

ISSN 2732-0189 (Online)

ISSN 1586-2070 (Print)

# JOURNAL OF COMPUTATIONAL AND APPLIED MECHANICS

An Open Access International Journal

Published by the University of Miskolc

VOLUME 16, NUMBER 1 (2021)



**MISKOLC UNIVERSITY PRESS**



ISSN 2732-0189 (Online)

ISSN 1586-2070 (Print)

# JOURNAL OF COMPUTATIONAL AND APPLIED MECHANICS

An Open Access International Journal

Published by the University of Miskolc

VOLUME 16 NUMBER 1 (2021)



MISKOLC UNIVERSITY PRESS



## EDITORS

László **BARANYI**, Institute of Energy Engineering and Chemical Machinery, University of Miskolc, H-3515 MISKOLC, Hungary, e-mail: [arambl@uni-miskolc.hu](mailto:arambl@uni-miskolc.hu)

Balázs **TÓTH**, Institute of Applied Mechanics, University of Miskolc, H-3515 MISKOLC, Hungary e-mail: [balazs.toth@uni-miskolc.hu](mailto:balazs.toth@uni-miskolc.hu)

## EDITORIAL ADVISORY BOARD

Edgár **BERTÓTI**, Institute of Applied Mechanics, University of Miskolc, H-3515 MISKOLC, Hungary, e-mail: [edgar.bertoti@uni-miskolc.hu](mailto:edgar.bertoti@uni-miskolc.hu)

Attila **BAKSA**, Institute of Applied Mechanics, University of Miskolc, H-3515 MISKOLC, Hungary, [attila.baksa@uni-miskolc.hu](mailto:attila.baksa@uni-miskolc.hu)

István **ECSEDI**, Institute of Applied Mechanics, University of Miskolc, H-3515 MISKOLC, Hungary, [mechecs@uni-miskolc.hu](mailto:mechecs@uni-miskolc.hu)

Ulrich **GABBERT**, Institut für Mechanik, Otto-von-Guericke-Universität Magdeburg, Universitätsplatz 2, 39106 MAGDEBURG, Germany, [ulrich.gabbert@mb.uni-magdeburg.de](mailto:ulrich.gabbert@mb.uni-magdeburg.de)

Zsolt **GÁSPÁR**, Department of Structural Mechanics, Budapest University of Technology and Economics, Műegyetem rkp. 3, 1111 BUDAPEST, Hungary, [gaspar@ep-mech.me.bme.hu](mailto:gaspar@ep-mech.me.bme.hu)

Robert **HABER**, Department of Theoretical and Applied Mechanics, University of Illinois at Urbana-Champaign, 216 Talbot Lab., 104 S. Wright St., URBANA, IL 61801, USA, [r-haber@uiuc.edu](mailto:r-haber@uiuc.edu)

Csaba **HŐS**, Department of Hydraulic Machines, Budapest University of Technology and Economics, Műegyetem rkp. 3, 1111 BUDAPEST, Hungary, [hoscscaba@vizgep.bme.hu](mailto:hoscscaba@vizgep.bme.hu)

Károly **JÁRMAI**, Institute of Energy Engineering and Chemical Industry, University of Miskolc, H-3515 MISKOLC, Hungary, [altjar@uni-miskolc.hu](mailto:altjar@uni-miskolc.hu)

László **KOLLÁR**, Department of Structural Engineering, Budapest University of Technology and Economics, Műegyetem rkp. 3. K.II.42., 1521 BUDAPEST, Hungary, [lkollar@eik.bme.hu](mailto:lkollar@eik.bme.hu)

József **KÖVECSES**, Mechanical Engineering Department 817 Sherbrooke Street West, MD163 MONTREAL, Quebec H3A 2K6 [jozsef.kovecses@mcgill.ca](mailto:jozsef.kovecses@mcgill.ca)

Márta **KURUTZ**, Department of Structural Mechanics, Budapest University of Technology and Economics, Műegyetem rkp. 3, 1111 BUDAPEST, Hungary, [kurutzm@eik.bme.hu](mailto:kurutzm@eik.bme.hu)

Lin **LU**, Center for Deepwater Engineering, Dalian University of Technology, Dalian, China [lulin@dlut.edu.cn](mailto:lulin@dlut.edu.cn)

Herbert **MANG**, Institute for Strength of Materials, University of Technology, Karlsplatz 13, 1040 VIENNA, Austria, [Herbert.Mang@tuwien.ac.at](mailto:Herbert.Mang@tuwien.ac.at)

Sanjay **MITTAL**, Department of Aerospace Engineering, Indian Institute of Technology, KANPUR, UP 208 016, India, [smittal@iitk.ac.in](mailto:smittal@iitk.ac.in)

Zenon **MRÓZ**, Polish Academy of Sciences, Institute of Fundamental Technological Research, Swietokrzyska 21, WARSAW, Poland [zmroz@ippt.gov.pl](mailto:zmroz@ippt.gov.pl)

Gyula **PATKÓ**, Institute of Machine Tools and Mechatronics, University of Miskolc, H-3515 MISKOLC, Hungary, [patko@uni-miskolc.hu](mailto:patko@uni-miskolc.hu)

István **PÁCZELT**, Institute of Applied Mechanics, University of Miskolc, 3515 MISKOLC, Hungary, [istvan.paczelt@uni-miskolc.hu](mailto:istvan.paczelt@uni-miskolc.hu)

Jan **SLADEK**, Ústav stavbeníctva a architektúry, Slovenskej akadémie vied, Dubrovská cesta 9, 842 20 BRATISLAVA, Slovakia, [usarslad@savba.sk](mailto:usarslad@savba.sk)

Gábor **STÉPÁN**, Department of Applied Mechanics, Budapest University of Technology and Economics, Műegyetem rkp. 3, 1111 BUDAPEST, Hungary, [stepan@mm.bme.hu](mailto:stepan@mm.bme.hu)

Barna **SZABÓ**, Department of Mechanical Engineering and Materials Science, Washington University, Campus Box 1185, ST. LOUIS, MO 63130, USA, [szabo@wustl.edu](mailto:szabo@wustl.edu)

## HONORARY EDITORIAL ADVISORY BOARD MEMBERS

Tibor **CZIBERE**, Institute of Energy Engineering and Chemical Machinery, University of Miskolc, H-3515 Miskolc-Egyetemváros, Hungary

Gábor **HALÁSZ**, Department of Hydraulic Machines, Budapest University of Technology and Economics, Műegyetem rkp. 3, 1111 BUDAPEST, Hungary

György **SZEIDL**, Institute of Applied Mechanics, University of Miskolc, H-3515 Miskolc-Egyetemváros, Hungary



# NONLINEAR VIBRATIONAL AND ROTATIONAL ANALYSIS OF MICROBEAMS IN NANOBIMATERIALS USING GALERKIN DECOMPOSITION AND DIFFERENTIAL TRANSFORM METHODS

OLUROTIMI ADELEYE

Department of Biomedical Engineering, University of Lagos  
Akoka, Lagos, Nigeria  
[oadeleye@unilag.edu.ng](mailto:oadeleye@unilag.edu.ng)

ABDULAH I ATITEBI

Department of Systems Engineering, University of Lagos  
Akoka, Lagos, Nigeria  
[ibnaganiyy@gmail.com](mailto:ibnaganiyy@gmail.com)

AHMED YINUSA

Department of Mechanical Engineering, University of Lagos  
Akoka, Lagos, Nigeria  
[aayinusa@unilag.edu.ng](mailto:aayinusa@unilag.edu.ng)

[Received: September 1, 2020; Accepted: March 15, 2021]

**Abstract.** In this paper, a nonlinear vibrational and rotational analysis of microbeams in nanobiomaterials using Galerkin Decomposition (GDM) and Differential Transform Methods (DTM) is presented. The dependency of cell migration and growth on nanoscaffold porosity and pore size architecture in tissue regeneration is governed by a dynamic model for the nonlinear vibration and rotation of the microbeams of nanobiomaterials and represented by a set of nonlinear partial differential equations. The solutions of the governing model are obtained by applying GDM and DTM and good agreement is achieved with numerical Runge-Kutta method (RK4). From the results, it is observed that an increase in Duffing term resulted in the increase of the frequency of the micro-beam. An increase in the foundation term also resulted in a corresponding increase in the frequency of the system for both free and forced dynamic responses. This study will enhance the application of tissue engineering in the regeneration of damaged human body tissues.

*Mathematical Subject Classification:* 35M86

*Keywords:* Nonlinear vibration, rotation, microbeams, nanobiomaterials, Galerkin Decomposition Method (GDM), Differential Transform Method (DTM)

## 1. INTRODUCTION

Cellular structured nanobiomaterials with extremely restrained micro-architectures have a wide range of applications which includes bone-substituting biomaterials in orthopaedics [1]. In these applications, the size and size distribution of the biomaterials are important [2]. The production of these biomaterials has been enabled by applying additive manufacturing techniques in engineering principles to produce

one or multiple types of unit cells. One of the most recent applications of the unit cell in the production of porous biomaterials is the diamond lattice unit cell [1, 3]. In the application of additively manufacturing to porous titanium implants as replacements for bone, it is observed that the excellent biocompatible properties of titanium are preserved, which shows that the stiffness of titanium is quite small when compared with that of the natural bones [4]. The porosity and permeability of materials have been linked to fractal dimensions through imbibition model for petro-physical applications [5].

Nanoporous biomaterials such as Metal-Organic Frameworks (MOFs) consist of metal ions joined by organic connective ligands which have unique chemical and physical characteristics. The application of MOFs in biological systems, drug delivery, material science, and nanotechnology is being explored [2]. The importance and applications of biomaterials with more recent findings of smart biomaterials cannot be overemphasized, as uses are being found in the medicine and healthcare sector; as implants for body organ replacements, tissue regeneration, drug delivery systems, medical devices, and immune engineering [6–9].

Mathematical models for size dependent dynamics of biomaterials have been developed for three-layered beams based on the hypothesis of the Grigolyuk–Chulkov and the modified couple stress theory. The governing model and its boundary/initial conditions for beam displacement are applied for motion of layers' beams on the micro and nano-scales [10]. Nanobeams with axially immovable ends and the geometrical nonlinearity caused by mid-plane stretching are considered in the developed model. In the Euler-Bernoulli beam model, the nano-device dynamic equation of motion is applied in the model kinematics [11]. The mathematical models of the nanoparticle are also affected by size and architecture, as shown in the normalized center deflections obtained in the study of size dependent composite laminated skew Mindlin plate. The Raleigh-Ritz method was applied to obtain a numerical solution to the model and it was observed that the normalized center deflections are always smaller than those obtained by the classical one [12, 13]. The mechanisms of the nanoparticles will aid the understanding of cell and nanoparticle size dependent toxicity. The electromechanical response of a nanostructure is observed to be influenced by the size of its element. This property of the nanostructure has been exhibited and it is further shown that the stability of the nanotweezers will be affected by the element size [14]. In the modeling of size effects of nanobeams, Reddy's shear deformation beam theory was applied to vibration characteristics of functional graded piezoelectric (FGP) nanobeams. Eringen's nonlocal elasticity theory was adopted to capture the small size effect. The obtained results showed that the applied Reddy's shear deformation model presented accurate frequency results of the FGP nanobeams [15].

Remarkably, mathematical models have provided the means to understand the physiochemical and physiological features of the behavior of nanomaterial in biological systems, as shown in the application of nanotechnology in inducing cytotoxic agents in cancer-nanomedicine [16], for predicting pore size distribution, and for the estimations of growth rates [17]. Nanomaterials of different shapes and sizes relate with cells in various ways, passively and actively. Recent studies on size-dependent

effects of nanomaterials have been done with spherical nanoparticles but special consideration has been given to critical cellular interaction [13]. In order to enhance the cellular interaction and nanoparticle internalization, it has been proposed that the best size for the nanoparticle is 50 nm [13], though most experimental data show that the approximate nanoparticle size preferred for cell internalization is 100 nm. Hence nanoparticle size influences the endocytic pathway which is followed by cell internalization. The microtubules and the actin filaments are biological elements in the living cells which serve as block builders for functional nanomaterials and nanostructures used for manufacturing nature—inspired small-scale devices or systems [18].

Analytical solutions have been obtained for wave dispersion in anisotropic doubly-curved nanoshells. The governing equation for the formulation was based on Hamilton's principles [19]. In a related study of free vibration of piezoelectric nanotubes, Hamilton's principles were applied to develop the governing equation and the enthalpy energy [20–22]. The effects of size as well as the geometrical and electromechanical effects on the nanotube and their effects on natural frequency of the vibration of the piezoelectric nanotubes were investigated. An explicit expression obtained for mechanical properties of nanoporous biomaterials. The expression was made in terms of the pore size from the lattice structure of the refined truncated cube by applying additive manufacturing in order to obtain appropriate mechanical properties [23]. The effectiveness, robustness and applicability of analytical solutions to complex problems cannot be overemphasized and this makes the analytical solution of the present problem of utmost importance. The study is focused on investigating the problems of nonlinear vibrational and rotational analysis of microbeams in nanobiomaterials using Galerkin Decomposition and Differential Transform Methods.

The developed nonlinear differential equations which describe the nonlinear vibrational and rotational analysis of microbeams in nanobiomaterials do not have closed form solutions, hence special analytical techniques are applied to obtain the solution: the Galerkin Decomposition Method and the Differential Transform Method. The Galerkin Decomposition Method is a numerical method which has proved to be effective in various applications, which include nonlinear elastic dynamics of a clamped laminated composite [24] and solution of wide range of weighted residual problems using Galerkin's Method [25]. Galerkin's method has also been applied to nonlinear vibrational problems in carbon nanotubes applications [26], and heat transfer problems for temperature-dependent thermal conductivity of a porous fin in [27]. Galerkin's method has been combined with other methods to obtain more efficient results, such as the Variational methods, in solving engineering problems in nonlinear ordinary differential equations [28] and Petrov–Galerkin methods for nonlinear systems without monotonicity [29].

In this study, the solution obtained by the Galerkin Decomposition Method is compared with the solutions of the differential transform method. The differential transform method (DTM) is an approximate analytical method for solving linear and nonlinear ordinary and partial differential equations. It was proposed by Zhou in 1986 [30]. The DTM has been applied in free and forced convection flow about inclined surfaces in porous media [31, 32], in Newtonian and non-Newtonian nanofluids flow

analysis [33], and nonlinear ordinary differential matrix equations [34]. DTM has proved to be effective when compared with the Adomian Decomposition Method (ADM) and with the Variation Iteration Method (VIM) and Homotopy Perturbation Method (HPM) [35, 36]. The DTM has some drawbacks which have been overcome by combining it with Laplace transform in studies for nonlinear Duffing oscillator with damping effect [37] and for non-linear oscillators by applying the multi-step differential transform method [38]. Further works on vibration theories and applications have also been presented [39, 40].

Therefore the main objective of this current study is to investigate the problem of nonlinear vibrational and rotational analysis of microbeams in nanobiomaterials using Galerkin Decomposition and the Differential Transform Methods. In replacing damaged human body tissues, novel approaches are emerging in tissues engineering to regenerate damaged tissues and the major elements in these approaches are the migration and growth of cells. These elements depend on the porosity of the nanoscaffolds and the pore size architecture of the cell. In order to investigate this dependency of the migration and growth of cell on pore size, the nonlocal strain gradient theory of elasticity is applied to develop the dynamic model for the nonlinear vibration and rotation of the microbeams made of nanobiomaterials. This dynamic model is a set of nonlinear partial differential equations whose solutions require special analytic techniques. The solutions are obtained by applying Galerkin Decomposition Method or the Differential Transform Method. The effects of modal number on steady state response, the effect of duffing term on stability response of the microbeam, the effect of elastic foundations on microbeam stability response, and the effect of elastic foundation on microbeam free and forced dynamic responses are then investigated.

The paper is organized into five sections. The first one, i.e., the present section considers the preliminary results and outlines the problem to be solved. Section 2 is devoted to the equations of motion which have a strongly non-linear character. The solution algorithm is detailed in Section 3 where analytical approximations are devised for the unknown quantities. The numerical results are evaluated and discussed in Section 4. Our conclusions are presented in Section 5 which is a short summary of our results. The last section is a Nomenclature. The readers are advised to refer to this section for the fundamental notations.

## 2. FORMULATING THE EQUATION OF MOTION

The degree of freedom of system for the microbeam's unit cell as well as the imposed boundary conditions are represented by Figures 1 and 2. In this present study, the biological system nanoporous microbeam is assumed to include the lattice structure of the refined truncated cube. With repeated cells, the unit cell is surrounded by truncated cubes and hence, results in each membrane of refined truncated cube. Consequently, analyzing a membrane of refined truncated cube is sufficient to obtain the mechanical response of the unit cell. If  $\eta_2 = 1$ ,  $\eta_1 = \eta_3$  and  $\eta_4 = \eta_5 = \eta_6 = 0$  it follows from Figure 1 that the point  $a_1$  (the vertices of links  $a_1b_1$ ,  $a_1b_2$ ,  $a_1b_3$ ,  $a_1b_4$  – the last three links are, however, not represented in Figure 1) displaces downwards by unity.

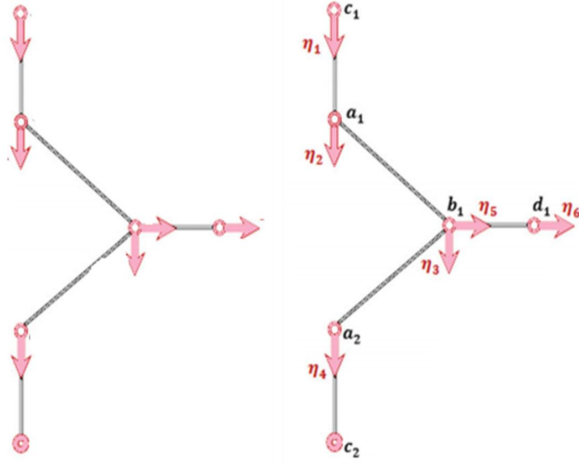


Figure 1. Cell unit with its degree of freedom

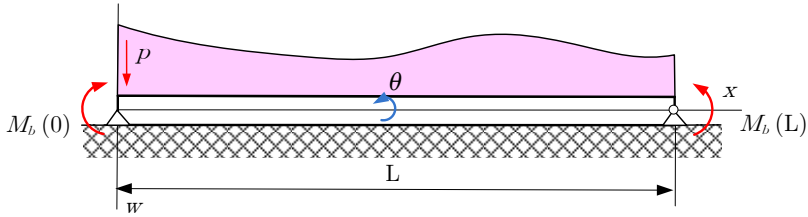


Figure 2. The system condition considered (pinned-pinned)

According to the refined hyperbolic shear deformable beam model proposed by Sahmani [41], the governing equations that capture the deflection and rotation are as follows:

$$\begin{aligned} \xi_1 \frac{\partial^4 w}{\partial x^4} - \xi_2 \frac{\partial^3 \theta}{\partial x^3} - \xi_3 \frac{\partial^6 w}{\partial x^6} + \xi_4 \frac{\partial^5 \theta}{\partial x^5} - p + \mu^2 \frac{\partial^2 p}{\partial x^2} - \xi_5 \frac{\partial^2 w}{\partial x^2} + \\ + \mu^2 \xi_6 \frac{\partial^2 w}{\partial x^2} + \mu^2 \xi_5 \frac{\partial^4 w}{\partial x^4} + \xi_7 \frac{\partial^2 w}{\partial t^2} - (\mu^2 \xi_7 + \xi_8) \frac{\partial^4 w}{\partial x^2 \partial t^2} + \xi_9 \frac{\partial^6 w}{\partial x^4 \partial t^2} - \\ - \xi_{10} \frac{\partial^3 w}{\partial x \partial t^2} + \mu^2 \xi_{10} \frac{\partial^5 w}{\partial x^3 \partial t^2} = 0, \quad (1a) \end{aligned}$$

$$\xi_1 \frac{\partial^3 w}{\partial x^3} - \xi_{11} \frac{\partial^2 \theta}{\partial x^2} + \xi_{12} \theta - \xi_{12} \frac{\partial^3 w}{\partial x \partial t^2} - \xi_{13} \frac{\partial^2 w}{\partial t^2} = 0. \quad (1b)$$

In this work, a nonlinear elastic foundation term will be incorporated. This makes the fully coupled governing equation strongly nonlinear as presented below:

$$\begin{aligned}
R_1(x, t) = & \xi_1 \frac{\partial^4 w}{\partial x^4} - \xi_2 \frac{\partial^3 \theta}{\partial x^3} - \xi_3 \frac{\partial^6 w}{\partial x^6} + \xi_4 \frac{\partial^5 \theta}{\partial x^5} - p + \mu^2 \frac{\partial^2 p}{\partial x^2} - \xi_5 \frac{\partial^2 w}{\partial x^2} + \\
& + \mu^2 \xi_6 \frac{\partial^2 w}{\partial x^2} + \mu^2 \xi_5 \frac{\partial^4 w}{\partial x^4} + \xi_7 \frac{\partial^2 w}{\partial t^2} - (\mu^2 \xi_7 + \xi_8) \frac{\partial^4 w}{\partial x^2 \partial t^2} + \xi_9 \frac{\partial^6 w}{\partial x^4 \partial t^2} - \\
& - \xi_{10} \frac{\partial^3 w}{\partial x \partial t^2} + \mu^2 \xi_{10} \frac{\partial^5 w}{\partial x^3 \partial t^2} + k_1 w + k_2 w^3 = 0, \\
R_2(x, t) = & \xi_1 \frac{\partial^3 w}{\partial x^3} - \xi_{11} \frac{\partial^2 \theta}{\partial x^2} + \xi_{12} \theta - \xi_{12} \frac{\partial^3 w}{\partial x \partial t^2} - \xi_{13} \frac{\partial^2 w}{\partial t^2} = 0.
\end{aligned} \tag{2}$$

The non-linear differential equations (2) are associated with the following boundary conditions valid for pinned-pinned beams [40]:

$$\begin{aligned}
w(0, t) = w''(0, t) = 0, \\
w(L, t) = w''(L, t) = 0.
\end{aligned} \tag{3a}$$

The initial conditions are of the form

$$w(t=0) = a = \lim_{t \rightarrow 0} \frac{\bar{w}}{10^{-6} m} \cos \bar{\omega} t = W_{\max} \cos \bar{\omega} t, \quad \dot{w}(t=0) = 0, \tag{3b}$$

$$\theta(t=0) = b = \lim_{t \rightarrow 0} b \cos \bar{\omega} t, \quad \dot{\theta}(t=0) = 0.$$

Here, the initial deflection and rotation of the microbeam, which are  $a$  and  $b$ , tend to zero [41]. Equation 2 will be solved using Galerkin Decomposition (DG) and Differential Transform Method (DTM) in order to obtain the dynamic response and rotation of the system under consideration.

### 3. MODELS AND SOLUTIONS

**3.1. Application of the Galerkin decomposition.** The Galerkin Decomposition method is applied to convert the governing partial differential equations into ordinary differential equations using an appropriate shape function that satisfies the boundary conditions. This approach is expressed as

$$\int_0^L R_i(x, t) \varphi(x) dx = 0, \quad (i = 1, 2) \tag{4}$$

where

$$w = w(x, t) = T(t) \varphi(x), \quad \text{and} \quad \theta = \theta(x, t) = J(t) \varphi(x), \tag{5}$$

while  $R_1$  and  $R_2$  are given by (2). Substituting them into (4) yields

$$\begin{aligned} & \int_0^L \left( \xi_1 \frac{\partial^4 w}{\partial x^4} - \xi_2 \frac{\partial^3 \theta}{\partial x^3} - \xi_3 \frac{\partial^6 w}{\partial x^6} + \xi_4 \frac{\partial^5 \theta}{\partial x^5} - p + \mu^2 \frac{\partial^2 p}{\partial x^2} - \xi_5 \frac{\partial^2 w}{\partial x^2} + \right. \\ & + \mu^2 \xi_6 \frac{\partial^2 w}{\partial x^2} + \mu^2 \xi_5 \frac{\partial^4 w}{\partial x^4} + \xi_7 \frac{\partial^2 w}{\partial t^2} - (\mu^2 \xi_7 + \xi_8) \frac{\partial^4 w}{\partial x^2 \partial t^2} + \xi_9 \frac{\partial^6 w}{\partial x^4 \partial t^2} - \\ & \left. - \xi_{10} \frac{\partial^3 w}{\partial x \partial t^2} + \mu^2 \xi_{10} \frac{\partial^5 w}{\partial x^3 \partial t^2} + k_1 w + k_2 w^3 \right) \varphi(x) dx = 0, \quad (6) \\ & \int_0^L \left( \xi_1 \frac{\partial^3 w}{\partial x^3} - \xi_{11} \frac{\partial^2 \theta}{\partial x^2} + \xi_{12} \theta - \xi_{12} \frac{\partial^3 w}{\partial x \partial t^2} - \xi_{13} \frac{\partial^2 w}{\partial t^2} \right) \varphi(x) dx = 0. \end{aligned}$$

from where by inserting (5) we have

$$\begin{aligned} & \int_0^L \left( \xi_1 \frac{\partial^4 T(t) \varphi(x)}{\partial x^4} - \xi_2 \frac{\partial^3 J(t) \varphi(x)}{\partial x^3} - \xi_3 \frac{\partial^6 T(t) \varphi(x)}{\partial x^6} + \xi_4 \frac{\partial^5 J(t) \varphi(x)}{\partial x^5} - \right. \\ & - p + \mu^2 \frac{\partial^2 p}{\partial x^2} - \xi_5 \frac{\partial^2 T(t) \varphi(x)}{\partial x^2} + \mu^2 \xi_6 \frac{\partial^2 T(t) \varphi(x)}{\partial x^2} + \mu^2 \xi_5 \frac{\partial^4 (T(t) \varphi(x))}{\partial x^4} + \\ & + \xi_7 \frac{\partial^2 T(t) \varphi(x)}{\partial t^2} - (\mu^2 \xi_7 + \xi_8) \frac{\partial^4 T(t) \varphi(x)}{\partial x^2 \partial t^2} + \xi_9 \frac{\partial^6 T(t) \varphi(x)}{\partial x^4 \partial t^2} - \xi_{10} \frac{\partial^3 T(t) \varphi(x)}{\partial x \partial t^2} + \\ & \left. + \mu^2 \xi_{10} \frac{\partial^5 T(t) \varphi(x)}{\partial x^3 \partial t^2} + k_1 T(t) \varphi(x) + k_2 (T(t) \varphi(x))^3 \right) \varphi(x) dx = 0 \quad (7) \end{aligned}$$

and

$$\begin{aligned} & \int_0^L \left( \xi_1 \frac{\partial^3 T(t) \varphi(x)}{\partial x^3} - \xi_{11} \frac{\partial^2 J(t) \varphi(x)}{\partial x^2} + \xi_{12} J(t) \varphi(x) - \right. \\ & \left. - \xi_{12} \frac{\partial^3 T(t) \varphi(x)}{\partial x \partial t^2} - \xi_{13} \frac{\partial^2 J(t) \varphi(x)}{\partial t^2} \right) \varphi(x) dx = 0. \quad (8) \end{aligned}$$

By introducing new notations equations, (7) and (8) can be manipulated into the following simple forms

$$\begin{aligned} M_1 \ddot{T} + K_1 T + K_2 J + VT^3 &= F, \\ M_2 \ddot{J} + K_{12} J + K_{21} T &= 0, \end{aligned} \quad (9)$$

where

$$\begin{aligned} M_1 = \int_0^L \left( \xi_7 \varphi(x) - (\mu^2 \xi_7 + \xi_8) \frac{d^2 \varphi(x)}{dx^2} + \xi_9 \frac{d^4 \varphi(x)}{dx^4} + \right. \\ \left. + \xi_{10} \frac{d\varphi(x)}{dx} + \mu^2 \xi_{10} \frac{d^3 \varphi(x)}{dx^3} \right) \varphi(x) dx, \quad (10a) \end{aligned}$$

$$K_1 = \int_0^L \left( \xi_1 \frac{d^4 \varphi(x)}{dx^4} - \xi_3 \frac{d^6 \varphi(x)}{dx^6} - \xi_5 \frac{d^2 \varphi(x)}{dx^2} + \mu^2 \xi_6 \frac{d^2 \varphi(x)}{dx^2} + \mu^2 \xi_5 \frac{d^4 \varphi(x)}{dx^4} + k_1 \varphi(x) \right) \varphi(x) dx, \quad (10b)$$

$$K_2 = \int_0^L \left( -\xi_2 \frac{d^3 J(t) \varphi(x)}{dx^3} + \xi_4 \frac{d^5 J(t) \varphi(x)}{dx^5} \right) \varphi(x) dx, \quad (10c)$$

$$V = \int_0^L k_2 (\varphi(x))^3 \varphi(x) dx \quad (10d)$$

and

$$M_2 = \int_0^L (\xi_{13} \varphi(x)) \varphi(x) dx, \quad (11a)$$

$$M_{21} = - \int_0^L \xi_{12} \frac{d\varphi(x)}{dx} \varphi(x) dx = 0, \quad (11b)$$

$$K_{12} = \int_0^L \left( \xi_{11} \frac{d^2 \varphi(x)}{dx^2} + \xi_{12} \varphi(x) \right) \varphi(x) dx, \quad (11c)$$

$$K_{21} = \int_0^L \xi_1 \frac{d^3 \varphi(x)}{dx^3} \varphi(x) dx. \quad (11d)$$

Equation (9) is the desired system of ODE from the Galerkin decomposition of the PDEs which will be solved using DTM. However, the natural frequency and frequency ratio of the system may be obtained as

$$\omega = \sqrt{\frac{K_1}{M_1}} \quad (12)$$

and

$$\Omega = \frac{\omega_{nl}}{\omega} = \sqrt{1 \pm \frac{3VW_{\max}^2}{4K_1}} \quad (13)$$

which in an expanded form are given by

$$\omega = \sqrt{\frac{\int_0^L \left( \xi_1 \frac{d^4 \varphi(x)}{dx^4} - \xi_3 \frac{d^6 \varphi(x)}{dx^6} - \xi_5 \frac{d^2 \varphi(x)}{dx^2} + \mu^2 \xi_6 \frac{d^2 \varphi(x)}{dx^2} + \mu^2 \xi_5 \frac{d^4 \varphi(x)}{dx^4} + k_1 \varphi(x) \right) \varphi(x) dx}{\int_0^L \left( \xi_7 \varphi(x) - (\mu^2 \xi_7 + \xi_8) \frac{d^2 \varphi(x)}{dx^2} + \xi_9 \frac{d^4 \varphi(x)}{dx^4} + \xi_{10} \frac{d\varphi(x)}{dx} + \mu^2 \xi_{10} \frac{d^3 \varphi(x)}{dx^3} \right) \varphi(x) dx}}, \quad (14)$$

$$\Omega = \frac{\omega_{nl}}{\omega} = \sqrt{1 \pm \frac{3W_{\max}^2 \int_0^L k_2(\varphi(x))^3 \varphi(x) dx}{4 \int_0^L \left( \xi_1 \frac{d^4 \varphi(x)}{dx^4} - \xi_3 \frac{d^6 \varphi(x)}{dx^6} - \xi_5 \frac{d^2 \varphi(x)}{dx^2} + \mu^2 \xi_6 \frac{d^2 \varphi(x)}{dx^2} + \mu^2 \xi_5 \frac{d^4 \varphi(x)}{dx^4} + k_1 \varphi(x) \right) \varphi(x) dx}}, \quad (15)$$

where  $\varphi = \sin \frac{n\pi}{L} x$  for the considered pinned-pinned beam,  $n$  is the modal number and  $F$  is the Galerkin form of  $p$  – applying Galerkin decomposition to  $p$  yields  $F$ .

**3.2. Analytical solution to the developed models and the basic concepts of the differential transform method (DTM).** Due to the presence of a nonlinearity in the derived coupled governing equation of motion, a method capable of transforming differential equations into another domain with a robust and easy way of inversion is required. The differential transform method (DTM) possesses this attribute. DTM maps a governing equation into an algebraic domain and then obtains an inversion using a series summation method. This approximate analytical method generates a solution with the controlling parameters adequately conserved. The recursive relations that constitute DTM for transforming differential equation into the desired form are shown in Table 1. As regards the notations used in this table we refer the reader to [30] and [34] which detail the way they should be applied. By applying this scheme to equations (9) we obtain the required analytical solutions of the governing equations.

Table 1. Recursive relations for the Differential Transform Method (DTM)

$Z(t) = U(t) \pm V(t), \quad Z(k) = U(k) \pm V(k);$
$Z(t) = \infty U(t), \quad Z(k) = \infty U(k);$
$Z(t) = \frac{dU(t)}{dt}, \quad Z(k) = (k + 1)U[k + 1];$
$Z(t) = \frac{d^2U(t)}{dt^2}, \quad Z(k) = (k + 1)(k + 2)U[k + 2];$
$Z(t) = \frac{d^m U(t)}{dt^m}, \quad Z(k) = (k + 1)(k + 2) \cdots U[k + m] = \frac{(k+m)!}{k!} U[k + m];$
$Z(t) = U(t) * V(t), \quad Z(k) = \sum_{\ell=0}^K V(L)U[K - \ell];$
$Z(t) = t^m, \quad Z(k) = \delta(k - m).$

After applying the scheme in Table 1 to equations (9) we have

$$M_1(k + 1)(k + 2)T_{k+2} + K_1T_k + K_2J_k + V \sum_{q=0}^k \left( \sum_{l=0}^q T_l T_{q-l} T_{k-q} \right) - \frac{F\omega^k \sin(1/2k\pi)}{k!} = 0 \quad (16)$$

and

$$M_2(k+1)(k+2)J_{k+2} + K_{12}J_k + K_{21}T_k = 0, \quad (17)$$

where with regard to the transformed initial conditions

$$T_0 = a, \quad T_1 = 0, \quad J_0 = b \quad \text{and} \quad J_1 = 0. \quad (18)$$

Performing the iteration steps on equations (16) and (17) by utilizing equations (18) leads to the following solutions for  $T_2, J_2, \dots, T_7, J_7$ :

$$T_2 = -\frac{Va^3 + K_1a + K_2b}{2M_1}, \quad (19)$$

$$J_2 = -\frac{K_{12}b + K_{21}a}{2M_2}, \quad (20)$$

$$T_3 = \frac{F\omega}{16M_1}, \quad (21)$$

$$J_3 = 0, \quad (22)$$

$$T_4 = \frac{1}{24M_1^2M_2} (3M_2V^2a^5 + 4K_1M_2Va^3 + 3K_2M_2Va^2b + K_1^2M_2a + K_1K_2M_2b + K_{12}K_2M_1b + K_2K_{21}M_1a), \quad (23)$$

$$J_4 = \frac{K_{21}M_2Va^3 + K_1K_{21}M_2a + K_{12}^2M_1b + K_{12}K_{21}M_1a + K_2K_{21}M_2b}{24M_1M_2^2}, \quad (24)$$

$$T_5 = -F\omega(M_1\omega^2 + 3Va^2 + K_1)/120M_1^2 \quad (25)$$

$$J_5 = -K_{21}F\omega/120M_1M_2, \quad (26)$$

$$T_6 = -\frac{1}{720M_1^3M_2^2} \left( 27M_2^2V^3a^7 + 51K_1M_2^2V^2a^5 + 45K_2M_2^2V^2a^4b + 25K_1^2M_2^2Va^3 + 42K_1K_2M_2^2Va^2b + 3K_{12}K_2M_1M_2Va^2b + 18K_2^2M_2^2Vab^2 + 4K_2K_{21}M_1M_2Va^3 + K_1^3M_2^2a + K_1^2K_2M_2^2b + K_1K_{12}K_2M_1M_2 + 2K_1K_2K_{21}M_1M_2a + K_{12}^2K_2M_1^2b + K_{12}K_2K_{21}M_1^2a + K_2^2K_{21}M_1M_2b \right), \quad (27)$$

$$J_6 = -\frac{1}{720M_1^2M_2^3} \left( 3K_{21}M_2^2V^2a^5 + 4K_1K_{21}M_2^2Va^3 + K_{12}K_{21}M_1M_2Va^3 + 3K_2K_{21}M_2^2Va^2b + K_1^2K_{21}M_2^2a + K_1K_{12}K_{21}M_1M_2a + K_1K_2K_{21}M_2^2b + K_{12}^3M_1^2b + K_{12}^2K_{21}M_1^2a + 2K_{12}K_2K_{21}M_1M_2b + K_2K_{21}^2M_1M_2a \right), \quad (28)$$

$$T_7 = \frac{F\omega}{5040M_1^3M_2} \left( M_1^2M_2\omega^4 + 3M_1M_2Va^2\omega^2 + 69M_2V^2a^4 + K_1M_1M_2\omega^2 + 66K_1M_2Va^2 + 60K_2M_2Vab + K_1^2M_2 + K_2K_{21}M_1 \right), \quad (29)$$

$$J_7 = \frac{K_{21}F\omega(M_1M_2\omega^2 + 3M_2Va^2 + K_1M_2 + K_{12}M_1)}{5040M_1^2M_2^2}. \quad (30)$$

With  $T_0, J_0, \dots, T_7, J_7$  we have the following analytical approximations

$$T(t) = \sum_{k=0}^7 T_k t^k, \quad J(t) = \sum_{k=0}^7 J_k t^k. \quad (31)$$

Equations (31), in which the coefficients are given by (18),...,(30), are the desired analytical solutions for  $T(t)$  and  $J(t)$ . In order to find the unknown deflections for a longer time history, the above technique is applied and the results obtained are utilized to analyze the dynamic behavior of the system in the present study. Furthermore, the computations require 16 iterations for achieving good accuracy.

#### 4. RESULTS AND DISCUSSIONS

In this study, the nonlinear vibration and rotation of microbeams in presented. The migration and growth of a cell depends on the porosity of the nanoscaffolds and the pore size architecture. In order to investigate this dependency of the cell migration and growth on pore size, the nonlocal strain gradient theory of elasticity is applied to develop a dynamic model for the nonlinear vibration and rotation of microbeams made of nanobiomaterials. This dynamic model, which is a set of coupled nonlinear ordinary differential equations, was solved by applying an approximate

Table 2. Validation of the Galerkin Decomposition Method with the Differential Transform Method

Time (Secs)	Deflection (nm)			Rotation (radian)		
	GDM	DTM	Residual	GDM	DTM	Residual
1	0.3000	0.3000	0.0000	0.1000	0.1000	0.0000
2	0.2384	0.2385	0.0001	0.0921	0.0921	0.0000
3	0.0787	0.0790	0.0003	0.0711	0.0711	0.0000
4	-0.1150	-0.1144	0.0006	0.0441	0.0440	0.0001
5	-0.2649	-0.2645	0.0004	0.0198	0.0197	0.0001
6	-0.3104	-0.3105	0.0001	0.0051	0.0050	0.0001
7	-0.2327	-0.2335	0.0008	0.0025	0.0023	0.0002
8	-0.0628	-0.0641	0.0013	0.0088	0.0087	0.0001
9	0.1316	-0.1302	0.0014	0.0173	0.0172	0.0001
10	0.2732	-0.2724	0.0008	0.0199	0.0199	0.0000
11	0.3056	0.3059	0.0003	0.0110	0.1112	0.0002
12	0.2160	0.2175	0.0015	-0.0104	-0.0100	0.0003
13	0.0413	0.0435	0.0022	-0.0398	-0.0395	0.0003
14	-0.1482	-0.1461	0.0021	-0.0693	-0.0690	0.0003
15	-0.2764	-0.2753	0.0011	-0.0901	-0.0900	0.0001
16	-0.2912	-0.2919	0.0007	-0.0964	-0.0965	0.0001
17	-0.1865	-0.1889	0.0008	-0.0874	-0.0876	0.0002
18	-0.0046	-0.0078	0.0032	-0.0675	-0.0678	0.0003
19	0.1818	0.1790	0.0028	-0.0446	-0.0449	0.0003
20	0.2980	0.2969	0.0011	-0.0272	-0.0272	0.0000

solution method; Galerkin Decomposition Method and an approximate analytical approach the Differential Transform Method. The results are shown in Table 2 and an excellent agreement is established between them.

The effects of modal number on steady state response are shown in Figures 3-6. This analysis is vital as it shows clearly the locations of nodes and anti-nodes. Based on the results obtained, an increase in modal number increases the number

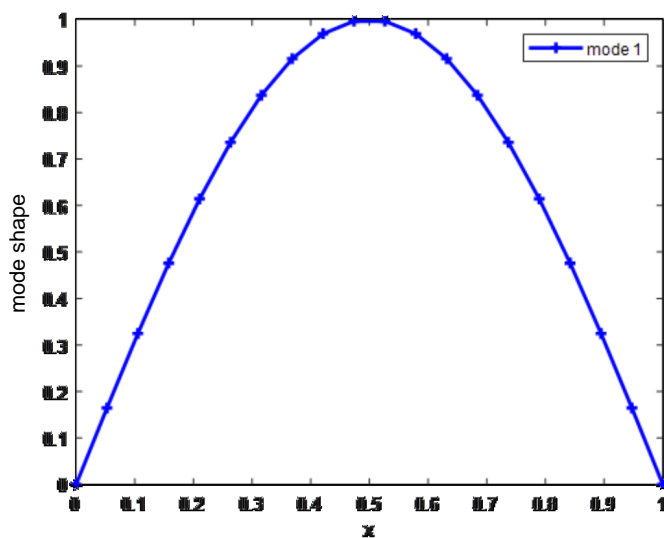


Figure 3. Steady state response for mode 1

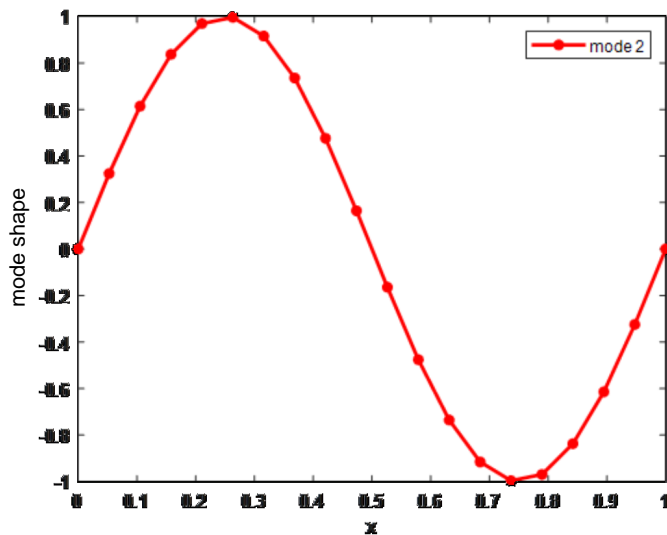


Figure 4. Steady state response for mode 2

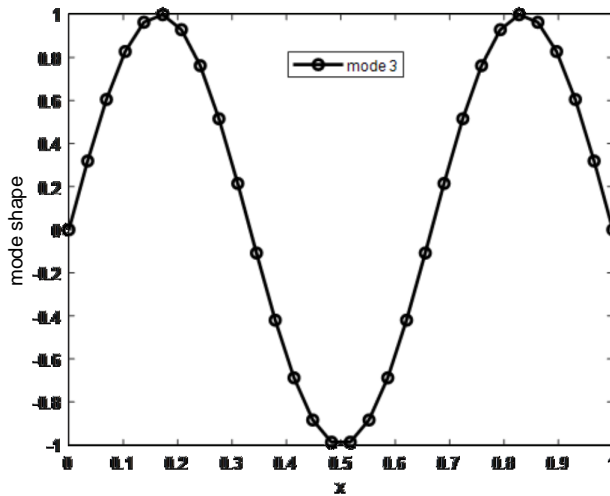


Figure 5. Steady state response for mode 3

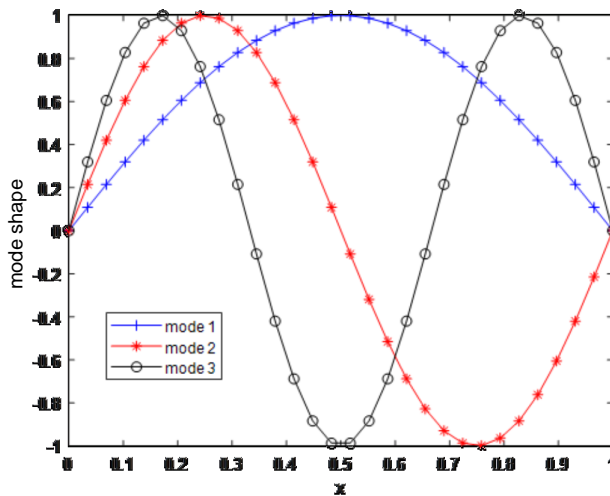
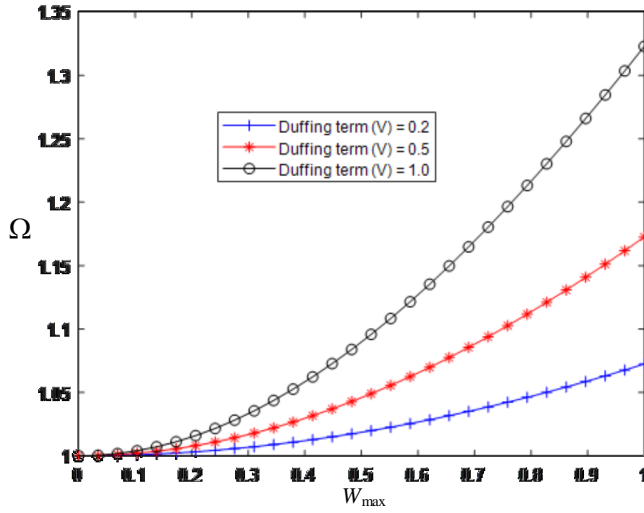
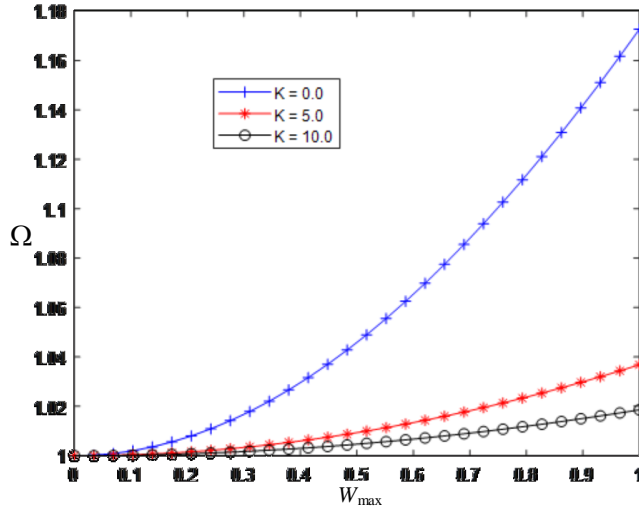


Figure 6. Super-imposed steady state responses

of nodes and anti-nodes. The locations of anti-nodes are very important during the system's vibration that may tend to resonance as reducing disturbances at these point automatically reduces vibration throughout the entire beam length.

The effect of the Duffing term on micro  $W_{\max}$  is shown in Figure 7. From the plot, it is obvious that when the system's deflection is low, the nonlinear term possesses negligible impact. However, at very large amplitudes, an increase in the Duffing term increases the dimensionless frequency of the nano-porous micro-beam. Figure 8 shows

Figure 7. The effect of the nonlinear term on  $W_{\max}$ Figure 8. The effect of the foundation term on  $W_{\max}$ 

the effect of elastic foundation term  $m$  (also referred to as the linear Winkler coefficient  $k = k_1$ ) on  $W_{\max}$ . From the plot, it is observed that when the micro-beam is foundation free, it gives a very large frequency ratio. This may result in instable behavior. However, when the elastic foundation parameter is introduced, the frequency ratio starts to decay even for high values of deflection. This reiterates the importance of an elastic foundation. Figures 7 and 8 are included in the study for monitoring the resonance of the microbeam.

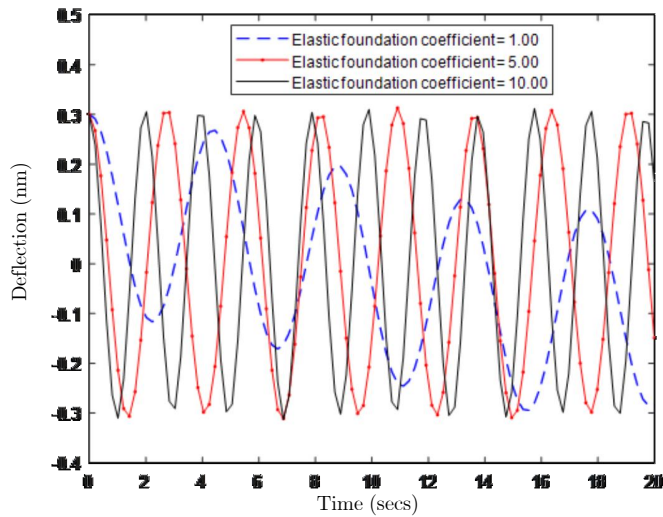


Figure 9. Effect of the foundation term on the free dynamic response

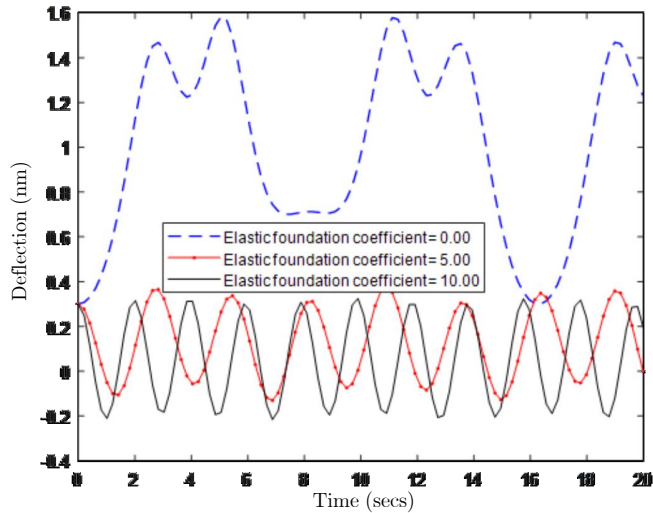


Figure 10. Effect of foundation term on the forced dynamic response

### 5. CONCLUSION

In this study, the nonlinear vibrational and rotational analysis of microbeams in nanobiomaterials using Galerkin Decomposition and the Differential Transform Method has been presented. The degeneration of human body tissues caused by congenital defects, diseases, trauma, etc. which were not replaced in times past, can now be

replaced today with the novel approaches emerging in tissue engineering to regenerate such damaged tissues even after been replaced. The major element in one of the novel approaches is the migration and growth of cells, which depends on the porosity of the nanoscaffolds and the pore size architecture. In order to investigate this dependency of the cell migration and growth on pore size, the nonlocal strain gradient theory of elasticity is applied to develop a dynamic model for the nonlinear vibration and rotation of the microbeams made of nanobiomaterials. This dynamic model, which is a set of coupled nonlinear ordinary differential equations, was solved by applying a decomposition scheme – Galerkin Decomposition Method and an approximate analytical technique, the Differential Transform Method. Good agreement is established between the solutions. The effects of the modal number on the steady state response, the effect of the Duffing term on stability response on microbeam, the effect of the elastic foundations on the stability response of the microbeam, and the effect of the elastic foundation on the free and forced dynamic responses of the microbeam were investigated. It is observed that an increase in the modal number increases the number of the nodes and anti-nodes. During system vibration that may tend to resonance, the increased anti-nodes reduce disturbances at these nodal points which automatically reduces the vibration in the entire beam length. An increase in Duffing term also resulted in the increases of the dimensionless frequency of the nano-porous micro-beam. When the elastic foundation is introduced and increased, there is a decrease in the frequency ration of the microbeam. And for the free and forced dynamic responses, an increase in the foundation term increases the frequency of the system for both conditions. This study will enhance a parametric study in vibration and rotation of nanobiomaterials and the application of tissue engineering to regenerate damaged tissues in the human body.

## 6. NOMENCLATURE

	<i>Latin notations</i>		
$a_1 b_1, \dots$	Links – see Figure 1	$t$	Time
$A$	Area	$T$	Temporal rotation
$E$	Modulus of elasticity	$V$	Duffing term
$F$	Galerkin force function	$w$	Deflection
$G$	Shear modulus of elasticity	$W_{\max}$	Maximum dimensionless deflection
$I$	Moment of inertia	$\bar{w}$	Deflection
$J$	Temporal rotation	$x$	Independent variable
$k_1$	Linear Winkler coefficient		<i>Greek notations</i>
$k_2$	Non-linear foundation coefficient	$\theta$	Rotation
$K$	Stiffness	$\mu$	Nonlocal term
$L$	Length of the microbeam	$\xi_1$	Flexural term
$M$	Mass	$\xi_{2, \dots, 13}$	Known coefficients [41]
$M_b$	Bending moment	$\varphi$	Shape function
$n$	Nodal number	$\omega$	Natural frequency
$p$	Distributed load	$\omega_{nl}$	Non-linear frequency
$R$	Galerkin Function	$\Omega$	Frequency ratio

## REFERENCES

1. O. V. Salata. “Applications of nanoparticles in biology and medicine.” *Journal of Nanobiotechnology*, **2**, (May 2004), pp. 1–6. DOI: 10.1186/1477-3155-2-3.
2. S. Beg, M. Rahman, A. Jain, S. Saini, P. Midoux, C. Pichon, F. J. Ahmad, and S. Akhter. “Nanoporous metal organic frameworks as hybrid polymer–metal composites for drug delivery and biomedical applications.” *Drug Discovery Today*, **22**(4) (2017), pp. 625–637. DOI: 10.1016/j.drudis.2016.10.001.
3. S. M. Ahmadi, G. Campoli, S. Amin Yavari, B. Sajadi, R. Wauthle, J. Schrooten, H. Weinans, and A. A. Zadpoor. “Mechanical behavior of regular open-cell porous biomaterials made of diamond lattice unit cells.” *Journal of the Mechanical Behavior of Biomedical Materials*, **34**, (2014), pp. 106–115. DOI: <https://doi.org/10.1016/j.jmbbm.2014.02.003>.
4. R. Hedayati, S. Amin Yavari, and A. A. Zadpoor. “Fatigue crack propagation in additively manufactured porous biomaterials.” *Materials Science and Engineering: C*, **76**, (2017), pp. 457–463. DOI: 10.1016/j.msec.2017.03.091.
5. A. Mumuni and P. Michal. “A mathematical determination of the pore size distribution and fractal dimension of a porous sample using spontaneous imbibition dynamics theory.” *Journal of Petroleum Exploration and Production Technology*, **9**, (2019), pp. 427–435. DOI: 10.1007/s13202-018-0477-9.
6. P. S. Kowalski, C. Bhattacharya, S. Afewerki, and R. Langer. “Smart Biomaterials: Recent Advances and Future Directions.” *ACS Biomaterials Science and Engineering*, **4**(11), (2018). DOI: 10.1021/acsbmaterials.8b00889.
7. D. Caccavo. “An overview on the mathematical modeling of hydrogels’ behavior for drug delivery systems.” *International Journal of Pharmaceutics*, **560**, (2019), pp. 175–190. DOI: 10.1016/j.ijpharm.2019.01.076.
8. M. E. Furth, A. Atala, and Mark E. Van Dyke. “Smart biomaterials design for tissue engineering and regenerative medicine.” *Biomaterials*, **28**(34), (2007). Festschrift honouring Professor David F. Williams, pp. 5068–5073. DOI: 10.1016/j.biomaterials.2007.07.042.
9. R. A. Perez, J. Won, J. C. Knowles, and H. Kim. “Naturally and synthetic smart composite biomaterials for tissue regeneration.” *Advanced Drug Delivery Reviews*, **65**(4), (2013), pp. 471–496. DOI: 10.1016/j.addr.2012.03.009.
10. J. Awrejcewicz, V. A. Krysko, S. P. Pavlov, M. V. Zhigalov, and A. V. Krysko. “Mathematical model of a three-layer micro- and nano-beams based on the hypotheses of the Grigolyuk–Chulkov and the modified couple stress theory.” *International Journal of Solids and Structures*, **117**, (2017), pp. 39–50. DOI: 10.1016/j.ijsolstr.2017.04.011.
11. S. Bornassi and H. Haddadpour. “Nonlocal vibration and pull-in instability analysis of electrostatic carbon-nanotube based NEMS devices.” *Sensors and Actuators A: Physical*, **266**, (2017), pp. 185–196. DOI: 10.1016/j.sna.2017.08.020.

12. D. He, W. Yang, and W. Chen. "A size-dependent composite laminated skew plate model based on a new modified couple stress theory." *Acta Mechanica Solida Sinica*, **30**(1), (2017), pp. 75–86. DOI: 10.1016/j.camss.2016.12.001.
13. F. Villanueva-Flores, A. Castro-Lugo, O. T. Ramírez, and L. A. Palomares. "Understanding cellular interactions with nanomaterials: towards a rational design of medical nanodevices." *Nanotechnology* 31.13 (2020), p. 132002. DOI: 10.1088/1361-6528/ab5bc8.
14. A. Farrokhbadi, A. Koochi, A. Kazemi, and M. Abadyan. "Effects of size-dependent elasticity on stability of nanotweezers." *Applied Mathematics and Mechanics*, **35**(12), (2014), 1573–1590. DOI: 10.1007/s10483-014-1880-6.
15. F. Ebrahimi and R. E. Fardshad. "Modeling the size effect on vibration characteristics of functionally graded piezoelectric nanobeams based on Reddy's shear deformation beam theory." *Advances in Nano Research*, **6**(2), (2018), pp. 113–133. DOI: 10.12989/anr.2018.6.2.113.
16. P. Dogra, J. D. Butner, Y. L. Chuang, S. Caserta, S. Goel, C. J. Brinker, V. Cristini, and Z. Wang. "Mathematical modeling in cancer nanomedicine: a review." *Biomedical Microdevices*, **21**(2), (2019). DOI: 10.1007/s10544-019-0380-2.
17. A. H. Faramarzi, T. Kaghazchi, H. A. Ebrahim, and A. A. Ebrahimi. "A mathematical model for prediction of pore size distribution development during activated carbon preparation." *Chemical Engineering Communications*, **202**(2), (2015), pp. 131–143. DOI: 10.1080/00986445.2013.830609.
18. K. C. Wu, C. Y. Yang, and C. M. Cheng. "Using cell structures to develop functional nanomaterials and nanostructures—case studies of actin filaments and microtubules." *Chemical Communications (Cambridge, England)*, **50**(32), (2014), 4148–4157. DOI: 10.1039/c4cc00005f.
19. B. Karami, M. Janghorban, and A. Tounsi. "Variational approach for wave dispersion in anisotropic doubly-curved nanoshells based on a new nonlocal strain gradient higher order shell theory." *Thin-Walled Structures*, **129**, (2018), pp. 251–264. DOI: 10.1016/j.tws.2018.02.025.
20. F. Kheibari and Y. T. Beni. "Size dependent electro-mechanical vibration of single-walled piezoelectric nanotubes using thin shell model." *Materials and Design*, **114**, (2017), pp. 572–583. DOI: <https://doi.org/10.1016/j.matdes.2016.10.041>.
21. Y. T. Beni. "Size-dependent electromechanical bending, buckling, and free vibration analysis of functionally graded piezoelectric nanobeams." *Journal of Intelligent Material Systems and Structures*, **27**(16), (2016), pp. 2199–2215. DOI: 10.1177/1045389X15624798.
22. M. Esmaeili and Y. T. Beni. "Vibration and buckling analysis of functionally graded flexoelectric smart beam." *Journal of Applied and Computational Mechanics*, **5**(5), (2019), pp. 900–917. DOI: 10.22055/jacm.2019.27857.1439.
23. R. Hedayati, M. Sadighi, M. Mohammadi-Aghdam, and A.A. Zadpoor. "Analytical relationships for the mechanical properties of additively manufactured porous biomaterials based on octahedral unit cells." *Applied Mathematical Modelling*, **46**, (2017), pp. 408–422. DOI: 10.1016/j.apm.2017.01.076.

24. H. Xe. “Modal decoupling using the method of weighted residuals for the nonlinear elastic dynamics of a clamped laminated composite.” *Mathematical Problems in Engineering*, **46**, (2009), pp. 1–19. DOI: 10.1155/2009/972930.
25. J. E. Cicelia. “Solution of weighted residual problems by using Galerkin’s method.” *Indian Journal of Science and Technology*, **7**(35), (Feb. 2014), pp. 52–54. DOI: 10.13140/2.1.3364.2883.
26. M. G. Sobamowo, Akanmu J. O., O. A. Adeleye, and A. A. Yinusa. “Nonlinear vibrations of single- and double-walled carbon nanotubes resting on two-parameter foundation in a magneto-thermal environment.” *SN Applied Sciences*, **1**, (2019). DOI: 10.1007/s42452-019-1158-0.
27. M. G. Sobamowo, O. M. Kamiyo, and O. A. Adeleye. “Further study on thermal performance of porous fin with temperature-dependent thermal conductivity and internal heat generation using Galerkin’s method of weighted residual.” *Scientific News, WSN*, **138**(2), (2019), pp. 167–191.
28. B. V. Reddy and K. R. Babu. “Application of variational methods and Galerkin method in solving engineering problems represented by ordinary differential equations.” *International Journal of Mechanical and Production Engineering*, **4**(4), (2016), pp. 75–80.
29. Y. Wang and B. Guo. “Petrov–Galerkin methods for nonlinear systems without monotonicity.” *Applied Numerical Mathematics*, **36**(1), (2001), pp. 57–78. DOI: [https://doi.org/10.1016/S0168-9274\(99\)00054-9](https://doi.org/10.1016/S0168-9274(99)00054-9).
30. J. K. Zhou. *Differential Transformation and its Applications for Electrical Circuits*. Huazhong University Press, Wuhan, China, 1986.
31. M. M. Rashidi, O. Anwar Bég, and N. Rahimzadeh. “A generalized differential transform method for combined free and forced convection flow about inclined surfaces in porous media.” *Chemical Engineering Communications*, **199**(2) (2012), pp. 257–282. DOI: 10.1080/00986445.2011.586757.
32. Bor-Lih Kuo. “Application of the differential transformation method to the solutions of the free convection problem.” *Applied Mathematics and Computation*, **165**(1), (2005), pp. 63–79. DOI: 10.1016/j.amc.2004.04.090.
33. M. Hatami and D. Jing. “Differential transformation method for Newtonian and non-Newtonian nanofluids flow analysis: Compared to numerical solution.” *Alexandria Engineering Journal*, **55**(2), (Jan. 2013), 731–739. DOI: 10.1016/j.aej.2016.01.003.
34. O. A. Adeleye, O. Ipinnimo, A. Yinusa, and P. E. Otobo. “Differential transformation method for Newtonian and non-Newtonian nanofluids flow analysis: Compared to numerical solution.” *Journal of Applied Computational Mechanics*, **6**(4), (2020), 893–907. DOI: 10.22055/jacm.2019.29361.1589.
35. M. Cakir and D. Arslan. “The Adomian Decomposition Method and the Differential Transform Method for numerical solution of multi-pantograph delay differential equations.” *Applied Mathematics*, **06**(8), (2015), pp. 1332–1343. DOI: 10.4236/am.2015.68126.

36. S. Ghafoori, M. Motevalli, M. G. Nejad, F. Shakeri, D. D. Ganji, and M. Jalaal. “Efficiency of differential transformation method for nonlinear oscillation: Comparison with HPM and VIM.” *Current Applied Physics*, **11**(4), (2011), pp. 965–971. DOI: 10.1016/j.cap.2010.12.018.
37. S. Nourazar and A. Mirzabeigy. “Approximate solution for nonlinear Duffing oscillator with damping effect using the modified differential transform method.” *Scientia Iranica*, **20**(2), (2013), pp. 364–368. DOI: 10.1016/j.scient.2013.02.023.
38. V. S. Erturk, Z. M. Odibat, and S. Momani. “The multi-step differential transform method and its application to determine the solutions of non-linear oscillators.” *Advances in Applied Mathematics and Mechanics*, **4**(4), (2012), pp. 422–438. DOI: 10.1017/S2070073300001727.
39. L. Kiss and G. Szeidl. “Vibrations of pinned–pinned heterogeneous circular beams subjected to a radial force at the crown point.” *Mechanics Based Design of Structures and Machines: An International Journal*, **43**(4), (2015), pp. 424–449. DOI: 10.1080/15397734.2015.1022659.
40. G. Szeidl and L. Kiss. *Theory of Vibrations, an Introduction*. Series: Foundations of Engineering Mechanics, Series Editor: Vladimir I. Babitsky. Switzerland: Springer Nature, 2020. DOI: 10.1007/978-3-030-45074-8.
41. Sahmani S. and Aghdam M. M. “Size-Dependent Nonlinear Mechanics of Biological Nanoporous Microbeams.” *Nanomaterials for Advanced Biological Applications*. Ed. by Rahmandoust M. and Ayatollahi M. Vol. 104. Advanced Structured Materials. Springer, 2019. DOI: 10.1007/978-3-030-10834-2\_7.

## DEFORMATION OF CANTILEVER CURVED BEAM WITH VARIABLE CROSS SECTION

I. ECSEDI, A. BAKSA

University of Miskolc, Institute of Applied Mechanics, Hungary

`istvan.ecsedi@uni-miskolc.hu` `attila.baksa@uni-miskolc.hu`

[Received: October 31, 2020; Accepted: January 15, 2021]

*Dedicated to Professor Barna Szabó on the occasion of his eighty-fifth birthday*

**Abstract.** This paper deals with the determination of the displacements and stresses in a curved cantilever beam. The considered curved beam has circular centerline and the thickness of its cross section depends on the circumferential coordinate. The kinematics of Euler-Bernoulli beam theory are used. The curved elastic beam is fixed at one end and on the other end is subjected to concentrated moment and force; three different loading cases are considered. The paper gives analytical solutions for radial and circumferential displacements and cross-sectional rotation and circumferential stresses. The presented examples can be used as benchmark for the other types of solutions as given in this paper.

*Mathematical Subject Classification:* 74K10, 74B05

*Keywords:* curved beam, cantilever, variable cross section

### 1. INTRODUCTION

The analysis of curved beam has been a topic of interest to researchers for over a century, it is a standard topic in the most text books of mechanics [1–3]. This theme is still relevant at the present time because curved elements are important components in many modern engineering structures. In this paper an analytical solution is presented for cantilever curved beams with variable cross sections. One of the ends of a curved beam is fixed and the other end is subjected to radial and circumferential forces and a couple. Elasticity solutions are presented in [4] for curved beams with orthotropic functionally graded layers by means of Airy stress functions. The developed method is illustrated in curved cantilever beams with different types of loading conditions. Pydah and Sabele [5] present an analytical model for the flexure of bidirectional functionally graded circular beam. The formulation of the considered problem is based on the Euler-Bernoulli beam theory. The governing equations are solved for statically determinate circular cantilever beams under the action of tip loads. Paper [6] deals with the determination of stress in circular curved beams with cross-sectional inhomogeneity. In Ecsedi and Lengyel [7] an analytical solution is presented for the determination of deformation of curved composite beams with uniform cross sections. The developed analytical solution is based on fundamental

solutions which are filling to the given loading and boundary conditions. Closed form formulae are derived for the displacements, cross-sectional rotation normal and shear forces and bending moment. Paper [7] gives the expressions of circumferential and normal stresses and of shearing stress. Several studies give finite element numerical solutions to the in-plane deformation static problems of curved beams with uniform curvature such as [8–10].

## 2. GOVERNING EQUATIONS

In the cylindrical coordinate system  $Or\varphi z$  the curved beam of variable cross section occupies the space domain (Figure 1)

$$B = \left\{ (r, \varphi, z) \mid R_1 \leq r \leq R_2, |z| \leq \frac{t(\varphi)}{2}, 0 < \varphi < \alpha < 2\pi \right\}, \quad (2.1)$$

where  $R_i$  ( $i = 1, 2$ ) is the radius of inner and outer cylindrical boundary surface of body  $B$ ,  $t = t(\varphi)$  is the cross-sectional thickness in direction of axis  $z$ . The radius of the circular centerline of curved beam is

$$r_c = \frac{1}{2}(R_1 + R_2). \quad (2.2)$$

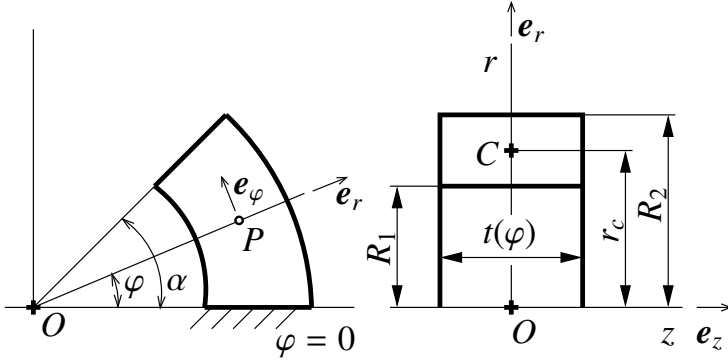


Figure 1. Cantilever curved beam and its cross section

The plane  $z = 0$  is the plane of symmetry of the curved beam and of the applied loads. Denote the unit vectors of cylindrical coordinate system  $Or\varphi z$   $e_r$ ,  $e_\varphi$  and  $e_z$ . We start from the next displacement field to describe the in-plane deformation of cantilever curved beam [11]

$$\mathbf{u} = u\mathbf{e}_r + v\mathbf{e}_\varphi + w\mathbf{e}_z, \quad (2.3)$$

$$u = U(\varphi), \quad v = r\phi(\varphi) + V(\varphi), \quad V(\varphi) = \frac{dU}{d\varphi}, \quad w = 0. \quad (2.4)$$

Application of the strain-displacement relationships of the linearized theory of elasticity gives [12, 13]

$$\varepsilon_r = \frac{\partial u}{\partial r} = 0, \quad \varepsilon_z = \frac{\partial w}{\partial z} = 0, \quad \gamma_{r\varphi} = \frac{1}{r} \left( \frac{\partial u}{\partial \varphi} - v \right) = 0, \quad \gamma_{\varphi z} = \frac{\partial v}{\partial z} + \frac{1}{r} \frac{\partial w}{\partial \varphi} = 0, \quad (2.5)$$

$$\gamma_{rz} = \frac{\partial u}{\partial z} + \frac{\partial w}{\partial r} = 0, \quad \varepsilon_\varphi = \frac{W(\varphi)}{r} + \frac{d\phi}{d\varphi}, \quad W(\varphi) = \frac{d^2 U}{d\varphi^2} + U. \quad (2.6)$$

The strain field given by equations (2.5), (2.6) satisfy the requirements of the Bernoulli-Euler beam theory, only the normal strain  $\varepsilon_\varphi$  is different from zero and all the other strains vanish. Based on paper [11] we define the stress resultant forces  $N = N(\varphi)$ ,  $S = S(\varphi)$  and stress couple resultant  $M = M(\varphi)$  as

$$N(\varphi) = \int_{A(\varphi)} \sigma_\varphi dA, \quad S(\varphi) = \int_{A(\varphi)} \tau_{r\varphi} dA, \quad M(\varphi) = \int_{A(\varphi)} r \sigma_\varphi d(A), \quad (2.7)$$

where  $\tau_{r\varphi} = \tau_{r\varphi}(r, \varphi)$  denotes the shearing stress. Here, we note, the shear force  $S = S(\varphi)$  will be computed by the use of equilibrium equation which is the usual in the case of Euler-Bernoulli beam theory. Figure 2 illustrates the stress and stress couple resultants in an arbitrary cross section of curved beam. Application of Hooke's law yields the formula of normal stresses  $\sigma_\varphi$  [13]

$$\sigma_\varphi = E \left( \frac{W(\varphi)}{r} + \frac{d\phi}{d\varphi} \right), \quad (2.8)$$

where  $E$  is the modulus of elasticity. From equations (2.7) it follows that

$$N(\varphi) = EA(\varphi) \left( \frac{W(\varphi)}{R} + \frac{d\phi}{d\varphi} \right), \quad (2.9)$$

$$M(\varphi) = EA(\varphi) \left( W(\varphi) + r_c \frac{d\phi}{d\varphi} \right). \quad (2.10)$$

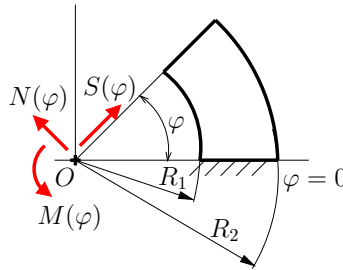


Figure 2. Illustration of  $N(\varphi)$ ,  $S(\varphi)$  and  $M(\varphi)$

In equations (2.9), (2.10)  $A = t(\varphi)(R_2 - R_1)$  is the area of the cross section,  $r_c = \frac{1}{2}(R_1 + R_2)$  is the radial coordinate of the center of cross section (Figure 1) and

$$R = \frac{R_2 - R_1}{\ln \frac{R_2}{R_1}}. \quad (2.11)$$

The equilibrium equations in terms of  $N$ ,  $S$  and  $M$  for curved cantilever beam which is loaded its end cross sections are [7, 11]

$$\frac{dN}{ds} + S = 0, \quad \frac{dS}{d\varphi} - N = 0, \quad \frac{dM}{d\varphi} = 0. \quad (2.12)$$

We remark that the considered cantilever curved beams satisfy the boundary conditions

$$U(0) = 0, \quad V(0) = 0, \quad \phi(0) = 0. \quad (2.13)$$

### 3. CANTILEVER CURVED BEAM LOADED BY BENDING MOMENT

Figure 3 shows the cantilever curved beam, which is loaded at its end cross section  $\varphi = \alpha$  by a bending moment  $M_1$ . From equilibrium equations (2.12) we have

$$N(\varphi) = S(\varphi) = 0, \quad M(\varphi) = M_1 = \text{constant}, \quad \varphi_1 \leq \varphi \leq \varphi_2. \quad (3.1)$$

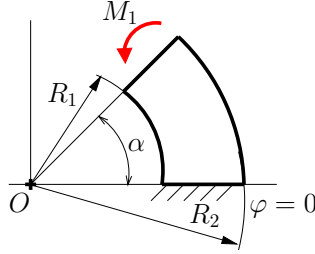


Figure 3. Cantilever curved beam with bending moment

Combination of equations (2.9) and (2.10) with equation (3.1) gives

$$W_1(\varphi) + R \frac{d\phi_1}{d\varphi} = 0, \quad (3.2)$$

$$W_1(\varphi) + r_c \frac{d\phi_1}{d\varphi} = \frac{M_1}{EA(\varphi)}. \quad (3.3)$$

The solution of the system of equations (3.2), (3.3) for  $W_1(\varphi)$  and  $\frac{d\phi_1}{d\varphi}$  is as follows:

$$W_1(\varphi) = -\frac{M_1}{eEA(\varphi)}, \quad \frac{d\phi_1}{d\varphi} = \frac{M_1}{eEA(\varphi)}, \quad e = r_c - R. \quad (3.4)$$

In the present problem

$$W_1(\varphi) = \frac{d^2U_1}{d\varphi^2} + U_1. \quad (3.5)$$

Here, we will use the result of the theory of ordinary differential equations [14, 15]:

**Theorem 1:** Let  $h = h(x)$  be a continuous bounded function defined for  $x \in [0, a > 0]$ . In this case the solution of the initial value problem

$$\frac{d^2y}{dx^2} + y = h(x), \quad 0 \leq x \leq a, \quad y(0) = 0, \quad \left. \frac{dy}{dx} \right|_{x=0} = 0, \quad (3.6)$$

can be represented as

$$y(x) = \int_0^x h(\lambda) \sin(x - \lambda) d\lambda, \quad (3.7)$$

and we have

$$\frac{dy}{dx} = \int_0^x h(\lambda) \cos(x - \lambda) d\lambda. \quad (3.8)$$

The application of Theorem 1 gives the next formulae for  $U_1 = U_1(\varphi)$  and  $V_1 = V_1(\varphi)$

$$U_1(\varphi) = -\frac{M_1 R}{e(R_2 - R_1)E} \int_0^\varphi \frac{\sin(\varphi - \vartheta)}{t(\vartheta)} d\vartheta, \quad (3.9)$$

$$V_1 = \frac{dU_1}{d\varphi} = -\frac{MR}{e(R_2 - R_1)E} \int_0^\varphi \frac{\cos(\varphi - \vartheta)}{t(\vartheta)} d\vartheta. \quad (3.10)$$

A direct integration of equation (3.4) yields the result

$$\phi_1(\varphi) = \frac{M_1}{e(R_2 - R_1)E} \int_0^\varphi \frac{d\vartheta}{t(\vartheta)}. \quad (3.11)$$

By the use of formula (2.8) we get the expression of circumferential normal stress

$$\sigma_\varphi = \frac{M_1}{e(R_2 - R_1)} \frac{r - R}{rt(\varphi)}. \quad (3.12)$$

The circumferential normal stress  $\sigma_\varphi$  is zero in all cross sections at the radial coordinate  $r = R$ .

#### 4. CANTILEVER CURVED BEAM LOADED BY RADIAL FORCE

The cantilever curved beam which is loaded at its end cross section  $\varphi = \alpha$  by a radial force  $F_2$  is shown in Figure 4. From equilibrium equations in this case we have

$$N(\varphi) = -F \sin(\varphi - \alpha), \quad S(\varphi) = F \cos(\varphi - \alpha), \quad M(\varphi) = 0, \quad 0 \leq \varphi \leq \alpha. \quad (4.1)$$

In the present problem the application of equations 2.9 and (2.10) gives

$$W_2(\varphi) + R \frac{d\phi_2}{d\varphi} = -\frac{F_2 R}{EA(\varphi)} \sin(\varphi - \alpha), \quad (4.2)$$

$$W_2(\varphi) + r_c \frac{d\phi_2}{d\varphi} = 0. \quad (4.3)$$

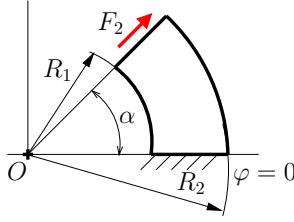


Figure 4. Cantilever curved beam subjected by radial force

Solution of the system of equations for  $W_2 = W_2(\varphi)$  and  $\frac{d\phi_2}{d\varphi}$  is as follows

$$W_2(\varphi) = -\frac{F_2 R r_2}{EA(\varphi)e} \sin(\varphi - \alpha), \quad \frac{d\phi_2}{d\varphi} = \frac{F_2 R}{EA(\varphi)e} \sin(\varphi - \alpha). \quad (4.4)$$

Substitution of the expression  $W_2 = W_2(\varphi)$  into equation (3.6) gives the formula of radial displacement function  $U_2 = U_2(\varphi)$

$$U_2(\varphi) = -\frac{F_2 R r_c}{e(R_2 - R_1)E} \int_0^\varphi \sin(\varphi - \alpha) \frac{\sin(\vartheta - \alpha)}{t(\vartheta)} d\vartheta. \quad (4.5)$$

A simple computation based on equation (4.5) yields the result

$$V_2(\varphi) = \frac{dU_2}{d\varphi} = -\frac{F_2 R r_c}{e(R_2 - R_1)E} \int_0^\varphi \cos(\varphi - \alpha) \frac{\sin(\vartheta - \alpha)}{t(\vartheta)} d\vartheta. \quad (4.6)$$

From equation (4.4) it follows that

$$\phi_2(\varphi) = \frac{F_2 R}{E(R_2 - R_1)e} \int_0^\varphi \frac{\sin(\vartheta - \alpha)}{t(\vartheta)} d\vartheta. \quad (4.7)$$

In the present case we obtain for the circumferential normal stress the formula

$$\sigma_\varphi = \frac{F_2 R}{(R_2 - R_1)e} \frac{r - r_c}{r} \frac{\sin(\varphi - \alpha)}{t(\varphi)}. \quad (4.8)$$

The circumferential normal stress  $\sigma_\varphi$  is zero in all cross sections at the radial coordinate  $r = r_c$ .

## 5. CANTILEVER CURVED BEAM LOADED BY NORMAL FORCE

The curved beam which is fixed at one end and loaded by normal force  $F_3$  at the other end is shown in Figure 5. In this case the solutions of equilibrium equations are as follows:

$$N(\varphi) = F_3 \cos(\varphi - \alpha), \quad S(\varphi) = -F_3 \sin(\varphi - \alpha), \quad M(\varphi) = 0, \quad 0 \leq \varphi \leq \alpha. \quad (5.1)$$

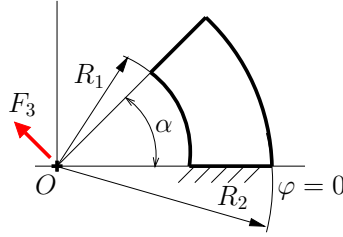


Figure 5. Cantilever curved beam loaded by normal force

In the present problem equations (2.9) and (2.10) lead to the system of equations for  $W_3 = W_3(\varphi)$  and  $\frac{d\phi_3}{d\varphi}$

$$W_3(\varphi) + R \frac{d\phi_3}{d\varphi} = \frac{F_3 R}{EA} \cos(\varphi - \alpha), \quad (5.2)$$

$$W_3(\varphi) + r_c \frac{d\phi_3}{d\varphi} = 0. \quad (5.3)$$

A simple computation gives

$$W_3(\varphi) = \frac{F_3 R r_c}{EeA(\varphi)} \cos(\varphi - \alpha), \quad \frac{d\phi_3}{d\varphi} = -\frac{F_3 R}{EeA(\varphi)} \cos(\varphi - \alpha). \quad (5.4)$$

Application of *Theorem 1* yields the expression of radial displacement  $U_3 = U_3(\varphi)$

$$U_3(\varphi) = \frac{F_3 R r_c}{Ee(R_2 - R_1)} \int_0^\varphi \frac{\cos \vartheta - \alpha}{t(\vartheta)} \sin(\varphi - \vartheta) d\vartheta. \quad (5.5)$$

The circumferential displacement  $V_3 = V_3(\varphi)$  is

$$V_3(\varphi) = \frac{dU_3}{d\varphi} = \frac{F_3 R}{Ee(R_2 - R_1)} \int_0^\varphi \frac{\cos(\vartheta - \alpha)}{t(\vartheta)} \cos(\varphi - \vartheta) d\vartheta. \quad (5.6)$$

Integration of equation (5.4<sub>2</sub>) gives the cross-sectional rotation function  $\phi_3 = \phi_3(\varphi)$

$$\phi_3(\varphi) = -\frac{F_3 R}{Ee(R_2 - R_1)} \int_0^\varphi \frac{\cos(\vartheta - \alpha)}{t(\vartheta)} d\vartheta. \quad (5.7)$$

From equation (2.8) we obtain the formula of the circumferential normal stress  $\sigma_\varphi$  as

$$\sigma_\varphi = \frac{F_3 R}{e(R_2 - R_1)} \frac{r_c - r \cos(\varphi - \alpha)}{r t(\varphi)}. \quad (5.8)$$

Here, we note that the circumferential normal stress  $\sigma_\varphi$  is zero in all cross sections at the radial coordinate  $r = r_c$ .

## 6. BETTI'S THEOREM FOR CANTILEVER CURVED BEAM

Let us consider two different equilibrium states of cantilever curved beam with end loads. The applied loads for the first equilibrium state are  $M'_1$ ,  $F'_2$  and  $F'_3$  which cause the displacements  $\tilde{U}(\varphi)$ ,  $\tilde{V}(\varphi)$  and  $\tilde{\phi}(\varphi)$ . The applied loads for the second equilibrium state are  $M''_1$ ,  $F''_2$  and  $F''_3$  and the corresponding displacements to the end cross sectional loads  $M''_1$ ,  $F''_2$  and  $F''_3$  are  $\overset{*}{U}(\varphi)$ ,  $\overset{*}{V}(\varphi)$  and  $\overset{*}{\phi}(\varphi)$ . A simple computation shows that the work done by system of forces on the displacement field  $\overset{*}{U}(\varphi)$ ,  $\overset{*}{V}(\varphi)$  and  $\overset{*}{\phi}(\varphi)$  is as follows

$$w_{12} = \int_A \sigma'_\varphi (r\phi^* + V^*) \Big|_{\varphi=\alpha} dA + \int_A \tau'_{r\varphi} U^* \Big|_{\varphi=\alpha} dA = M'_1 \phi^*(\alpha) + F'_3 V^*(\alpha) + F'_2 U^*(\alpha). \quad (6.1)$$

It is evident the work done by system of forces  $M''_1$ ,  $F''_2$  and  $F''_3$  on the displacement field  $\tilde{U}(\varphi)$ ,  $\tilde{V}(\varphi)$  and  $\tilde{\phi}(\varphi)$  is obtained from the equation

$$w_{21} = M''_1 \tilde{\phi}(\alpha) + F''_3 \tilde{V}(\alpha) + F''_2 \tilde{U}(\alpha). \quad (6.2)$$

According to Betti's theorem [12, 13] we have

$$w_{12} = w_{21}. \quad (6.3)$$

We will use Betti's theorem for the following three equilibrium states

$$M'_1 = M_1, \quad F'_2 = F'_3 = 0, \quad \tilde{U}(\varphi) = U_1(\varphi), \quad \tilde{V}(\varphi) = V_1(\varphi), \quad \tilde{\phi}(\varphi) = \phi_1(\varphi);$$

$$M''_1 = 0, \quad F''_2 = F_2, \quad F''_3 = 0, \quad \overset{*}{U}(\varphi) = U_2(\varphi), \quad \overset{*}{V}(\varphi) = V_2(\varphi), \quad \overset{*}{\phi} = \phi_2(\varphi).$$

We remark that the third equilibrium state is defined as

$$M'''_1 = 0, \quad F'''_2 = 0, \quad F'''_3 = F_2, \quad \hat{U}(\varphi) = U_3(\varphi), \quad \hat{V}(\varphi) = V_3(\varphi), \quad \hat{\phi} = \phi_3(\varphi).$$

For these equilibrium states the following equations must be valid according to Betti's theorem:

$$w_{12} = w_{21}, \quad w_{13} = w_{31}, \quad w_{23} = w_{32}. \quad (6.4)$$

In the present problems we have

$$w_{12} = M_1 \phi_2(\alpha) = \frac{M_1 F_2 R}{E(R_2 - R_1)e} \int_0^\alpha \frac{\sin(\vartheta - \alpha)}{t(\vartheta)} d\vartheta, \quad (6.5)$$

$$w_{21} = F_2 U_1(\alpha) = -\frac{F_2 M_1 R}{E(R_2 - R_1)e} \int_0^\alpha \frac{\sin(\alpha - \vartheta)}{t(\vartheta)} d\vartheta, \quad (6.6)$$

$$w_{13} = M_1 \phi_3(\alpha) = -\frac{M_1 F_3 R}{E(R_2 - R_1)e} \int_0^\alpha \frac{\cos(\vartheta - \alpha)}{t(\vartheta)} d\vartheta, \quad (6.7)$$

$$w_{31} = F_3 V_1(\alpha) = -\frac{M_1 F_3 R}{E(R_2 - R_1)e} \int_0^\alpha \frac{\cos(\alpha - \vartheta)}{t(\vartheta)} d\vartheta, \quad (6.8)$$

$$\begin{aligned}
 w_{23} &= F_2 U_3(\alpha) = \\
 &= \frac{F_2 F_3 R r_c}{E(R_2 - R_1)e} \int_0^\alpha \frac{\cos(\vartheta - \alpha)}{t(\vartheta)} \sin(\alpha - \vartheta) d\vartheta, \quad (6.9)
 \end{aligned}$$

$$\begin{aligned}
 w_{32} &= F_3 V_2(\alpha) = \\
 &= -\frac{F_2 F_3 R r_c}{E(R_2 - R_1)e} \int_0^\alpha \frac{\cos(\alpha - \vartheta)}{t(\vartheta)} \sin(\vartheta - \alpha) d\vartheta. \quad (6.10)
 \end{aligned}$$

The validity of equations (6.4)<sub>1,2,3</sub> follows from equations (6.5-6.10).

## 7. NUMERICAL EXAMPLES

The following data are used in the numerical example:  $E = 2 \times 10^5$  MPa,  $R_1 = 0.015$  m,  $R_2 = 0.025$  m,  $t_0 = 0.015$  m,  $\alpha = \frac{\pi}{3}$ ,  $t(\varphi) = t_0 \cos \varphi$ .

**7.1. Example 1.** (see Figure 3)  $M_1 = 50$  Nm,  $F_2 = F_3 = 0$  The graphs of the radial displacement  $U_1 = U_1(\varphi)$  and circumferential displacement  $V_1 = V_1(\varphi)$  are shown in Figure 6 and the cross sectional rotation  $\phi_1 = \phi_1(\varphi)$  is presented in Figure 7. The plots of  $\sigma_\varphi(r, \varphi)$  for four different values of polar angle  $\varphi$  ( $\varphi = 0$ ,  $\varphi = \frac{\pi}{6}$ ,  $\varphi = \frac{\pi}{4}$ ,  $\varphi = \frac{\pi}{3}$ ) are shown in Figure 8.

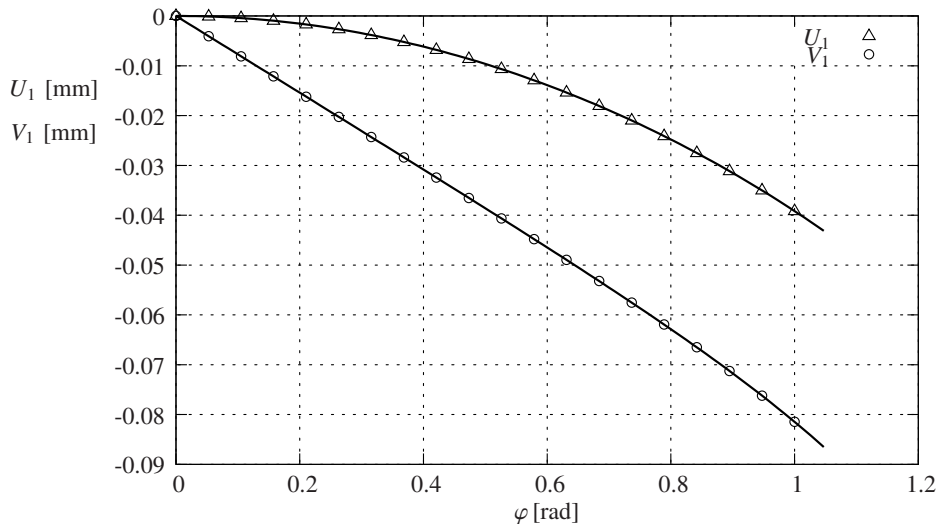
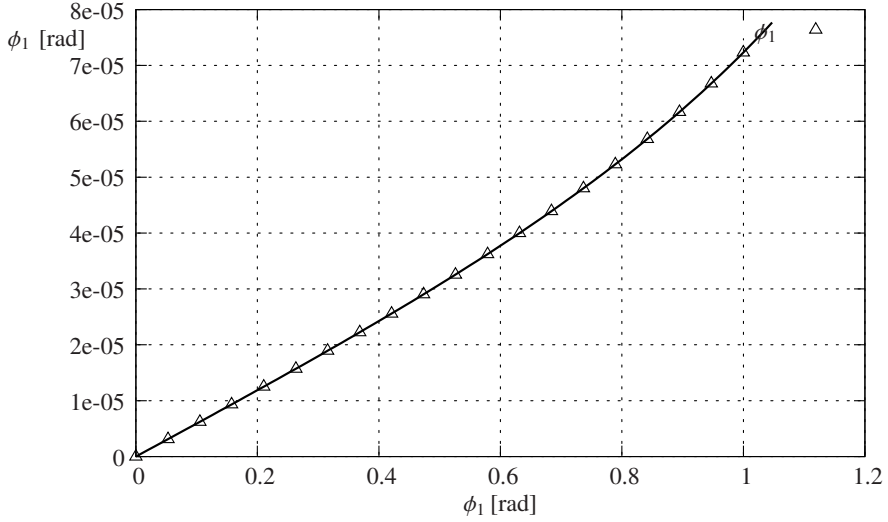
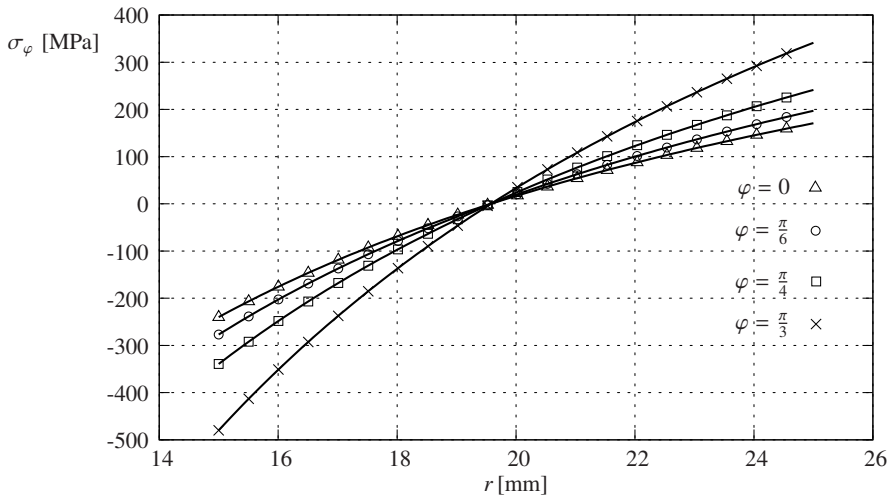


Figure 6. Plots of  $U_1$  and  $V_1$

Figure 7. Plot of  $\phi_1$ Figure 8. The plots of  $\sigma_\varphi$  (Example 1)

**7.2. Example 2.** (see Figure 4)  $F_2 = 1400\text{ N}$ ,  $M_1 = 0$ ,  $F_3 = 0$ . The graphs of radial displacement  $U_2 = U_2(\varphi)$  and circumferential displacement  $V_2 = V_2(\varphi)$  are given in Figure 9. The plots of cross-sectional rotation  $\phi_2 = \phi_2(\varphi)$  is shown in Figure 10. The plots of the circumferential stress  $\sigma_\varphi(r, \varphi)$  for four different values of polar angle  $\varphi$  ( $\varphi = 0$ ,  $\varphi = \frac{\pi}{6}$ ,  $\varphi = \frac{\pi}{4}$ ,  $\varphi = \frac{\pi}{3}$ ) are shown in Figure 11.

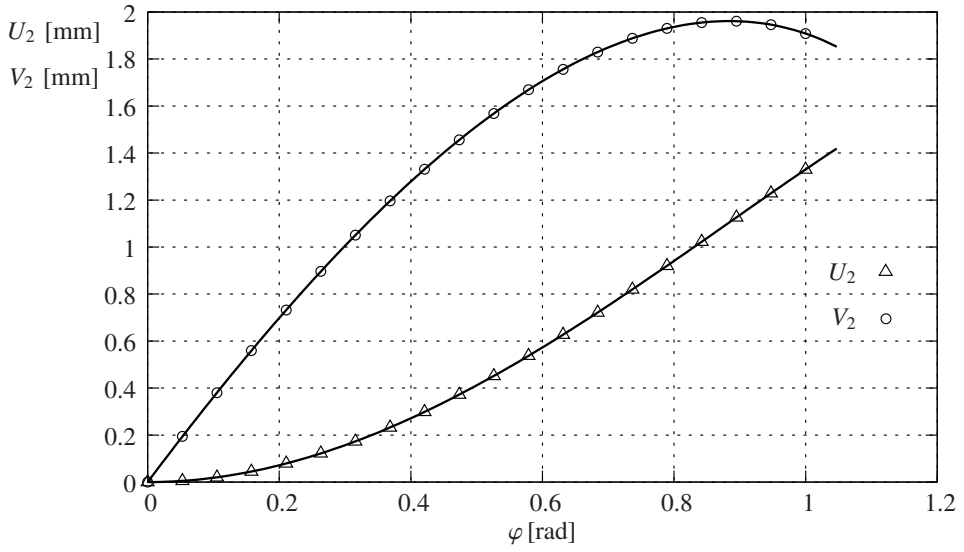


Figure 9. Plots of  $U_2$  and  $V_2$

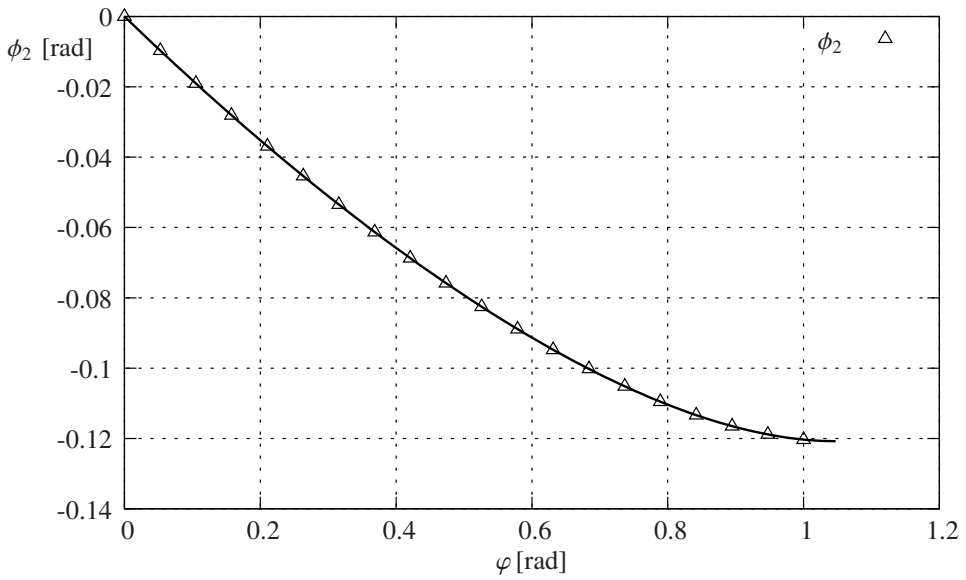
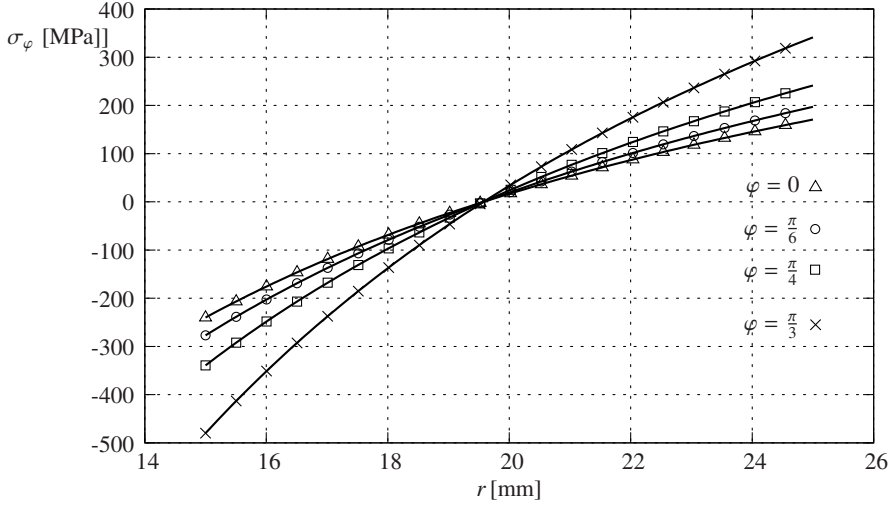
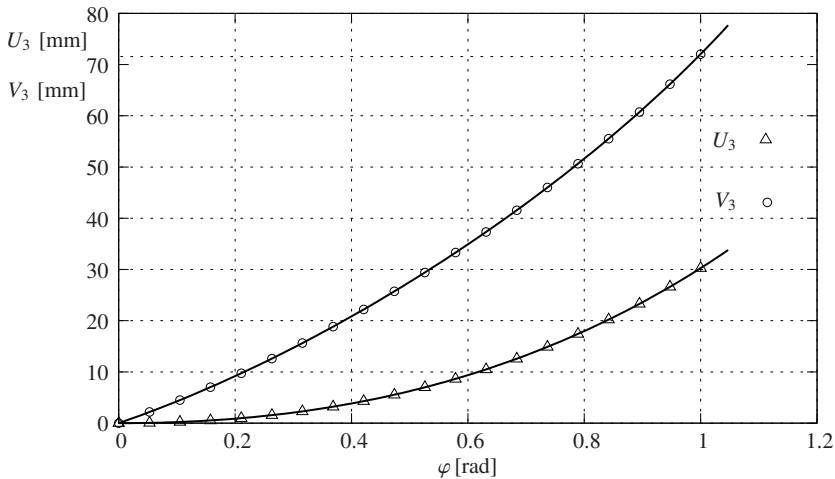
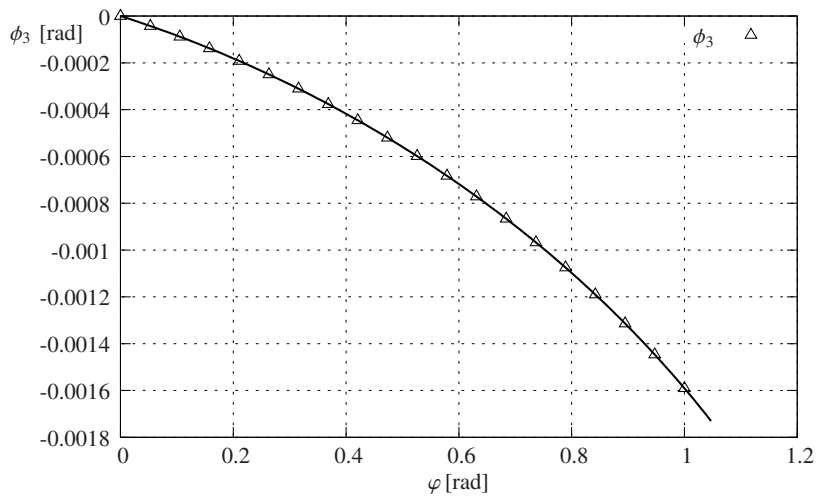
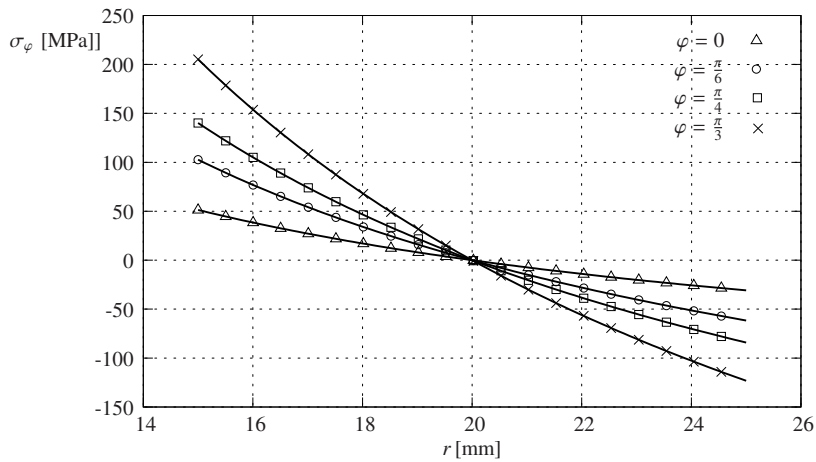


Figure 10. Plot of  $\phi_2$

Figure 11. Plots of  $\sigma_\varphi$ 

**7.3. Example 3.** (see Figure 5)  $F_3 = 1000 \text{ N}$ ,  $M_1 = 0$ ,  $F_2 = 0$ . In this case the plots of radial displacement  $U_3 = U_3(\varphi)$ , and circumferential displacement  $V_3 = V_3(\varphi)$  are given in Figure 12. The graph of  $\phi_3 = \phi_3(\varphi)$  is presented in Figure 13. The plots of circumferential stress  $\sigma_\varphi(r, \varphi)$  for four different values of the polar angle  $\varphi$  ( $\varphi = 0$ ,  $\varphi = \frac{\pi}{6}$ ,  $\varphi = \frac{\pi}{4}$ ,  $\varphi = \frac{\pi}{3}$ ) are shown in Figure 14.

Figure 12. Plots of  $U_3$  and  $V_3$ .

Figure 13. Plot of  $\phi_3$ Figure 14. Plots of  $\sigma_\phi$ 

## 8. CONCLUSIONS

In this paper an elastic cantilever curved beam of variable cross section is studied. At one end of the beam its cross section is fixed and at the other end it is loaded by concentrated forces and couples. Three different loading cases are considered. The paper presents an analytical solution to obtain the radial and circumferential displacements, cross sectional rotation and circumferential normal stress. Formulation of the considered equilibrium problems is based on the Euler-Bernoulli beam theory.

The validity of the obtained result is supported by Betti's theorem. Three numerical examples illustrate the application of the developed analytical solutions.

**Acknowledgement.** The present research was partially supported by the Hungarian Academy of Sciences, by grant NKFIH 115701.

#### REFERENCES

1. A. P. Boresi and R. J. Schmidt. *Advanced Mechanics of Materials*. Wiley and Sons, Inc., New York, 2003. DOI: 10.1111/j.1475-1305.1993.tb00852.x.
2. R. Solecki and R. J. Conant. *Advanced Mechanics of Materials*. Oxford University Press, Oxford, 2003.
3. R. D. Cook and W. C. Young. *Advanced Mechanics of Materials*. Macmillan, New York, 1985.
4. M. Wang and Y. Liu. "Elasticity solutions for orthotropic functionally graded curved beams." *European Journal of Mechanics-A/Solids*, **37**, (2013), pp. 8–13. DOI: 10.1016/j.euromechsol.2012.04.005.
5. A. Pydah and A. Sabela. "Static analysis of bidirectional functionally graded beams." *Composite Structures*, **160**, (2017), pp. 867–876. DOI: 10.116/compstruc.2016.10.120.
6. L. Kiss and Gy. Szeidl. "Stresses in curved beams made of heterogeneous materials." *International Journal of Mechanical Systems of Engineering*, **1**(2), (2015), p. 8 id. 107. DOI: 10.15344/2455-7412/2015/107.
7. I. Ecsedi and Á. J. Lengyel. "An analytical solution for static problems of curved composite beams." *Curved and Layered Structures*, **6**(1), (2019), pp. 105–116. DOI: 10.1515/c1s-2019-0009.
8. L. Ascione and F. Fraternali. "A penalty model for the analysis of curved composite beams." *Computers and Structures*, **45**(5-6), (1992), pp. 985–999. DOI: 10.1016/0045-7949(92)90057-7.
9. A. Ibrahimbegoric and F. Frey. "Finite element analysis on linear and non-linear planar deformation of elastic initially curved beams." *International Journal for Numerical Methods in Engineering*, **36**(9), (1993), pp. 3239–3528. DOI: 10.1002/nme.1620361903.
10. G. J. Kim. "An effective composite laminated curved beam element." *Communications in Numerical Methods in Engineering*, **22**(6), (2006), pp. 453–466. DOI: 10.002/cnm.829.
11. I. Ecsedi and K. Dluhi. "A linear model for the static and dynamic analysis of non-homogeneous curved beams." *Applied Mathematical Modelling* **29**(12), (2005), pp. 1211–1231. DOI: 10.1016/j.apm.2005.03.006.
12. I. S. Sokolnikoff. *Mathematical Theory of Elasticity*. McGraw-Hill, 1956. DOI: 10.2307/3608899.
13. A. D. Saade. *Elastic Theory and Applications*. Pergamon Press Inc., 1974. DOI: 10.1016/C2013-0-02524-8.
14. E. Kamke. "Differentialgleichungen. Lösungsmethoden and Lösungen I-II." Akademische Verlagsgesellschaft Gest and Portig K.-G. Leipzig, 1951.
15. A. R. Forsyth. *A Treatise on Differential Equations*. Macmillan, London, 1929.

## THE AVERAGE METHOD IS MUCH BETTER THAN AVERAGE

LÍVIA BODA AND ISTVÁN FARAGÓ

Department of Differential Equations, Budapest University of Technology and Economics,  
Műgytem rkp. 3., H-1111 Budapest, Hungary  
[faragois@gmail.com](mailto:faragois@gmail.com), [bodalivi@math.bme.hu](mailto:bodalivi@math.bme.hu)

TAMÁS KALMÁR-NAGY

Department of Fluid Mechanics, Budapest University of Technology and Economics,  
Műgytem rkp. 3., H-1111 Budapest, Hungary  
[kalmarnagy@ara.bme.hu](mailto:kalmarnagy@ara.bme.hu)

[Received: October 14, 2020; Accepted: November 21, 2020]

*Dedicated to Professor Barna Szabó on the occasion of his eighty-fifth birthday*

**Abstract.** Operator splitting is a powerful method for the numerical investigation of complex time-dependent models, where the stationary (elliptic) part consists of a sum of several structurally simpler sub-operators. As an alternative to the classical splitting methods, a new splitting scheme is proposed here, the Average Method with sequential splitting. In this method, a decomposition of the original problem is sought in terms of commuting matrices. We demonstrate that third-order accuracy can be achieved with the Average Method. The computational performance of the method is investigated, yielding run times 1-2 orders of magnitude faster than traditional methods.

*Mathematical Subject Classification:* 65L05, 76G25

*Keywords:* Operator splitting, Cauchy problem, numerical solution

### 1. INTRODUCTION

Operator splitting entails the decomposition (splitting) of the spatial differential operator of the problem into a sum of different sub-operators having simpler forms. Operator splitting methods are commonly used in many applications. The decomposition can be motivated mathematically (equations of different types, elliptic, parabolic, etc.) or by the presence of subsystems described by different areas of physics (coupled flow-structure or thermo-mechanical problems, for example).

McLahlan and Quispel [1] survey splitting methods for the numerical integration of ODE's. A nice exposition of splitting methods can be found in [2]. Different communities use different names for the same concept. Operator splitting is also called staggered methods (schemes), decomposition, co-simulation, etc. Gu and Asada [3] discuss the concept of co-simulation, which refers to simultaneous numerical solution

(discretization) of multiple interacting subsystem. A simple mathematical model for co-simulation is proposed in [4], together with the study of the resulting stability charts. Csomós and Nickel introduce splitting methods for delay equations in an abstract setting [5] and prove the convergence of the method.

The structure of this paper is the following. In Section 2 we discuss two basic splitting methods: sequential and Strang-Marchuk splitting. Then we introduce the Average Method in Section 3. In the same section we discuss the possible reduction of the terms needed for the Average Method by using a matrix decomposition of pairwise commuting matrices. In Section 4 we state a condition that makes the Average Method with sequential splitting third-order in accuracy. Here we also show that third-order accuracy cannot be achieved when basing the Average Method on Strang-Marchuk splitting. In Section 5 an example problem is given, motivated by an aerodynamic model. In Section 6 results of eight runtimes of the various methods. Section 7 summarizes the findings of this work.

## 2. SEQUENTIAL AND STRANG-MARCHUK SPLITTING

This section is based on [2]. We consider the following Cauchy problem in  $\mathbb{R}^m$

$$\begin{cases} \dot{y}(t) = Ay(t) = \sum_{i=1}^d A_i y(t) & t \in [0, T] \\ y(0) = y_0, \end{cases} \quad (1)$$

where  $y : [0, T] \rightarrow \mathbb{R}^m$  is the unknown function,  $y_0 \in \mathbb{R}^m$  is the given initial vector,  $A_i \in \mathbb{R}^{m \times m}$  ( $i = 1, \dots, d$ ) are matrices.

The exact solution of the Cauchy problem (1) can be written directly as

$$y(t) = \exp(tA)y(0). \quad (2)$$

Our aim is to approximate the exact solution (2) numerically on the grid

$$\omega_h = \{t_n = n \cdot h, h = \frac{T}{N}, n = 0, 1, \dots, N\}. \quad (3)$$

In *sequential splitting* we decompose the original problem (1) into  $d$  sub-problems ( $i = 1, 2, \dots, d$ )

$$\begin{cases} \dot{y}_i^n(t) = A_i y_i^n(t), & t \in ((n-1)h, nh], \\ y_i^n((n-1)h) = y_{i-1}^n(nh). \end{cases} \quad (4)$$

The solution is

$$y_{seq}^N(nh) = y_d^n(nh), \quad (5)$$

where  $y_0^n(nh) = y_{seq}^N((n-1)h)$ , and  $y_{seq}^N(0) = y(0) = y_0$ .

Sequential splitting is a first-order method.

The main difference between sequential and *Strang-Marchuk splitting* is that the latter computes the values in the midpoints of the subintervals. First

$$\begin{cases} \dot{y}_i^n(t) = A_i y_i^n(t), & t \in ((n-1)h, (n-\frac{1}{2})h], \\ y_i^n((n-1)h) = y_{i-1}^n((n-\frac{1}{2})h) \end{cases} \quad (6)$$

is computed for  $i = 1, 2, \dots, d - 1$ . For  $i = d$  the slightly different

$$\begin{cases} \dot{y}_d^n(t) = A_d y_d^n(t), & t \in ((n-1)h, nh], \\ y_d^n((n-1)h) = y_{d-1}^n((n-\frac{1}{2})h) \end{cases} \quad (7)$$

is evaluated. For  $i = d + 1, \dots, 2d - 1$  the following formula is used

$$\begin{cases} \dot{y}_i^n(t) = A_i y_i^n(t), & t \in ((n-\frac{1}{2})h, nh], \\ y_i^n((n-\frac{1}{2})h) = y_{i-1}^n(nh). \end{cases} \quad (8)$$

The solutions are given by

$$y_{SM}^N(nh) = y_{2d-1}^n(nh),$$

where  $y_0^n((n-\frac{1}{2})h) = y_{SM}^N((n-1)h)$  and  $y_{SM}^N(0) = y(0) = y_0$ .

The Strang-Marchuk method is a second-order method.

### 3. THE AVERAGE METHOD

A new method is introduced here (referred to as the Average Method) based on the following idea: dividing the Cauchy problem (1) into  $d$  subproblems, using sequential splitting in all possible sequences, calculating the numerical solutions and then taking their arithmetic mean and letting it be the numerical solution in  $\omega_h$ .

Let  $\mathcal{P}^n$  denote the set for the permutations of the indices  $\{1, 2, \dots, n\}$ . For  $p = \{p_1, p_2, \dots, p_n\} \in \mathcal{P}^n$  we introduce the notation

$$\exp\{p_1, p_2, \dots, p_n\} = \exp(hA_{p_1}) \exp(hA_{p_2}) \cdot \dots \cdot \exp(hA_{p_n}). \quad (9)$$

Solving the Cauchy-problem (1) using sequential splitting for all possible permutations and then averaging the resulting numerical solutions yields a second-order method, i.e.

**Statement 1.**

$$\exp(h(A_1 + \dots + A_d)) = \frac{1}{d!} \sum_{p \in \mathcal{P}^d} \exp\{p_1, p_2, \dots, p_n\} + \mathcal{O}(h^3). \quad (10)$$

See Appendix 1 for the proof.

Since  $\mathcal{P}^d$  has  $d!$  elements, we examine conditions that reduce the complexity of the Average Method. Consider the case of  $d = 3$ , i.e.  $A = A_1 + A_2 + A_3$ . By Statement 1 we have

$$\exp(h(A_1 + \dots + A_d)) = \frac{1}{3!} \sum_{p \in \mathcal{P}^3} \exp\{p_1, p_2, p_3\}, \quad (11)$$

with  $3! = 6$  terms on the right-hand side. We utilize the usual definition of the commutator  $[A, B] = AB - BA$ . If, for example,  $A_1$  and  $A_3$  commute, i.e.  $[A_1, A_3] = \mathbf{0}$ , then we have

$$\exp\{p_2, p_1, p_3\} = \exp\{p_2, p_3, p_1\}, \quad (12)$$

$$\exp\{p_1, p_3, p_2\} = \exp\{p_3, p_1, p_2\}, \quad (13)$$

and

$$\begin{aligned} \sum_{p \in \mathcal{P}^3} \exp\{p_1, p_2, p_3\} &= \\ &= \exp\{p_1, p_2, p_3\} + \exp\{p_3, p_2, p_1\} + 2 \exp\{p_2, p_1, p_3\} + 2 \exp\{p_1, p_3, p_2\}, \end{aligned} \quad (14)$$

where the number of terms was reduced from six to four.

Let us now consider the general case. Let  $A = A_1 + A_2 + \dots + A_d$ , and suppose that  $\exists i, j \in \mathbb{N}, i \neq j$  such that  $[A_i, A_j] = 0$ . Then instead of all the  $d!$  permutations, we have  $d! - (d-1)! = (d-1)(d-1)!$  elements. If the decomposition includes more commuting pairs of matrices, the reduction might be more significant. An interesting question is the decomposition of a given matrix into pairwise commuting matrices. Even the study of the pairs of  $n \times n$  commuting matrices  $A$  and  $B$  yields non-trivial results (i.e. Schur's theorem, Gerstenhaber's theorem, see, for example, Section 5 of [6]). The so-called commuting variety generated by the  $n^2$  equations  $(AB)_{ij} - (BA)_{ij} = 0$  can be investigated with the tools of algebraic geometry or linear algebraic conditions can be sought for commutativity. For  $k$  matrices one deals with commutative  $k$ -generated subalgebras, where even the best upper bound for their dimension is an open problem.

#### 4. MAKING THE AVERAGE METHOD THIRD-ORDER

Now we consider if third-order accuracy can be achieved with the Average Method based on sequential splitting. Assume that we have the Cauchy problem (1), with  $d = 2$ . We then have the following

**Statement 2.** *If and only if  $A = A_1 + A_2$ , and  $A_1$  and  $A_2$  satisfy the condition*

$$\begin{aligned} \left[ A_1, [A_1, A_2] \right] &= \left[ A_2, [A_1, A_2] \right] \text{ then} \\ \exp(h(A_1 + A_2)) &= \frac{\exp(hA_1) \exp(hA_2) + \exp(hA_2) \exp(hA_1)}{2} + \mathcal{O}(h^4). \end{aligned} \quad (15)$$

See Appendix 2 for the proof.

Now we consider the Strang-Marchuk splitting as the base method of average splitting. Can third-order accuracy be obtained by the Average Method?

The decomposition  $A = A_1 + A_2$  with weights  $\alpha$  and  $\beta$  ( $\alpha, \beta \neq 0$  and  $\alpha + \beta \neq 0$ ) has to satisfy

$$\begin{aligned} \exp(h(A_1 + A_2)) &= \\ &= \frac{\alpha \left( \exp\left(\frac{hA_1}{2}\right) \exp(hA_2) \exp\left(\frac{hA_1}{2}\right) \right) + \beta \left( \exp\left(\frac{hA_2}{2}\right) \exp(hA_1) \exp\left(\frac{hA_2}{2}\right) \right)}{\alpha + \beta} + \\ &\quad + \mathcal{O}(h^4). \end{aligned} \quad (16)$$

The right-hand side of equation (16) can be written as

$$\begin{aligned}
 & \frac{(\alpha + \beta)I + h(\alpha + \beta)(A_1 + A_2) + \frac{h^2}{2!}(\alpha + \beta)(A_1^2 + A_2^2 + A_1A_2 + A_2A_1)}{\alpha + \beta} + \\
 & + \frac{h^3}{3!} \left( \frac{(\alpha + \beta)(A_1^3 + A_2^3)}{\alpha + \beta} + \frac{(\frac{3}{4}\alpha + \frac{3}{2}\beta)A_1^2A_2 + (\frac{3}{4}\alpha + \frac{3}{2}\beta)A_2A_1^2 + (\frac{3}{2}\alpha + \frac{3}{4}\beta)A_2^2A_1}{\alpha + \beta} + \right. \\
 & \left. + \frac{(\frac{3}{2}\alpha + \frac{3}{4}\beta)A_1A_2^2 + \frac{3}{2}\alpha A_1A_2A_1 + \frac{3}{2}\beta A_2A_1A_2}{\alpha + \beta} \right) + O(h^4) = \\
 & = I + h(A_1 + A_2) + \frac{h^2}{2!}(A_1^2 + A_2^2 + A_1A_2 + A_2A_1) + \frac{h^3}{3!} \left( (A_1^3 + A_2^3) + \right. \\
 & + \frac{(\frac{3}{4}\alpha + \frac{3}{2}\beta)A_1^2A_2 + (\frac{3}{4}\alpha + \frac{3}{2}\beta)A_2A_1^2 + (\frac{3}{2}\alpha + \frac{3}{4}\beta)A_2^2A_1}{\alpha + \beta} + \\
 & \left. + \frac{(\frac{3}{2}\alpha + \frac{3}{4}\beta)A_1A_2^2 + \frac{3}{2}\alpha A_1A_2A_1 + \frac{3}{2}\beta A_2A_1A_2}{\alpha + \beta} \right) + O(h^4). \tag{17}
 \end{aligned}$$

The left-hand side of Equation (16) is

$$\begin{aligned}
 \exp(h(A_1 + A_2)) &= I + h(A_1 + A_2) + \frac{h^2}{2!}(A_1 + A_2)^2 + \frac{h^3}{3!}(A_1 + A_2)^3 + \mathcal{O}(h^4) = \\
 &= I + h(A_1 + A_2) + \frac{h^2}{2} \left( A_1^2 + A_2^2 + A_1A_2 + A_2A_1 \right) + \\
 &+ \frac{h^3}{6} \left( A_1^3 + A_2^3 + A_1A_2^2 + A_2A_1^2 + A_2A_1^2 + A_2^2A_1 + A_1A_2A_1 + A_2A_1A_2 \right) + \mathcal{O}(h^4). \tag{18}
 \end{aligned}$$

The equality (16) is only true under the conditions

$$\frac{\frac{3}{4}\alpha + \frac{3}{2}\beta}{\alpha + \beta} = 1, \tag{19}$$

$$\frac{\frac{3}{2}\alpha + \frac{3}{4}\beta}{\alpha + \beta} = 1, \tag{20}$$

$$\frac{\frac{3}{2}\alpha}{\alpha + \beta} = 1, \tag{21}$$

$$\frac{\frac{3}{2}\beta}{\alpha + \beta} = 1. \tag{22}$$

Equations (19) and (21) give the condition  $\alpha = 2\beta$ , while Equation (22) yields the condition  $\beta = 2\alpha$ . This implies  $\alpha = \beta = 0$ , which contradicts our assumption.

Third-order accuracy thus cannot be achieved with the Average Method based on Strang-Marchuk splitting.

## 5. EXAMPLE APPLICATION

As seen in Section 3, the number of terms needed for the Average Method can be reduced by decomposing the underlying matrix into a set of matrices that have commuting elements.

We now investigate the efficacy of the three splitting methods discussed above on a physical problem. The model was chosen because of the structure of the matrices involved, i.e. sparse matrices whose decomposition into a partially commuting set was easy.

A piecewise-linear model of flutter was investigated in [7] and [8]. The affine model equations contain the three system matrices ( $k = 0, 1, 2$ )

$$A_k = \begin{pmatrix} 0 & 1 & 0 & 0 \\ -1 & -(p_1 + p_2\mu c_k) & -\mu^2 c_k p_2 & 0 \\ 0 & 0 & 0 & 1 \\ 0 & c_k \mu & -(p_4 - c_k \mu^2) & -p_3 \end{pmatrix},$$

with the model parameters given in Table 1 (see [7]) and  $\mu \in (0, \infty)$  represents the nondimensional wind speed.

Table 1. Parameters of the model

Parameter	$c_0$	$c_1$	$c_2$	$d_1$	$d_2$	$p_1$	$p_2$	$p_3$	$p_4$
Value	5.932	-6.846	2.662	2.56	-0.2515	0.1485	0.0147	0.0540	0.2748

Motivated by this model, we consider the following 4-dimensional Cauchy problem

$$\begin{cases} \dot{\mathbf{x}}(t) = A_k \mathbf{x}(t), \\ \mathbf{x}(0) = \mathbf{x}_0. \end{cases} \quad (23)$$

**5.1. Decompositions of matrix  $A_k$ .** All three  $A_k$  matrices have the same structure, thus we can discuss the symbolic decompositions of  $A_k$ .

First, we analyze the decomposition

$$A_k = A_{k(1)} + A_{k(2)}, \quad (24)$$

where

$$A_{k(1)} = \begin{pmatrix} 0 & 1 & 0 & 0 \\ 0 & -(p_1 + p_2\mu c_k) & -\mu^2 c_k p_2 & 0 \\ 0 & 0 & 0 & 1 \\ 0 & 0 & 0 & -p_3 \end{pmatrix}, \quad A_{k(2)} = \begin{pmatrix} 0 & 0 & 0 & 0 \\ -1 & 0 & 0 & 0 \\ 0 & 0 & 0 & 0 \\ 0 & c_k \mu & -(p_4 - c_k \mu^2) & 0 \end{pmatrix}.$$

Clearly,  $A_{k(1)}$  is an upper triangular matrix. On the other hand,  $A_{k(2)}$  is a strictly lower triangular matrix and hence it is nilpotent. Therefore  $(A_{k(2)})^m = \mathbf{0}$  for  $m > 2$ . This means that the exponential of the matrix  $A_{k(2)}$  can be computed exactly. Thus, when we realize the splitting methods, the solution of the subproblem with this matrix can be calculated exactly. We can also define a decomposition in which the exponential of each matrix can be calculated exactly. For example, the decomposition

$$A_k = A_{k(1)} + A_{k(2)} + A_{k(3)}, \quad (25)$$

with

$$A_{k(1)} = \begin{pmatrix} 0 & 1 & 0 & 0 \\ 0 & 0 & -\mu^2 c_k p_2 & 0 \\ 0 & 0 & 0 & 1 \\ 0 & 0 & 0 & 0 \end{pmatrix}, \quad A_{k(2)} = \begin{pmatrix} 0 & 0 & 0 & 0 \\ 0 & -(p_1 + p_2 \mu c_k) & 0 & 0 \\ 0 & 0 & 0 & 0 \\ 0 & 0 & 0 & -p_3 \end{pmatrix},$$

$$A_{k(3)} = \begin{pmatrix} 0 & 0 & 0 & 0 \\ -1 & 0 & 0 & 0 \\ 0 & 0 & 0 & 0 \\ 0 & c_k \mu & -(p_4 - c_k \mu^2) & 0 \end{pmatrix}$$

has this property because it is the sum of two nilpotent matrices and a diagonal matrix.

Now we define three decompositions which consist of commuting matrices. First, we consider the decomposition:

$$A_k = A_{k(1)} + A_{k(2)} + A_{k(3)}, \quad (26)$$

where

$$A_{k(1)} = \begin{pmatrix} 0 & 1 & 0 & 0 \\ -1 & -(p_1 + p_2 \mu c_k) & 0 & 0 \\ 0 & 0 & 0 & 0 \\ 0 & 0 & 0 & 0 \end{pmatrix}, \quad A_{k(2)} = \begin{pmatrix} 0 & 0 & 0 & 0 \\ 0 & 0 & 0 & 0 \\ 0 & 0 & 0 & 1 \\ 0 & 0 & -(p_4 - c_k \mu^2) & -p_3 \end{pmatrix},$$

$$A_{k(3)} = \begin{pmatrix} 0 & 0 & 0 & 0 \\ 0 & 0 & -\mu^2 c_k p_2 & 0 \\ 0 & 0 & 0 & 0 \\ 0 & c_k \mu & 0 & 0 \end{pmatrix}.$$

$A_{k(3)}$  is a nilpotent matrix with  $(A_{k(3)})^m = \mathbf{0}$  for  $m > 2$ , hence its exponential can be given exactly. For the matrices  $A_{k(1)}$  and  $A_{k(2)}$   $A_{k(1)}A_{k(2)} = \mathbf{0}$  and  $A_{k(2)}A_{k(1)} = \mathbf{0}$ , so  $[A_{k(1)}, A_{k(2)}] = \mathbf{0}$ . On the one hand we win some advantage, due to the Statement 1, and on the other hand, this decomposition has a disadvantage, namely we lost the property of exact solvability.

In the following decomposition, the original matrix  $A_k$  is written as the sum of four matrices, two of them are commuting, and each has the property of exact solvability. The decomposition is the following:

$$A_k = A_{k(1)} + A_{k(2)} + A_{k(3)} + A_{k(4)}, \quad (27)$$

where

$$A_{k(1)} = \begin{pmatrix} 0 & 0 & 0 & 0 \\ 0 & -(p_1 + p_2 \mu c_k) & 0 & 0 \\ 0 & 0 & 0 & 0 \\ 0 & 0 & 0 & 0 \end{pmatrix}, \quad A_{k(2)} = \begin{pmatrix} 0 & 0 & 0 & 0 \\ 0 & 0 & 0 & 0 \\ 0 & 0 & 0 & 0 \\ 0 & 0 & 0 & -p_3 \end{pmatrix},$$

$$A_{k(3)} = \begin{pmatrix} 0 & 1 & 0 & 0 \\ 0 & 0 & -\mu^2 c_k p_2 & 0 \\ 0 & 0 & 0 & 1 \\ 0 & 0 & 0 & 0 \end{pmatrix}, \quad A_{k(4)} = \begin{pmatrix} 0 & 0 & 0 & 0 \\ -1 & 0 & 0 & 0 \\ 0 & 0 & 0 & 0 \\ 0 & c_k \mu & -(p_4 - c_k \mu^2) & 0 \end{pmatrix}.$$

$A_{k(1)}$  and  $A_{k(2)}$  are diagonal matrices (so they commute), therefore in both cases we can solve the subproblems exactly. Further, matrices  $A_{k(3)}$  and  $A_{k(4)}$  are nilpotent, so we can produce the exact solutions of the subproblems.

The last decomposition is the following:

$$A_k = A_{k(1)} + A_{k(2)} + A_{k(3)} + A_{k(4)}, \quad (28)$$

where

$$A_{k(1)} = \begin{pmatrix} 0 & 1 & 0 & 0 \\ -1 & 0 & 0 & 0 \\ 0 & 0 & 0 & 0 \\ 0 & 0 & 0 & 0 \end{pmatrix}, \quad A_{k(2)} = \begin{pmatrix} 0 & 0 & 0 & 0 \\ 0 & 0 & 0 & 0 \\ 0 & 0 & 0 & 1 \\ 0 & 0 & -(p_4 - c_k \mu^2) & 0 \end{pmatrix},$$

$$A_{k(3)} = \begin{pmatrix} 0 & 0 & 0 & 0 \\ 0 & -(p_1 + p_2 \mu c_k) & 0 & 0 \\ 0 & 0 & 0 & 0 \\ 0 & 0 & 0 & -p_3 \end{pmatrix}, \quad A_{k(4)} = \begin{pmatrix} 0 & 0 & 0 & 0 \\ 0 & 0 & -\mu^2 c_k p_2 & 0 \\ 0 & 0 & 0 & 0 \\ 0 & c_k \mu & 0 & 0 \end{pmatrix}.$$

In this set matrices  $A_{k(1)}$  and  $A_{k(2)}$  commute, and the exponential of  $A_{k(1)}$  can be computed exactly (it is actually a rotation matrix). Matrices  $A_{k(3)}$  and  $A_{k(4)}$  are nilpotent and diagonal matrices, already discussed in previous decompositions.

## 6. NUMERICAL EXPERIMENTS

For the numerical implementation of operator splitting, the question is the following: what kind of methods to use for computing the solutions of subproblems? Here we considered three possibilities.

The first and perhaps the most obvious choice is when at every step we solve the subproblems by a numerical method with the same order of accuracy as that of the splitting method. This means that for sequential splitting we have to use a first-order method, such as the explicit or implicit Euler method. For Strang-Marchuk splitting and the Average Method we have to use a second-order method, e.g. second-order Euler or trapezoidal method.

The solution of the subproblems can also be given by truncating the infinite exponential sequence at the order of the splitting method. Finally, we can produce exact solutions by using decompositions of matrix  $A_k$  to yield exactly solvable subproblems. We have already seen such decompositions in the previous section.

We performed the following eight experiments to solve the Cauchy problem (23):

- E1:** Sequential splitting with decomposition (24), solving the subproblems corresponding to  $A_{k(1)}$  and  $A_{k(2)}$  with explicit Euler method and exactly, respectively.
- E2:** Sequential splitting with decomposition (25), all subproblems solved exactly.
- E3:** Explicit Euler solution of the full problem (no splitting).
- E4:** Strang-Marchuk splitting with decomposition (24), solving the subproblems corresponding to  $A_{k(1)}$  and  $A_{k(2)}$  with improved Euler method and exactly, respectively.
- E5:** Strang-Marchuk splitting with decomposition (25), all subproblems solved exactly.
- E6:** Average Method with sequential splitting and decomposition (24), solving the subproblems corresponding to  $A_{k(1)}$  and  $A_{k(2)}$  with explicit Euler method and exactly, respectively.
- E7:** Average Method with sequential splitting and decomposition (26) all subproblems solved with explicit Euler method in parallel.
- E8:** Improved Euler solution of the full problem (no splitting).

We now detail the results of the above numerical experiments. The parameter value  $\mu = 0.2$  and the initial condition  $\mathbf{x}_0 = (1, 1, 1)$  was used in all computations.

- E1:** Figure 1 shows component  $x_3(t)$  of the solution on the time interval  $[0, 100]$ . The figure shows how the splitting solution (red line) approximates the exact solution (blue line) by reducing the step size  $h$ .

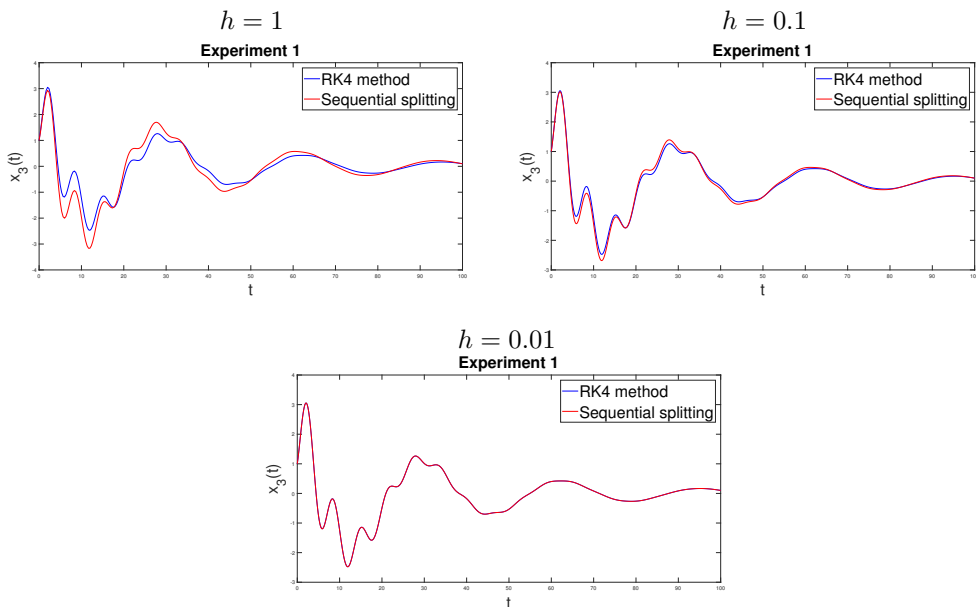


Figure 1. Experiment 1:  $x_3(t)$  on time interval  $[0, 100]$

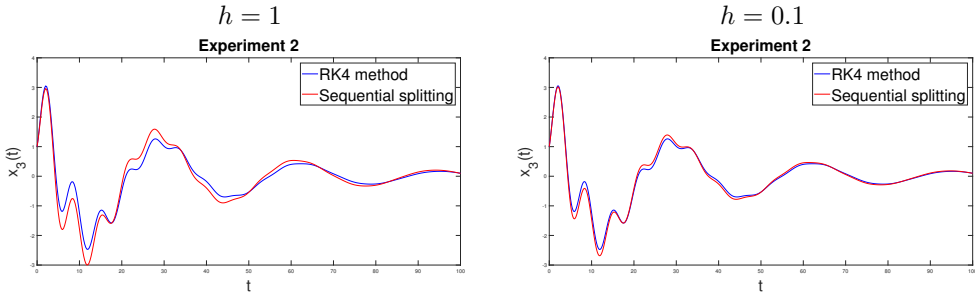


Figure 2. Experiment 2:  $x_3(t)$  on the time interval  $[0, 100]$

**E2:** In Figure 2 we see how the splitting solution approximates the exact solution by reducing the step size  $h$ . Figure 2 shows component  $x_3$  of the solution on the time interval  $[0, 100]$ . The first 3 experiments utilized first-order methods. Runtimes are shown in Table 2.

Table 2. Comparison of runtimes (in seconds) for E1-3

<b>h</b>	<b>1.</b>	<b>2.</b>	<b>3.</b>
1.0	$7.02 \times 10^{-5}$	$2.51 \times 10^{-5}$	$2.39 \times 10^{-3}$
0.1	$8.44 \times 10^{-4}$	$8.93 \times 10^{-4}$	$5.32 \times 10^{-3}$
0.01	$1.70 \times 10^{-3}$	$8.11 \times 10^{-3}$	$1.09 \times 10^{-2}$
0.001	$1.37 \times 10^{-2}$	$4.02 \times 10^{-2}$	$7.14 \times 10^{-1}$

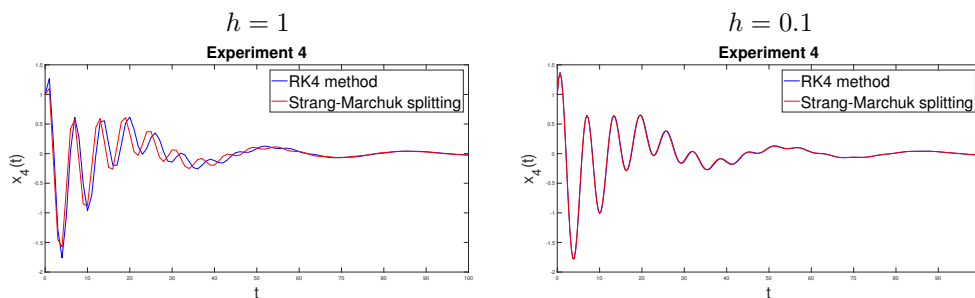
As expected, we see that for the same order of accuracy splitting methods are faster than the full numerical solution. It can be seen that by reducing the step size  $h$ , the solvers containing splitting produce the numerical solution 1-2 orders of magnitude faster than the Euler method.

Table 3 shows the errors for Experiments 1 and 2. The methods give approximately the same error.

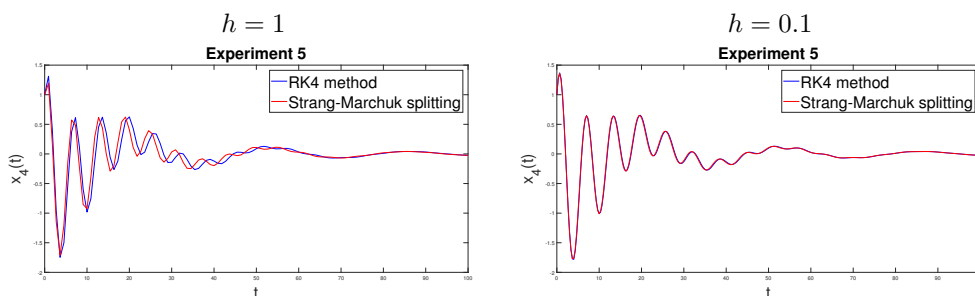
Table 3. Comparison of errors for Experiments 1 and 2

<b>h</b>	<b>1.</b>	<b>2.</b>
1.0	$2.56 \times 10^{-1}$	$2.64 \times 10^{-1}$
0.1	$2.53 \times 10^{-2}$	$2.09 \times 10^{-2}$
0.01	$2.09 \times 10^{-3}$	$2.05 \times 10^{-3}$
0.001	$2.08 \times 10^{-4}$	$2.04 \times 10^{-4}$

**E4:** Since the Strang-Marchuk method is second-order, the choice of a bigger step size  $h$  is also sufficient to obtain a well-approximating splitting solution. This is illustrated in Figure 3, which shows  $x_4(t)$  for the time interval  $[0, 100]$ . We see that even for  $h = 0.3$  the splitting solution and the exact solution are very close.

Figure 3. Experiment 4:  $x_4(t)$  on the time interval  $[0, 100]$ 

**E5:** We see in Figure 4 how the splitting solution behaves when the step size  $h$  is reduced. The figures show the component  $x_4$  of the splitting solution on time interval  $[0, 100]$ .

Figure 4. Experiment 5:  $x_4(t)$  of the splitting solution on interval  $[0, 100]$ 

For E4 and E5 the errors as well as the runtimes are similar. It is interesting to compare the errors between the Strang-Marchuk splitting method and using a second-order numerical method without splitting. We used the second-order Euler method to solve the system (23) without splitting in Experiment 8. In Table 4 we show the errors. The errors are two orders of magnitude smaller for the same stepsize  $h$  using the splitting method than using the second-order Euler method.

Table 4. Comparison of errors in case of Experiment 4 and 8

$h$	Experiment 4	Experiment 8
1.0	$7.20 \times 10^{-4}$	$8.21 \times 10^{-2}$
0.1	$4.90 \times 10^{-7}$	$8.24 \times 10^{-5}$
0.01	$4.78 \times 10^{-10}$	$7.52 \times 10^{-8}$
0.001	$4.76 \times 10^{-13}$	$7.43 \times 10^{-11}$

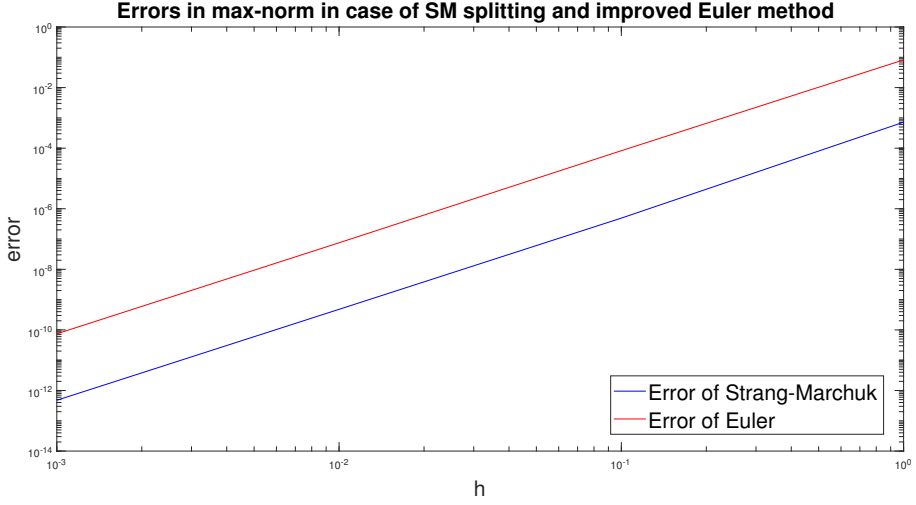


Figure 5. Error as a function of the stepsize  $h$  in Experiments 4 and 8

Figure 5 shows how errors change with decreasing  $h$  for Experiments 4 and 8.

**E6:** In this experiment we apply the average sequential splitting. At first we use the decomposition (24) requiring 2 numerical solutions. For this case, we have to solve the following two subproblems at each step:

$$\begin{cases} \dot{y}_1(t) = A_{0(1)}y_1(t) & t \in [t_i, t_{i+1}], \\ y_1(t_i) = x_{sp(1)}(t_i), \end{cases} \quad \begin{cases} \dot{y}_2(t) = A_{0(2)}y_2(t) & t \in [t_i, t_{i+1}], \\ y_2(t_i) = y_1(t_{i+1}). \end{cases} \quad (29) \quad (30)$$

The splitting solution at  $t_{i+1}$  ( $i = 0, \dots, n-1$ ) is

$$x_{sp(1)}(t_{i+1}) = \exp(A_{0(2)}(t_{i+1} - t_i))y_1(t_{i+1}) \exp(A_{0(1)}(t_{i+1} - t_i))x_{sp(1)}(t_i). \quad (31)$$

We have to solve the following subproblems at each step:

$$\begin{cases} \dot{y}_1(t) = A_{0(2)}y_1(t) & t \in [t_i, t_{i+1}], \\ y_1(t_i) = x_{sp(2)}(t_i), \end{cases} \quad \begin{cases} \dot{y}_2(t) = A_{0(1)}y_2(t) & t \in [t_i, t_{i+1}], \\ y_2(t_i) = y_1(t_{i+1}). \end{cases} \quad (32) \quad (33)$$

The form of the splitting solution at  $t_{i+1}$  ( $i = 0, \dots, n-1$ ) is

$$x_{sp(2)}(t_{i+1}) = \exp(A_{0(1)}(t_{i+1} - t_i))y_1(t_{i+1}) \exp(A_{0(2)}(t_{i+1} - t_i))x_{sp(2)}(t_i). \quad (34)$$

The second-order approximate splitting solution is given by the average of the solutions  $x_{sp(1)}(t_{i+1})$  and  $x_{sp(2)}(t_{i+1})$ , i.e.

$$x_{sp}(t_{i+1}) = \frac{x_{sp(1)}(t_{i+1}) + x_{sp(2)}(t_{i+1})}{2}. \quad (35)$$

Figure 6 shows how the splitting solution approximates the exact solution with decreasing  $h$ . The figures show  $x_4(t)$  on the  $[0, 100]$  time interval.

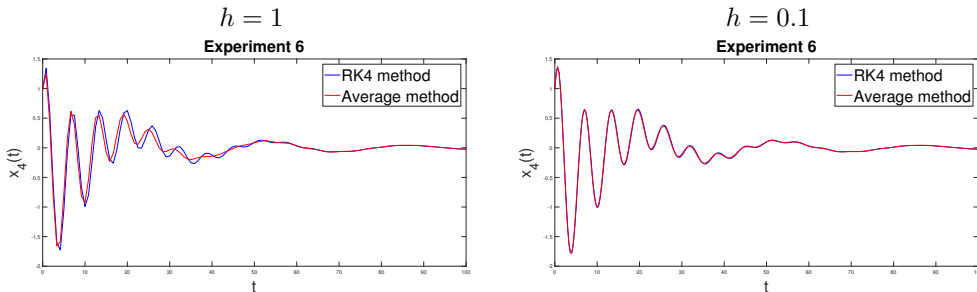


Figure 6. Experiment 6:  $x_4(t)$  of the splitting solution on time interval  $[0, 100]$

**E7:** We consider the decomposition (26) where the first two matrices are commuting. Therefore, for using the Average Method instead of  $3! = 6$  split problems we have to solve four subproblems, only.

The decomposition has the following form

$$A_0 = A_{0_{(3)}} + A_{0_{(4)}}, \quad (36)$$

where we use the notation  $A_{0_{(4)}}$  for the sum of the two commuting matrices, i.e.  $A_{0_{(4)}} := A_{0_{(1)}} + A_{0_{(2)}}$ , which means that

$$A_{0_{(4)}} = \begin{pmatrix} 0 & 1 & 0 & 0 \\ -1 & -(p_1 + p_2\mu c_k) & 0 & 0 \\ 0 & 0 & 0 & 1 \\ 0 & 0 & -(p_4 - c_k\mu^2) & -p_3 \end{pmatrix}.$$

Thus, in these cases, we solve the following sequences of sub-problems.

First, we solve the following two subproblems where the commutativity is not present.

The ordering  $A_1 \rightarrow A_3 \rightarrow A_2$  results in the following split sub-problems:

$$\begin{cases} y_1(t) = A_{0_{(1)}}y_1(t) & t \in [t_i, t_{i+1}], \\ y_1(t_i) = x_{sp(1)}(t_i), \end{cases} \quad \begin{cases} y_2(t) = A_{0_{(3)}}y_2(t) & t \in [t_i, t_{i+1}], \\ y_2(t_i) = y_1(t_{i+1}), \end{cases} \quad (37) \quad (38)$$

$$\begin{cases} \dot{y}_3(t) = A_{0(2)}y_3(t) & t \in [t_i, t_{i+1}], \\ y_3(t_i) = y_2(t_{i+1}). \end{cases} \quad (39)$$

Then the splitting solution at  $t = t_{i+1}$  is

$$\begin{aligned} x_{sp(1)}(t_{i+1}) &= \\ &= \exp(A_{0(2)}(t_{i+1} - t_i))y_2(t_{i+1}) \exp(A_{0(3)}(t_{i+1} - t_i))y_1(t_{i+1}) \exp(A_{0(1)}(t_{i+1} - t_i))x_{sp(1)}(t_i). \end{aligned} \quad (40)$$

The ordering  $A_2 \rightarrow A_3 \rightarrow A_1$  results in the sub-problems following three subproblems:

$$\begin{cases} \dot{y}_1(t) = A_{0(2)}y_1(t) & t \in [t_i, t_{i+1}], \\ y_1(t_i) = x_{sp(2)}(t_i), \end{cases} \quad (41) \quad \begin{cases} \dot{y}_2(t) = A_{0(3)}y_2(t) & t \in [t_i, t_{i+1}], \\ y_2(t_i) = y_1(t_{i+1}), \end{cases} \quad (42)$$

$$\begin{cases} \dot{y}_3(t) = A_{0(1)}y_1(t) & t \in [t_i, t_{i+1}], \\ y_3(t_i) = y_2(t_{i+1}). \end{cases} \quad (43)$$

Then the splitting solution at  $t_{i+1}$  is

$$\begin{aligned} x_{sp(2)}(t_{i+1}) &= \\ &= \exp(A_{0(1)}(t_{i+1} - t_i))y_2(t_{i+1}) \exp(A_{0(3)}(t_{i+1} - t_i))y_1(t_{i+1}) \exp(A_{0(2)}(t_{i+1} - t_i))x_{sp(2)}(t_i). \end{aligned} \quad (44)$$

Due to the commutativity, the remaining two problems, which we solve, consist of only two subproblems. These are the following.

For the ordering  $A_4 \rightarrow A_3$  the subproblems are the following:

$$\begin{cases} \dot{y}_1(t) = A_{0(4)}y_1(t) & t \in [t_i, t_{i+1}], \\ y_1(t_i) = x_{sp(3)}(t_i), \end{cases} \quad (45) \quad \begin{cases} \dot{y}_2(t) = A_{0(3)}y_2(t) & t \in [t_i, t_{i+1}], \\ y_2(t_i) = y_1(t_{i+1}). \end{cases} \quad (46)$$

The splitting solution at  $t_{i+1}$  is

$$\begin{aligned} x_{sp(3)}(t_{i+1}) &= \\ &= \exp(A_{0(3)}(t_{i+1} - t_i))y_1(t_{i+1}) \exp(A_{0(4)}(t_{i+1} - t_i))x_{sp(3)}(t_i). \end{aligned} \quad (47)$$

Finally, for the ordering  $A_3 \rightarrow A_4$  we get

$$\begin{cases} \dot{y}_1(t) = A_{0(3)}y_1(t) & t \in [t_i, t_{i+1}], \\ y_1(t_i) = x_{sp(4)}(t_i), \end{cases} \quad (48) \quad \begin{cases} \dot{y}_2(t) = A_{0(4)}y_2(t) & t \in [t_i, t_{i+1}], \\ y_2(t_i) = y_1(t_{i+1}). \end{cases} \quad (49)$$

Then

$$x_{sp(4)}(t_{i+1}) = \exp(A_{0(4)}(t_{i+1} - t_i))y_1(t_{i+1}) \exp(A_{0(3)}(t_{i+1} - t_i))x_{sp(4)}(t_i). \quad (50)$$

Using the Average Method, the second-order accurate approximation is defined as

$$x_{sp}(t) = \frac{x_{sp(1)}(t) + x_{sp(2)}(t) + 2 \cdot x_{sp(3)}(t) + 2 \cdot x_{sp(4)}(t)}{6}. \quad (51)$$

Figure 7 shows how the 4th component ( $x_4(t)$ ) of the splitting solution approaches the exact solution with decreasing  $h$ . The advantage of the method is

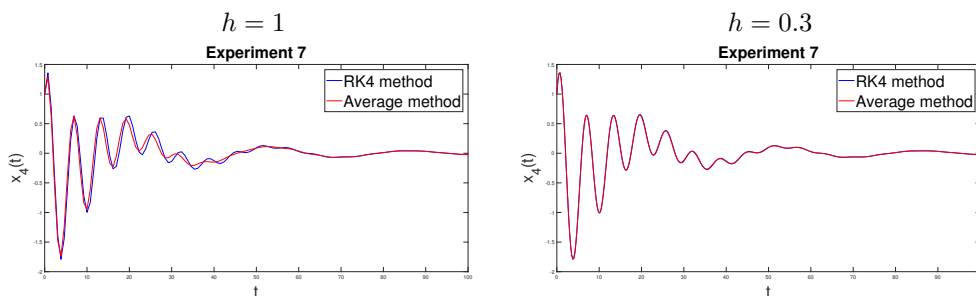


Figure 7. Experiment 7:  $x_4(t)$  on time interval interval  $[0, 100]$

that the solutions (40), (44), (47) and (50) can be independently calculated, i.e., the computation is parallelizable.

Table 5. Comparison of runtimes (in seconds) for Experiments 4-8.

<b>h</b>	<b>E4</b>	<b>E5</b>	<b>E6</b>	<b>E7</b>	<b>E8</b>
1.0	$4.32 \times 10^{-2}$	$7.57 \times 10^{-2}$	$1.15 \times 10^{-4}$	$4.54 \times 10^{-4}$	$8.18 \times 10^{-3}$
0.1	$7.55 \times 10^{-1}$	$8.71 \times 10^{-1}$	$1.01 \times 10^{-3}$	$1.52 \times 10^{-3}$	$1.96 \times 10^{-2}$
0.01	$5.20 \times 10^0$	$6.39 \times 10^0$	$3.65 \times 10^{-3}$	$7.81 \times 10^{-3}$	$8.44 \times 10^{-2}$
0.001	$1.53 \times 10^1$	$2.06 \times 10^1$	$1.89 \times 10^{-2}$	$6.47 \times 10^{-2}$	$1.13 \times 10^0$

Table 5 collects the comparison of runtimes for Experiments 4-8. These results show that sequential and Strang-Marchuk splitting is about two orders of magnitude slower than the improved Euler method, while the Average Method is about two orders of magnitude faster. This is an encouraging result for the applicability of the Average Method.

## 7. SUMMARY

By performing several numerical experiments we demonstrated that the benefits of the Average Method are the following:

- easy implementation when  $d$  is small,
- provides a second-order approximation solution using a first-order method,
- the numerical solutions of the subproblems can be independently computed, therefore the method can be parallelized.

The drawback of the Average Method is the large number ( $d!$ ) of solutions to be computed. This number can be reduced by finding a decomposition of the system matrix into a set of pairwise commuting matrices.

**Acknowledgements.** This work was completed in the ELTE Institutional Excellence Program (TKP2020-IKA-05) financed by the Hungarian Ministry of Human Capacities, Istvan Farago has been supported by the European Union, and co-financed by the European Social Fund (EFOP-3.6.3-VEKOP-16-2017-00002) and was also supported by the Hungarian Scientific Research Fund OTKA, SNN125119. The work of T. Kalmár-Nagy is supported by the NRDI Funds (TKP2020 IES, Grant No. BME-IE-WAT; TKP2020 NC, Grant No. BME-NC) based on the charter of bolster issued by the NRDI Office under the auspices of the Ministry for Innovation and Technology.

## APPENDIX 1

**Statement 1.** *Assume that we have the Cauchy problem (1) Solving this problem in all possible sequences using sequential splitting, and then taking the average of the resulting numerical solutions, the method is second-order, i.e.*

$$\exp(h(A_1 + \dots + A_d)) = \frac{1}{d!} \sum_{p \in \mathcal{P}^d} \exp\{p_1, p_2, \dots, p_n\} + \mathcal{O}(h^3). \quad (10)$$

**Proof.** We prove the statement by induction. First we consider the case  $k = 2$ , i.e. the validity of the formula

$$\exp(h(A_1 + A_2)) = \frac{\exp(hA_1)\exp(hA_2) + \exp(hA_2)\exp(hA_1)}{2!} + \mathcal{O}(h^3). \quad (52)$$

Obviously, for any matrix  $C$  we have

$$\exp(hC) = I + hC + \frac{h^2}{2}C^2 + \mathcal{O}(h^3). \quad (53)$$

Hence,

$$\begin{aligned} & \frac{\exp(hA_1)\exp(hA_2) + \exp(hA_2)\exp(hA_1)}{2!} = \\ &= \frac{[I + hA_1 + \frac{h^2}{2!}A_1^2][I + hA_2 + \frac{h^2}{2!}A_2^2] + [I + hA_2 + \frac{h^2}{2!}A_2^2][I + hA_1 + \frac{h^2}{2!}A_1^2]}{2!} = \\ &= \frac{2I + 2h(A_1 + A_2) + h^2(A_1^2 + A_2^2 + A_1A_2 + A_2A_1)}{2!} = \\ &= I + h(A_1 + A_2) + \frac{h^2}{2!}(A_1^2 + A_2^2 + A_1A_2 + A_2A_1) \quad (54) \end{aligned}$$

which proves (52).

Now we suppose that the statement is true for  $k = d$  and prove its validity for  $k = d + 1$ .

$$\begin{aligned} & \exp(h(A_1 + A_2 + \dots + A_d + A_{d+1})) = \\ & = I + h \sum_{j=1}^{d+1} A_j + \frac{h^2}{2!} \left( \sum_{j=1}^{d+1} A_j^2 + \sum_{i=1}^d \sum_{j=i+1}^{d+1} A_i A_j + \sum_{i=2}^{d+1} \sum_{j=1}^{i-1} A_i A_j \right) + \mathcal{O}(h^3). \end{aligned} \quad (55)$$

Using the notation  $B = A_1 + A_2 + \dots + A_d$ , we have

$$\begin{aligned} & \exp(h(A_1 + A_2 + \dots + A_d + A_{d+1})) = \\ & = \exp(h(B + A_{d+1})) = \frac{\exp(hB) \exp(hA_{d+1}) + \exp(hA_{d+1}) \exp(hB)}{2!} + \mathcal{O}(h^3) = \\ & = \frac{1}{2} \left[ I + h \sum_{j=1}^d A_j + \frac{h^2}{2!} \left( \sum_{j=1}^d A_j^2 + \sum_{i=1}^{d-1} \sum_{j=i+1}^d A_i A_j + \sum_{i=2}^d \sum_{j=1}^{i-1} A_i A_j \right) + \right. \\ & \quad \left. + hA_{d+1} + h^2 \sum_{j=1}^d A_j A_{d+1} + \frac{h^2}{2} A_{d+1}^2 \right] + \\ & + \frac{1}{2} \left[ I + h \sum_{j=1}^d A_j + \frac{h^2}{2!} \left( \sum_{j=1}^d A_j^2 + \sum_{i=1}^{d-1} \sum_{j=i+1}^d A_i A_j + \sum_{i=2}^d \sum_{j=1}^{i-1} A_i A_j \right) + \right. \\ & \quad \left. + hA_{d+1} + h^2 \sum_{j=1}^d A_{d+1} A_j + \frac{h^2}{2} A_{d+1}^2 \right] + \mathcal{O}(h^3) = \\ & = \frac{1}{2} \left[ 2I + 2h \left( \sum_{j=1}^d A_j + A_{d+1} \right) + h^2 \left( \sum_{j=1}^d A_j^2 + A_{d+1}^2 + \sum_{i=1}^{d-1} \sum_{j=i+1}^d A_i A_j + \right. \right. \\ & \quad \left. \left. + \sum_{i=2}^d \sum_{j=1}^{i-1} A_i A_j + \sum_{j=1}^d A_{d+1} A_j + A_j A_{d+1} \right) \right] + \mathcal{O}(h^3) = \\ & = \frac{1}{2} \left[ 2I + 2h \sum_{j=1}^{d+1} A_j + h^2 \left( \sum_{j=1}^{d+1} A_j^2 + \sum_{i=1}^d \sum_{j=i+1}^{d+1} A_i A_j + \right. \right. \\ & \quad \left. \left. + \sum_{i=2}^{d+1} \sum_{j=1}^{i-1} A_i A_j \right) \right] + \mathcal{O}(h^3) = \\ & = I + h \sum_{j=1}^{d+1} A_j + \frac{h^2}{2} \left( \sum_{j=1}^{d+1} A_j^2 + \sum_{i=1}^d \sum_{j=i+1}^{d+1} A_i A_j + \right. \\ & \quad \left. + \sum_{i=2}^{d+1} \sum_{j=1}^{i-1} A_i A_j \right) + \mathcal{O}(h^3). \end{aligned} \quad (56)$$

This proves our statement.  $\square$

## APPENDIX 2

**Statement 2.** *If and only if  $A = A_1 + A_2$ , and  $A_1$  and  $A_2$  satisfy the condition*

$$\left[ A_1, [A_1, A_2] \right] = \left[ A_2, [A_1, A_2] \right] \text{ then}$$

$$\exp(h(A_1 + A_2)) = \frac{\exp(hA_1)\exp(hA_2) + \exp(hA_2)\exp(hA_1)}{2} + \mathcal{O}(h^4). \quad (15)$$

**Proof.** Let  $x, y \in \mathbb{R} \setminus \{0\}$ ,  $x + y \neq 0$  and  $d = 2$  and we want to prove the following relation:

$$\exp(h(A_1 + A_2)) = \frac{x \exp(hA_1)\exp(hA_2) + y \exp(hA_2)\exp(hA_1)}{x + y} + \mathcal{O}(h^4). \quad (57)$$

Clearly

$$\begin{aligned} \exp(h(A_1 + A_2)) &= \\ &= I + h(A_1 + A_2) + \frac{h^2}{2!}(A_1 + A_2)^2 + \frac{h^3}{3!}(A_1 + A_2)^3 + \mathcal{O}(h^4) = \\ &= I + h(A_1 + A_2) + \frac{h^2}{2} \left( A_1^2 + A_2^2 + A_1A_2 + A_2A_1 \right) + \frac{h^3}{6} \left( A_1^3 + A_2^3 + \right. \\ &\quad \left. + A_1A_2^2 + A_1^2A_2 + A_2A_1^2 + A_2^2A_1 + A_1A_2A_1 + A_2A_1A_2 \right) + \mathcal{O}(h^4). \quad (58) \end{aligned}$$

Then, the right-hand side of (57):

$$\begin{aligned} &\frac{x \exp(hA_1)\exp(hA_2) + y \exp(hA_2)\exp(hA_1)}{x + y} + \mathcal{O}(h^4) = \\ &= \frac{1}{x + y} \left[ x \left( I + hA_1 + \frac{h^2}{2!}A_1^2 + \frac{h^3}{3!}A_1^3 + \mathcal{O}(h^4) \right) \left( I + hA_2 + \frac{h^2}{2!}A_2^2 + \frac{h^3}{3!}A_2^3 + \mathcal{O}(h^4) \right) \right] + \\ &+ \frac{1}{x + y} \left[ y \left( I + hA_2 + \frac{h^2}{2!}A_2^2 + \frac{h^3}{3!}A_2^3 + \mathcal{O}(h^4) \right) \left( I + hA_1 + \frac{h^2}{2!}A_1^2 + \frac{h^3}{3!}A_1^3 + \mathcal{O}(h^4) \right) \right] = \\ &= \frac{1}{x + y} \left[ x \left( I + h(A_1 + A_2) + h^2 \left( \frac{1}{2}A_1^2 + \frac{1}{2}A_2^2 + A_1A_2 \right) + \right. \right. \\ &\quad \left. \left. + h^3 \left( \frac{1}{6}A_1^3 + \frac{1}{6}A_2^3 + \frac{1}{2}A_1^2A_2 + \frac{1}{2}A_1A_2^2 \right) \right) \right] + \\ &+ \frac{1}{x + y} \left[ y \left( I + h(A_1 + A_2) + h^2 \left( \frac{1}{2}A_1^2 + \frac{1}{2}A_2^2 + A_2A_1 \right) + \right. \right. \\ &\quad \left. \left. + h^3 \left( \frac{1}{6}A_1^3 + \frac{1}{6}A_2^3 + \frac{1}{2}A_2^2A_1 + \frac{1}{2}A_2A_1^2 \right) \right) \right] = \\ &= I + h(A_1 + A_2) + \frac{1}{x + y} \left\{ x \left[ \left( \frac{1}{2}A_1^2 + \frac{1}{2}A_2^2 + A_1A_2 \right) + y \left( \frac{1}{2}A_1^2 + \frac{1}{2}A_2^2 + A_2A_1 \right) \right] + \right. \\ &\quad \left. + h^3 \left[ x \left( \frac{1}{6}A_1^3 + \frac{1}{6}A_2^3 + \frac{1}{2}A_1^2A_2 + \frac{1}{2}A_1A_2^2 \right) + y \left( \frac{1}{6}A_1^3 + \frac{1}{6}A_2^3 + \frac{1}{2}A_2^2A_1 + \frac{1}{2}A_2A_1^2 \right) \right] \right\}. \quad (59) \end{aligned}$$

(57) will be true if coefficients of (58) and (59) are the same. The coefficients of  $h^i$ ,  $i = 0, 1, 2, 3$  are the following.

Coefficient of  $h^0$ :

$$\frac{(x+y)I}{(x+y)} = I \implies I = I.$$

Coefficient of  $h^1$ :

$$\frac{(x+y)(A_1 + A_2)}{(x+y)} = (A_1 + A_2) \implies (A_1 + A_2) = (A_1 + A_2).$$

Coefficient of  $h^2$ :

$$\begin{aligned} x\left(\frac{1}{2}A_1^2 + \frac{1}{2}A_2^2 + A_1A_2\right) + y\left(\frac{1}{2}A_1^2 + \frac{1}{2}A_2^2 + A_2A_1\right) &= \\ &= \frac{1}{2}(A_1 + A_2) + \frac{1}{2}(A_1A_2 + A_2A_1) \\ \frac{1}{2}(A_1 + A_2) + \frac{xA_1A_2 + yA_2A_1}{x+y} &= \frac{1}{2}(A_1 + A_2) + \frac{1}{2}(A_1A_2 + A_2A_1), \\ \frac{xA_1A_2 + yA_2A_1}{x+y} &= \frac{1}{2}(A_1A_2 + A_2A_1), \\ xA_1A_2 + yA_2A_1 &= \frac{1}{2}(x+y)A_1A_2 + \frac{1}{2}(x+y)A_2A_1. \\ &\downarrow \\ x = y &= \frac{1}{2}(x+y), \\ x &= y. \end{aligned} \tag{60}$$

Coefficient of  $h^3$ :

$$\begin{aligned} \frac{1}{x+y} \left[ x\left(\frac{1}{6}A_1^3 + \frac{1}{6}A_2^3 + \frac{1}{2}A_1^2A_2 + \frac{1}{2}A_1A_2^2\right) + y\left(\frac{1}{6}A_1^3 + \frac{1}{6}A_2^3 + \frac{1}{2}A_2^2A_1 + \frac{1}{2}A_2A_1^2\right) \right] &= \\ = \frac{1}{6} \left( A_1^3 + A_2^3 + A_1A_2^2 + A_1^2A_2 + A_2A_1^2 + A_2^2A_1 + A_1A_2A_1 + A_2A_1A_2 \right). \end{aligned}$$

After some calculations we get

$$\begin{aligned} \frac{x(A_1^2A_2 + A_1A_2^2) + y(A_2^2A_1 + A_2A_1^2)}{2(x+y)} &= \\ = \frac{A_1A_2^2 + A_1^2A_2 + A_2A_1^2 + A_2^2A_1 + A_1A_2A_1 + A_2A_1A_2}{6}, \end{aligned}$$

Utilizing equation (60) yields

$$\begin{aligned} \frac{x(A_1^2A_2 + A_1A_2^2 + A_2^2A_1 + A_2A_1^2)}{4x} &= \\ = \frac{A_1A_2^2 + A_1^2A_2 + A_2A_1^2 + A_2^2A_1 + A_1A_2A_1 + A_2A_1A_2}{6} \end{aligned}$$

or

$$A_1^2 A_2 + A_1 A_2^2 + A_2^2 A_1 + A_2 A_1^2 = 2A_1 A_2 A_1 + 2A_2 A_1 A_2$$

and

$$A_1 [A_1, A_2] + [A_2, A_1] A_1 + A_2 [A_2, A_1] + [A_1, A_2] A_2 = 0.$$

On the basis of the well known equality  $[A, B] = -[B, A]$  we have

$$A_1 [A_1, A_2] - [A_1, A_2] A_1 - A_2 [A_1, A_2] + [A_1, A_2] A_2 = 0,$$

or

$$\left[ A_1, [A_1, A_2] \right] + \left[ [A_1, A_2], A_2 \right] = 0,$$

and

$$\left[ A_1, [A_1, A_2] \right] - \left[ A_2, [A_1, A_2] \right] = 0.$$

Hence, the condition of third order is as follows

$$\left[ A_1, [A_1, A_2] \right] = \left[ A_2, [A_1, A_2] \right]. \quad (61)$$

This means that for a decomposition of two matrices the method will be third-order if and only if condition (61) is satisfied.  $\square$

#### REFERENCES

1. R. I. McLachlan and G. Reinout W. Quispel. "Splitting methods." *Acta Numerica*, **11**, (2002), pp. 341–434. DOI: 10.1017/S0962492902000053.
2. István Faragó and Ágnes Havasy. *Operator splittings and their applications*. Nova Science Publ., 2009.
3. Bei Gu and H. Harry Asada. "Co-Simulation of Algebraically Coupled Dynamic Subsystems Without Disclosure of Proprietary Subsystem Models." *Journal of Dynamic Systems, Measurement, and Control*, **126**(1) (2004), pp. 1–13. DOI: 10.1115/1.1648307.
4. Tamás Kalmár-Nagy and Ilinca Stanciulescu. "Can complex systems really be simulated?" *Applied Mathematics and Computation*, **227**, (2014), pp. 199–211.
5. Petra Csomós and Gregor Nickel. "Operator splitting for delay equations." *Computers & Mathematics with Applications*, **55**(10), (2008), pp. 2234–2246. DOI: 10.1016/j.camwa.2007.11.011.
6. Kevin O'Meara, John Clark, and Charles Vinsonhaler. *Advanced Topics in Linear Algebra: Weaving Matrix Problems through the Weyr Form*. Oxford University Press, 2011.
7. Tamás Kalmár-Nagy, Rudolf Csikja, and Tarek A Elgohary. "Nonlinear analysis of a 2-DOF piecewise linear aeroelastic system." *Nonlinear Dynamics*, **85**,(2) (2016), pp. 739–750. DOI: 10.1007/s11071-016-2719-z.
8. János Lelkes and Tamás Kalmár-Nagy. "Analysis of a piecewise linear aeroelastic system with and without tuned vibration absorber." *Nonlinear Dynamics*, (2020), pp. 1–22. DOI: 10.1007/s11071-016-2719-z.

## SIMULATION OF CELLULAR STRUCTURES WITH A COUPLED FEM-FCM APPROACH BASED ON CT DATA

ULRICH GABBERT AND MATHIAS WÜRKNER  
Otto von Guericke University of Magdeburg  
Universitaetsplatz 2, 39114 Magdeburg, Germany  
[ulrich.gabbert@ovgu.de](mailto:ulrich.gabbert@ovgu.de), [mathias.wuerkner@ovgu.de](mailto:mathias.wuerkner@ovgu.de)

[Received: October 30, 2020; Accepted: December 11, 2020]

*Dedicated to Professor Barna Szabó on the occasion of his eighty-fifth birthday*

**Abstract.** The application of cellular structural materials provide new light-weight capabilities in many engineering fields. But the microstructure significantly influences the strength, the fatigue and fracture behavior as well as the life span of a structure made from cellular materials. The current paper illustrates the general idea how to take into account the cellular microstructure in the stress and strain analysis. The detailed geometry, including all discontinuities in the microstructure is available, for instance from measurements provided by the computed tomography (CT). The proposed simulation methodology is a combination of the finite element method (FEM) and the finite cell method (FCM). The FCM approach is applied in regions where discontinuities occur, avoiding a body-fitted mesh. As basis of the FEM-FCM coupling the commercial FEA package Abaqus is used. The theoretical background and the overall simulation workflow along with specific implementation details are discussed. Finally, academic benchmark problems are used to verify the developed coupling method.

*Mathematical Subject Classification:* 65L05, 76G25

*Keywords:* Finite element method (FEM), finite cell method (FCM) , computed tomography (CT), cellular structures, coupling of the FEM with the FCM

### 1. INTRODUCTION

The application of ultra-light-weight constructions contributes to a reduction of natural resources in many fields of engineering. There are several types of light-weight materials available, such as cellular materials made of aluminium or plastic foam, sandwich materials with a core layer from honeycomb, hollow spheres or foam, etc. The increasing application of additive manufacturing technologies also allows the production of complex light-weight components with a special designed porosity, which can also be seen as a cellular structure as well. The general application of cellular materials provides new design capabilities in several engineering fields, such as in automotive and aerospace industries, electro engineering, wind power industries, machine and plant engineering, container constructions, etc. Besides the application of specially designed cellular materials there are other lightweight structures with great advantages, particularly in mass production, e.g. aluminium die cast parts.

Components produced with the die cast technology and with additive manufacturing have local inhomogeneities, such as pores in die cast parts and voids in additive produced parts, which are unavoidable. Such local porosities can be recognised with help of computed tomography (CT).

The desired and also the undesired inhomogeneities in the microstructure have to be taken into account in the simulation, because they significantly influence the strength, the fatigue and fracture behavior and, consequently, also the life span of a structure.

The main approach to analyse engineering structures is the application of the finite element method [1–3]. The typical method to take into account the microstructure in a global FE analysis is a homogenisation of the microstructure. Homogenisation means, that with help of different methods the microstructure is smeared, resulting in a homogenised reference material with the same global behavior as the original material with the microstructure. One standard homogenisation approach is based on the Hill theory [4]. There are several homogenisation methods available, such as the Eshelby-based methods, the Mori-Tanaka method, the generalised self-consistent method, the asymptotic homogenisation method, the representative volume element approach (RVE) etc.; for an overview see [5–9]. Of course, the local behaviour, e.g. the local stress-strain state, is lost when applying homogenisation methods. In FEM the microstructure can be taken into account, e.g. by a substructure approach [10] or by a multilevel finite element method (FE2) approach [11, 12]. In both cases the microstructure has to be meshed in some detail, which results in an increase of the computational effort.

One important problem is the generation of a high quality body-fitted mesh as a basis for the FEM. This pre-processing step calls for an experienced designer and can account for up to 80% of the overall analysis time [13]. In order to capture the microstructure a refined finite element mesh is needed to ensure an accurate approximation of the geometry. Most cellular materials have a randomly sized and distributed microstructure. To simplify the meshing procedure a reference microstructure can be used, which is regular and statistically equivalent to the original microstructure. In this case the finite element mesh can be generated automatically. The disadvantage is the loss of the irregularity of the microstructure. Alternatively, the micro-structure can be obtained from computed tomography (CT) images [14].

The most promising approach to avoid a finite element mesh fitting the geometry of the cellular microstructure is the application of the finite cell method (FCM). The FCM can also simply process CT data [15, 16]. The method can be automated straightforwardly and thus reduces the required input data. In [17] we have successfully implemented the FCM in order to analyse the propagation of ultrasonic waves in heterogeneous structures. The application of higher order finite elements increases the accuracy and reduces the required computational effort [18]. In this case a rough finite element approximation results in very accurate solutions even if a fine microstructure has to be analysed. A first in-house code based on the higher order FCM has been developed by S. Duczak [19, 20].

The FCM has also great advantages for structures with a cellular microstructure, which is often limited to small regions, such as in die cast parts [21]. The remaining parts of a structure can be well approximated by the classical FEM. Consequently, a combination of the FEM and the FCM, where the FCM is only applied in regions with local heterogeneities, could be of great advantage. The regions with a local microstructure known from CT scans can be simply meshed with hexagonal cells, avoiding complicated body adapted mesh generation.

Most of the FE simulations in industry are performed with commercial FEA tools, such as Abaqus, Ansys, Nastran and others. Therefore, it would be of a great industrial interest if the FCM approach would be a part of commercial FEA software [22]. In the following a concept of an overall workflow to combine the FCM with the commercial FE software Abaqus is presented and tested, where also specific implementation details and application problems are discussed. The paper is organized as follows. In Section 2 the fundamental principles of the three-dimensional finite cell method are briefly recalled. This also includes the main differences to the classical finite element method. In Section 3 the coupling concept based on the commercial analysis tool Abaqus is described. In Section 4 some information and trouble shooting according to the STL data derived from CT measurements is given. In Section 5 the developed coupling procedure is tested by analyzing an academic test example, which demonstrates the capability of the developed simulation concept. The paper finishes with conclusions in Section 6.

## 2. THE FINITE CELL METHOD

In the following we briefly summarize the basics of the FCM, assuming that the FEM is well known. The FCM slightly differs from the FEM, and, consequently, we start with the typical basics from the FEM. We assume a linear elastic static boundary value problem. The solution  $\mathbf{u}$  in a region  $\Omega$  is equivalent to the solution of the variational form

$$B(\mathbf{u}, \mathbf{v}) = F(\mathbf{v}), \quad \forall \mathbf{v} \in V. \quad (2.1)$$

This is the weak form of the equilibrium conditions of the problem. Here  $\mathbf{u}$  is the displacement vector and  $\mathbf{v}$  represents the vector of arbitrary test functions in the space  $V$  of admissible functions. The bilinear form  $B$  and the linear form  $F$  are given as follows

$$B(\mathbf{u}, \mathbf{v}) = \int_{\Omega} [\mathbf{L}\mathbf{v}]^T \mathbf{C} [\mathbf{L}\mathbf{u}] \, d\Omega, \quad (2.2)$$

$$F(\mathbf{v}) = \int_{\Omega} \mathbf{v}^T \bar{\mathbf{f}} \, d\Omega + \int_{\Gamma_N} \mathbf{v}^T \bar{\mathbf{t}} \, d\Gamma. \quad (2.3)$$

Here  $\mathbf{L}$  denotes the linear strain-displacement operator,  $\mathbf{C}$  stands for the Hook elasticity matrix,  $\mathbf{f}$  denotes the vector of body forces and  $\mathbf{t}$  is the traction vector. A bar over a variable signifies a prescribed value. The prescribed tractions are defined on the Neumann boundary  $\Gamma_N$  as

$$\boldsymbol{\sigma} \mathbf{n} = \bar{\mathbf{t}} \quad \text{on } \Gamma_N \quad (2.4)$$

where here  $\boldsymbol{\sigma}$  denotes the stress tensor and  $\mathbf{n}$  constitutes the outward normal vector of unit length. Furthermore the displacements are prescribed on the Dirichlet boundary  $\Gamma_D$ , resulting in

$$\mathbf{u} = \bar{\mathbf{u}} \quad \text{on } \Gamma_D \quad (2.5)$$

Equations (2.1)–(2.5) are the general basis of FEM [3]. In order to solve a problem with the help of FEM a mesh of finite elements is required which approximately coincides with the geometry of the structural region of interest  $\Omega$ . But in FCM the mesh in general must not fit the structural geometry. The physical domain  $\Omega$  is extended by a fictitious domain  $\Omega_{\text{fic}}$ . The union of these two domains forms the extended domain  $\Omega_{\text{ex}}$  – see Figure 1.

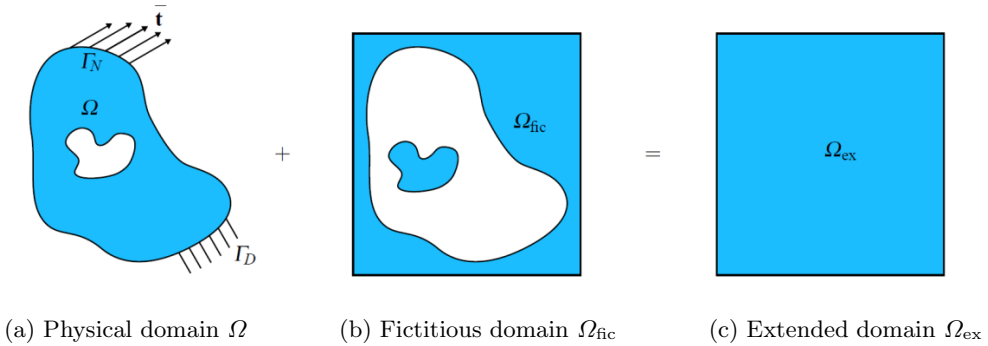


Figure 1. Fictitious domain approach

Instead of equation (2.1) the weak form is now solved over the extended region

$$B_{\text{ex}}(\mathbf{u}, \mathbf{v}) = F_{\text{ex}}(\mathbf{v}), \quad \forall \mathbf{v} \in V. \quad (2.6)$$

The main advantage of the fictitious domain approach is that the extended domain is of a much simpler geometry and can, therefore, be simply meshed by regular non-distorted finite elements. Quadrilateral and hexagonal elements and triangular and tetrahedral elements can be used for 2D and 3D problems, respectively. During the analysis it is imported to distinguish between normal (not cut) finite elements and elements cut by the physical boundary. This differentiation is controlled by the so-called indicator function  $\alpha$  as

$$\alpha(\mathbf{x}) = \begin{cases} 1 & \forall \mathbf{x} \in \Omega \\ a_0 = 10^{-q} & \forall \mathbf{x} \in \Omega_{\text{ex}} \setminus \Omega \end{cases} \quad (2.7)$$

If  $\mathbf{x}$  is in the fictitious region, the indicator function can be taken as zero. In order to avoid numerical problems a small value  $a_0$  is used instead of zero. The exponent  $q$  is typically taken in the range from 4 to 15, depending on the material properties [23]. With the value  $\alpha$  equations (2.2) and (2.3) are modified as

$$B_{\text{ex}}(\mathbf{u}, \mathbf{v}) = \int_{\Omega_{\text{ex}}} [\mathbf{L}\mathbf{v}]^T \alpha \mathbf{C} [\mathbf{L}\mathbf{u}] \, d\Omega, \quad (2.8)$$

$$F_{\text{ex}}(\mathbf{v}) = \int_{\Omega_{\text{ex}}} \mathbf{v}^T \alpha \bar{\mathbf{f}} \, d\Omega + \int_{\Gamma_N} \mathbf{v}^T \bar{\mathbf{t}} \, d\Gamma. \quad (2.9)$$



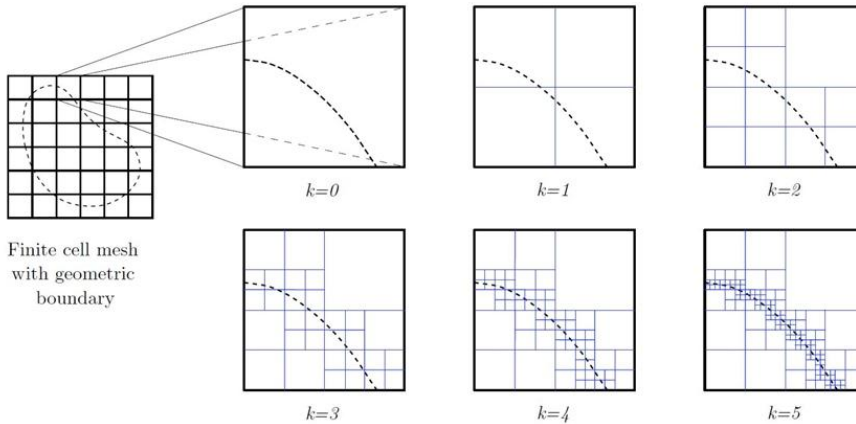


Figure 3. Adaptive subdivision of one element in integration cells

Here  $\mathbf{N}_e$  contains the element shape functions,  $\mathbf{U}_e$  represents the vector of unknowns, and  $\mathbf{V}_e$  stands for the coefficients of the test functions for one single finite element, which in the context of FCM is usually named a finite cell. Inserting equations (2.10) and (2.11) into the weak form of equation (2.6) finally yields the well known linear system of equations

$$\mathbf{K}\mathbf{U} = \mathbf{F}, \quad (2.12)$$

where  $\mathbf{K}$  denotes the global stiffness matrix and  $\mathbf{F}$  represents the global load vector. The most important difference of the finite cell method to the standard finite element approach is the integration over the finite elements (finite cells), which are cut by the boundary (Figure 3).

For a more detailed insight into FCM we refer the reader to the comprehensive review article by Schillinger et al. [25] and the works by Düster et al. [15] and Parvizian et al. [16]. Here also several methods to include Dirichlet and Neumann types of boundary conditions are presented.

### 3. APPLICATION OF CT DATA IN FCM SIMULATION

CT measurements result in a three-dimensional voxel data set containing all necessary information with respect to the microstructure. The voxel data can be further processed to obtain a boundary representation of the structure, e.g. via the surface tessellation language (STL) representation [26]. The determination of the material properties is based on the Hounsfield units (HU) of CT data. Both voxel data and STL data can be used as input data for simulation purposes.

The data from CT scans, given in STL format, can be processed by almost every CAD program. The file format can be either ASCII or binary. For processing STL data it is important that the triangular surface is closed and unique. Unfortunately,

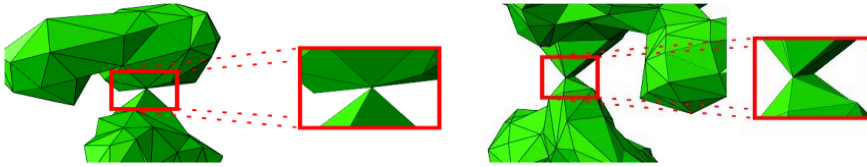


Figure 4. Problems of identifying closed STL surfaces [22]: left: two surfaces connected by a unit point; right: two surfaces connected by a unit line

the simplicity of STL format using unstructured triangular facets means some trouble shootings regarding the 3D finite element meshing process. The STL data often describe unclosed surfaces, or overlapping facets and incorrect normal directions. Additionally, sometimes two closed surface triangulations are connected to each other, as for instance by a line segment or by a point (see Figure 4).

The above mentioned problems complicate the unique identification of surface regions in an automated algorithm. Therefore a mesh repair or a remeshing procedure is absolutely essential for an FCM application. This is a highly complex issue and the topic of several publications [27, 28].

#### 4. INTEGRATION OF FCM INTO A COMMERCIAL FE PACKAGE

Initially we developed and applied FCM for the analysis of ultrasonic waves propagating in heterogeneous materials. This development was part of an interdisciplinary research project, which was aimed at new wave based methods for structural health monitoring. The developed methods are focused on light-weight structures made from fiber and particle reinforced structures for airplanes or the rotor blades of wind power stations. Our FCM software development is a Matlab based in-house code, see [19, 29]. But, the FCM approach is also an interesting approach in other fields of applications, such as for the stress analysis of structures made from materials with a cellular microstructure. One important industrial application is the evaluation of aluminum die cast parts and their quality assurance by taking into account their inevitable porosity [21, 22]. Today highly stressed parts are inline measured with CT in order to eliminate manufactured parts that do not meet the quality standards of the pore specification.

The FCM method cannot be well applied utilizing a university based in-house software which was developed for scientific reasons only. With regard to practical applications we are convinced that a robust implementation of the FCM methodology within a wide-spread and established software tool like Abaqus would create higher applicability to practical engineering problems. Therefore, we developed a software concept to couple the FCM with the commercial software package Abaqus, including open source software products for the pre- and post-processing tasks. The general workflow of our software concept is illustrated in Figure 5.

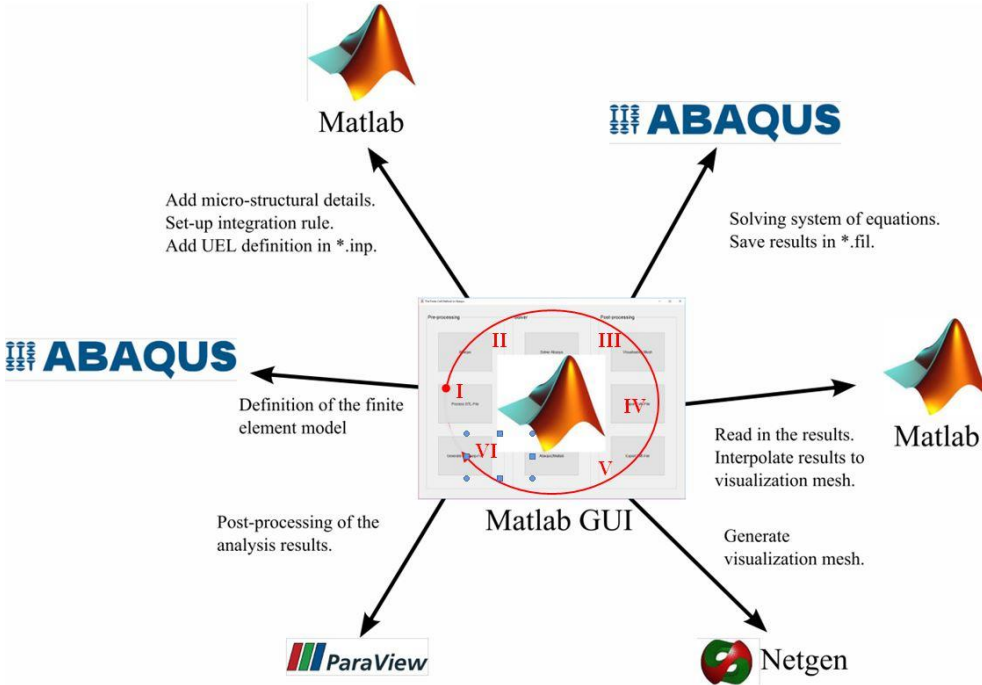


Figure 5. Workflow of the coupling of FCM with the FEM package Abaqus; the numbers I-VI denote the sequence of the application of the subprograms

For the coupling only free of access available software interfaces of Abaqus are used. To this end, we have defined a user subroutine with help of the Abaqus routine UEL that is able to incorporate the required functionality. In 3D the FCM can be applied if the FEM basis elements are hexahedral as well as tetrahedral finite elements [30]. Details concerning the required input data and the necessary pre- as well as post-processing tools – although not directly related to Abaqus – are provided as well. Besides microstructural data from CT measurements, also virtual generated STL data can be applied in the design process of the constructions under investigation.

The initial model is set up in the pre-processing module of Abaqus. Here, the material properties and the element types are defined. In the next step an Abaqus input file is generated. This file is further processed in MATLAB and adjusted to incorporate the user defined element routine (UEL). At this stage the micro-structural details from CT measurements are added to the analysis and also the necessary details to perform the composed numerical integration are generated. During the solution of the governing equations these data are read in by the UEL. For the post-processing a geometry-conforming visualization mesh is created. This can be achieved using

powerful mesh generators (e.g. Netgen [31]) or Abaqus itself. The analysis results are accordingly interpolated onto the new visualization nodes using the finite element shape functions of the coupled FEM-FCM model and saved in a vtk-file format. This format can be processed by ParaView, which offers all capabilities of commercial FE post-processing tools.

## 5. TEST EXAMPLE

The developed coupled FEM-FCM concept based on Abaqus has been tested with help of several simple test examples, where as reference solutions overkill pure Abaqus solutions were used. The following test example demonstrates the capability of the developed coupling procedure [22].

In Figure 6 a cube with an edge length of  $a = 10$  m is shown. A tensile load of  $p = 100$  N/m<sup>2</sup> is applied normal to the positive  $z$ -direction. On the opposite surface the displacements in  $z$ -direction are constrained to zero. Additionally the displacements at two edges are also constrained to zero in  $x$ - and in  $y$ -direction, respectively. A Young's modulus of 70000 N/mm<sup>2</sup> and a Poisson ratio of 0.33 are used.

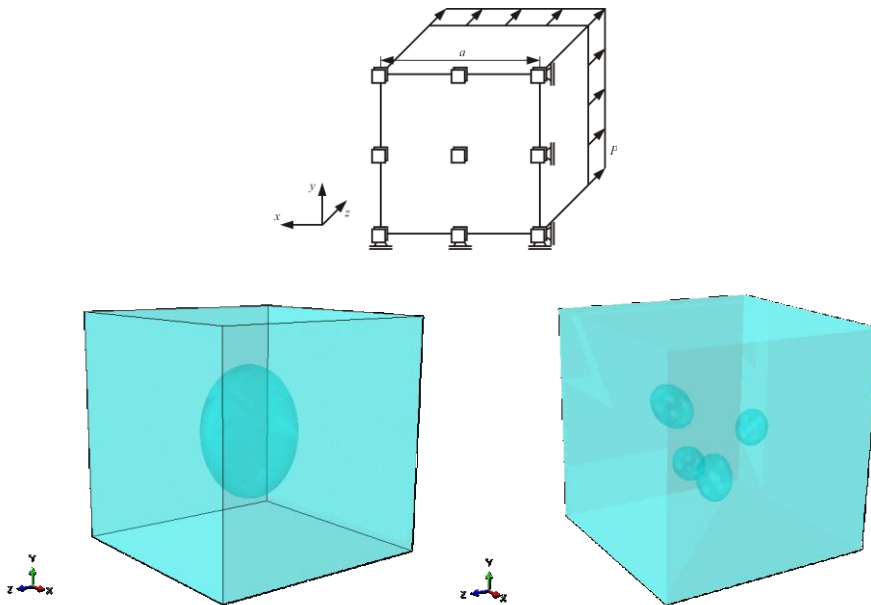


Figure 6. Cube with two types of inclusions: one centrally placed ellipsoid, and four randomly distributed ellipsoids

In the solid cube two versions of pores are embedded, a centrally embedded ellipsoidal pore in the first example and four randomly distributed embedded ellipsoidal pores in the second example, where the pores have different volumes and size (see Figure 6).

### Cube with one central placed ellipsoid

The FE-FC model consists of  $25 \times 25 \times 25$  hexahedral elements of second polynomial order (20 node hexahedrons). The cut elements are integrated with a subdivision level  $k = 3$  (for  $k$  see Figure 3). The overkill reference Abaqus model consists of 180,325 second order tetrahedral elements (764,424 DOFs). In Figure 7 the von Mises stress results of the coupled FEM-FCM approach and the pure Abaqus solution are compared. The results are in a very good agreement, with an error of about 0.6%.

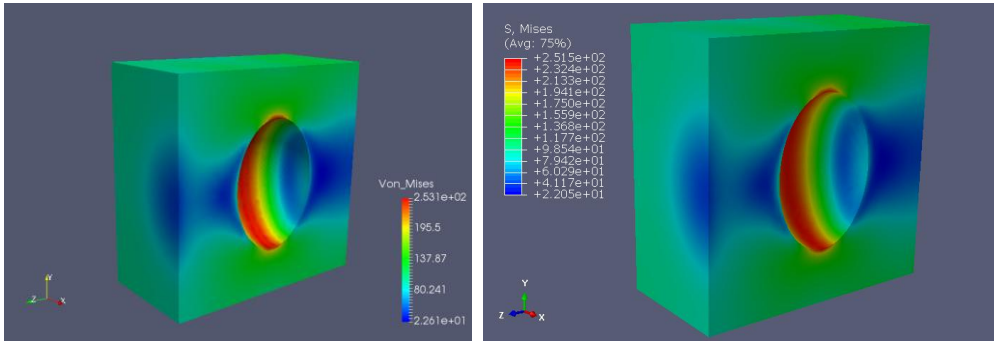


Figure 7. Von Mises stresses in a cube with a central ellipsoid; left: coupled FE-FC solution; right: overkill Abaqus reference solution

### Cube with four randomly distributed ellipsoids

The FE-FC model consists again of  $25 \times 25 \times 25$  hexahedral elements of second polynomial order (20 node hexahedrons). The cut elements are here integrated with a subdivision level  $k=4$  due to the smaller and more closely placed ellipsoids. The reference Abaqus model consists of 300,864 tetrahedral elements (1,263,081 DOFs). In Figure 7 the von Mises stress results of the coupled FEM-FCM approach and the pure overkill Abaqus solution are compared. The results are again in a good agreement, with a maximum error of 6%.

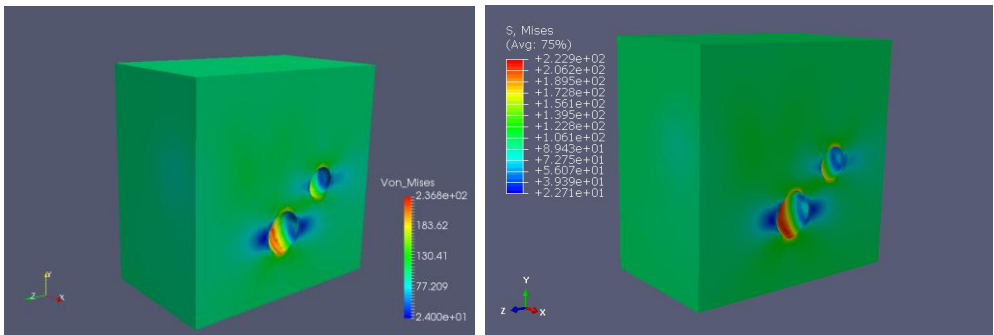


Figure 8. Von Mises stresses in a cube with a central ellipsoid; left: coupled FE-FC solution; right: overkill Abaqus reference solution

Regarding the convergence of FCM we refer to [16], where the convergence properties of FCM are investigated in detail. It is shown that the convergence properties of the FCM can be directly derived from those of the associated finite element computation. In our case the FCM approach is coupled with the Abaqus software, where the accuracy can be increased with h-refinements only. In this case the convergence rate of the coupled FE-FC approach is algebraic and identical to the well known h-extension of the applied finite elements. It is important that the stiffness matrices of the cut finite elements are sufficiently accurately integrated, e.g. by an adaptive integration approach (see Figure 3). For more details regarding the numerical integration we refer to [15, 24, 32]. If the mesh of the above given test examples is refined by increasing the number of hexahedral elements, the solution will converge to the Abaqus reference solution.

## 6. CONCLUSION

In the paper a concept for an implementation of the finite cell method (FCM) within the commercial software Abaqus is presented. The FCM can be efficiently applied for the stress and strain analysis of structures made from light-weight materials with a cellular or porous microstructure. The great advantage is inherent automated mesh generation with a quite regular hexahedron or tetrahedron mesh, which is not forced to match with the physical geometry of the structure. The real geometry is taken into account in the integration process of the element stiffness and load matrices of the cut finite elements (finite cells). The uncut finite elements are processed as in the standard FEM procedure. The cut elements are treated with an adaptive integration algorithm, as shown in Figure 3. The FCM provides a fast convergence rate if high order shape functions are used for the approximation of the displacement field in the finite elements. This is especially important if a very fine microstructure has to be taken into account with relative large finite elements/cells. In order to apply this methodology for the solution of engineering problems the FCM should be coupled with any standard commercial FEA software, such as Abaqus, Ansys, Nastran etc., which are powerful tools for solving complex engineering problems. In this paper the concept of a coupled FEM-FCM methodology has been presented and realized by using the Abaqus software. It is necessary to provide the microstructure in the form of a STL data file. The STL data can be derived by the CT measurements or can also be automatically generated. It is important that these STL data are unique and provide closed surfaces. This is a great problem if CT data in form of voxel data are used that are automatically transformed in STL data. Typically such data have to be repaired to be usable for the coupled FEM-FCM simulation. The applicability of the developed coupling method has been shown with academic test examples. The coupled FEM-FCM approach can also be used to solve industrial problems.

With the proposed methodology to couple FCM with a commercial finite element package like Abaqus, an important step has been taken towards a standardized analysis method for light-weight structures made from materials with a cellular microstructure.

## REFERENCES

1. O. C. Zienkiewicz and R. L. Taylor. *The Finite Element Method – Solid Mechanics*. 5th ed. Vol. 2. Butterworth-Heinemann, 2000.
2. K. J. Bathe. *Finite Element Procedures*. 2nd ed. Watertown, 2014.
3. B. Szabó and I. Babuška. *Introduction to Finite Element Analysis: Formulation, Verification and Validation*. John Wiley & Sons, 2011.
4. R. Hill. “Continuum micromechanics of elastoplastic polycrystals.” *Journal of the Mechanics and Physics of Solids*, **13**(2), (1965), 89–101. DOI: 10.1016/0022-5096(65)90023-2.
5. S. J. Hollister and N. Kikuehi. “A comparison of homogenization and standard mechanics analyses for periodic porous composites.” *Computational Mechanics*, **10**, (1992), 73–95. DOI: 10.1007/BF00369853.
6. G. Lielens. “Micro-macro modeling of structured materials.” PhD. Université Catholique de Louvain, 1999. 141 pp. URL: <https://d-nb.info/1005303312/34>.
7. S. Kari. “Micromechanical modeling and numerical homogenization of fibre and particle reinforced composites.” PhD. Düsseldorf: in Fortschritt-Berichte VDI, Reihe 18, Mechanik/Bruchmechanik; nr. 308: University of Magdeburg, Germany, 2007.
8. R. Rodríguez-Ramos, R. Guinovart-Díaz, J. Bravo-Castillero, F. J. Sabina, H. Berger, S. Kari, and U. Gabbert. “Variational bounds for anisotropic elastic multiphase composites with different shapes of inclusions.” *Archive of Applied Mechanics*, **79**, (2009), 695–708. DOI: 10.1007/s00419-008-0246-1.
9. A. Düster, H. G. Sehlhorst, and E. Rank. “Numerical homogenization of heterogeneous and cellular materials utilizing the finite cell method.” *Computational Mechanics*, **50**, (2012), 413–431. DOI: 10.1007/s00466-012-0681-2.
10. Chen Yang, L. Dong, B. Wang, Chen Yuli, Z. Qiu, and Z. Guo. “A substructure-based homogenization approach for systems with periodic microstructures of comparable sizes.” *Computational Mechanics*, **50**, (2017), pp. 97–104. DOI: 10.1016/j.compstruct.2017.01.050.
11. F. Feyel. “A multilevel finite element method (FE<sup>2</sup>) to describe the response of highly non-linear structures using generalized continua.” *Computer Methods in Applied Mechanics and Engineering*, **192**(28-30), (2017), 3233–3244. DOI: 10.1016/S0045-7825(03)00348-7.
12. H. G. Sehlhorst. *Numerical Homogenization Strategies for Cellular Materials with Applications in Structural Mechanics*. Fortschritt-Berichte VDI: Reihe 18, Mechanik/Bruchmechanik. 2012. URL: <https://books.google.hu/books?id=5tg8MwEACAAJ>.
13. J. A. Cottrell, T. J. R. Hughes, and Y. Bazilevs. “Isogeometric Analysis: Toward integration of CAD and FEA.” Wiley, Hoboken, Sept. 2009. DOI: 10.1002/9780470749081.ch7.
14. J. Kastner and C. Heinzl. “X-ray computed tomography for non-destructive testing and materials characterization.” *Integrated Imaging and Vision Techniques*

- for *Industrial Inspection*. Ed. by Liu Z., H. Ukida, P. Ramuhalli, and K. Niel. Springer, 2015, pp. 227–250. DOI: 10.1007/978-1-4471-6741-9\_8.
15. A. Düster, J. Parvizian, Z. Yang, and E. Rank. “The finite cell method for three-dimensional problems of solid mechanics.” *Computational Methods in Applied Mechanics and Engineering*, **197**(45), (2008), 3768–3782. DOI: 10.1016/j.cma.2008.02.036.
  16. J. Parvizian, A. Düster, and E. Rank. “The finite cell method for three-dimensional problems of solid mechanics.” *Computational Mechanics*, **45**, (2007), 121–133. DOI: 10.1007/s00466-007-0173-y.
  17. M. Joulaian, S. Duczec, U. Gabbert, and A. Düster. “Finite and spectral cell method for wave propagation in heterogeneous materials.” *Computational Mechanics*, **54**, (2014), 661–675. DOI: 10.1007/s00466-014-1019-z.
  18. C. Willberg, S. Duczec, J. M. Vivar Perez, D. Schmicker, and U. Gabbert. “Comparison of different higher order finite element schemes for the simulation of Lamb waves.” *Computer Methods in Applied Mechanics and Engineering*, **54**, (2014), pp. 241–244. DOI: 10.1016/j.cma.2012.06.011.
  19. S. Duczec. “Higher order finite elements and fictitious domain concept for wave propagation analysis.” PhD. Düsseldorf: in Fortschritt-Berichte VDI., Reihe 20, Mechanik/Bruchmechanik; nr. 437: University of Magdeburg, Germany, 2014.
  20. S. Duczec and U. Gabbert. “The Finite Cell Method: A higher order fictitious domain approach for wave propagation analysis in heterogeneous structures.” *Lamb-Wave Based Structural Health Monitoring in Polymer Composites*, ed. by R. Lammering, U. Gabbert, M. Sinapius, T. Schuster, and P. Wierach. Springer, 2018, pp. 217–239. DOI: 10.1007/978-3-319-49715-0.
  21. S. Duczec, H. Berger, and U. Gabbert. “The Finite Pore Method: A new approach to evaluate gas pores in cast parts by combining computed tomography and the finite cell method.” *International Journal of Cast Metals Research*, **28**(4), (2015), pp. 221–228. DOI: 10.1179/1743133615Y.0000000003.
  22. M. Würkner, S. Duczec, H. Berger, H. Köppe, and U. Gabbert. “A software platform for the analysis of die-cast parts with pores by the finite cell method,” *Analysis and Modelling of Advanced Structures and Smart Systems*, ed. by H. Altenbach, E. Carrera, and G. Kulikov. Series: Advanced Structured Materials. Springer, Singapore, 2018, pp. 327–341. DOI: 10.1007/978-981-10-6895-9\_14.
  23. M. Ruess, D. Schillinger, Y. Bazilevs, V. Varduhn, and E. Rank. “Weakly enforced essential boundary conditions for NURB-embedded and trimmed NURBS geometries on the basis of the finite cell method.” *International Journal of Numerical Methods in Engineering*, **95**, (2013), pp. 811–846. DOI: 10.1002/nme.4522.
  24. S. Duczec and U. Gabbert. “Efficient integration method for fictitious domain approaches.” *Computational Mechanics*, **56**(4), (2015), pp. 725–738. DOI: 10.1007/s00466-015-1197-3.
  25. D. Schillinger, Q. Cai, R. P. Mundani, and E. Rank. “A review of the finite cell method for nonlinear structural analysis of complex CAD and image based geometric models.” *Advanced Computing, Lecture Notes in Computational Science and Engineering*, **93**, (2013), pp. 1–23. DOI: 10.1007/978-3-642-38762-3\_1.

26. E. Bechet, J. C. Cuilliere, and F. Trochu. “Generation of a finite element mesh from stereolithography (STL) files.” *Computer-Aided Design*, **34**(1), (2002), pp. 1–17. DOI: 10.1016/S0010-4485(00)00146-9.
27. F. Liu, H. Zhou, and D. Li. “Repair of STL errors.” *International Journal of Production Research*, **47**(1), (2009), pp. 1–23. DOI: 10.1080/00207540701424539.
28. M. Attene. “Direct repair of self-intersecting meshes.” *Graphical Models*, **76**(6), (2014), 658–668. DOI: 10.1016/j.gmod.2014.09.002.
29. R. Lammering, U. Gabbert, M. Sinapius, T. Schuster, and P. Wierach, eds. *Lamb-Wave Based Structural Health Monitoring in Polymer Composites*. Springer International Publishing, 2018. URL: 10.1007/978-3-319-49715-0.
30. S. Ducek, F. Duvigneau, and U. Gabbert. “The finite cell method for tetrahedral meshes.” *Finite Elements in Analysis and Design*, **121**, (2016), 18–32. DOI: 10.1016/j.finel.2016.07.004.
31. J. Schöberl. “NETGEN: An advancing front 2D/3D-mesh generator based on abstract rules.” *Computing and Visualization in Science*, **1**, (1997), 41–52. DOI: 10.1007/s007910050004.
32. Z. Yang, M. Ruess, S. Kollmannsberger, A. Düster, and E. Rank. “An efficient integration technique for the voxel-based finite cell method.” *Journal for Numerical Methods in Engineering*, **91**(5), (2012), 457–471.

## Notes for Contributors

### to the Journal of Computational and Applied Mechanics

**Aims and scope.** The aim of the journal is to publish research papers on theoretical and applied mechanics. Special emphasis is given to articles on computational mechanics, continuum mechanics (mechanics of solid bodies, fluid mechanics, heat and mass transfer) and dynamics. Review papers on a research field and materials effective for teaching can also be accepted and are published as review papers or classroom notes. Papers devoted to mathematical problems relevant to mechanics will also be considered.

**Frequency of the journal.** Two issues a year (approximately 80 pages per issue).

**Submission of Manuscripts.** Submission of a manuscript implies that the paper has not been published, nor is being considered for publication elsewhere. Papers should be written in standard grammatical English. The manuscript is to be submitted in electronic, preferably in pdf, format. The text is to be 130 mm wide and 190 mm long and the main text should be typeset in 10pt CMR fonts. Though the length of a paper is not prescribed, authors are encouraged to write concisely. However, short communications or discussions on papers published in the journal must not be longer than 2 pages. Each manuscript should be provided with an English Abstract of about 50–70 words, reporting concisely on the objective and results of the paper. The Abstract is followed by the Mathematical Subject Classification – in case the author (or authors) give the classification codes – then the keywords (no more than five). References should be grouped at the end of the paper in numerical order of appearance. Author’s name(s) and initials, paper titles, journal name, volume, issue, year and page numbers should be given for all journals referenced.

The journal prefers the submission of manuscripts in L<sup>A</sup>T<sub>E</sub>X. Authors should select the  $\mathcal{A}\mathcal{M}\mathcal{S}$ -L<sup>A</sup>T<sub>E</sub>X article class and are not recommended to define their own L<sup>A</sup>T<sub>E</sub>X commands. Visit our home page for further details concerning how to edit your paper.

For the purpose of refereeing the manuscripts should be sent either to Balázs Tóth ([Balazs.TOTH@uni-miskolc.hu](mailto:Balazs.TOTH@uni-miskolc.hu)) or László BARANYI ([arambl@uni-miskolc.hu](mailto:arambl@uni-miskolc.hu)).

The eventual supply of an accepted for publication paper in its final camera-ready form will ensure more rapid publication. Format requirements are provided by the home page of the journal from which sample L<sup>A</sup>T<sub>E</sub>X files can be downloaded:

<http://www.mech.uni-miskolc.hu/jcam>

These sample files can also be obtained directly (via e-mail) from Balázs TÓTH ([Balazs.TOTH@uni-miskolc.hu](mailto:Balazs.TOTH@uni-miskolc.hu)), upon request.

One issue of the journal and ten offprints will be provided free of charge and mailed to the correspondent author. Since JCAM is an open access journal each paper can be downloaded freely from the homepage of the journal.

The Journal of Computational and Applied Mechanics is abstracted in Zentralblatt für Mathematik and in the Russian Referativnij Zhurnal.

Secretariat of the Vice-Rector for Research and International Relations, University of Miskolc

Responsible for publication: Prof. Dr. Zita Horváth, rector

Published by the Miskolc University Press under the leadership of Attila Szendi

Responsible for duplication: Works manager Erzsébet Pásztor

Number of copies printed: 75

Put to the Press on May 18, 2021

Number of permission: MERT.2021-70.ME.

**ISSN 2732-0189** (Online)

**ISSN 1586-2070** (Print)

## **A Short History of the Publications of the University of Miskolc**

The University of Miskolc (Hungary) is an important center of research in Central Europe. Its parent university was founded by the Empress Maria Teresia in Selmecebánya (today Banská Štiavnica, Slovakia) in 1735. After the first World War the legal predecessor of the University of Miskolc moved to Sopron (Hungary) where, in 1929, it started the series of university publications with the title *Publications of the Mining and Metallurgical Division of the Hungarian Academy of Mining and Forestry Engineering* (Volumes I.-VI.). From 1934 to 1947 the Institution had the name Faculty of Mining, Metallurgical and Forestry Engineering of the József Nádor University of Technology and Economic Sciences at Sopron. Accordingly, the publications were given the title *Publications of the Mining and Metallurgical Engineering Division* (Volumes VII.-XVI.). For the last volume before 1950 – due to a further change in the name of the Institution – *Technical University, Faculties of Mining, Metallurgical and Forestry Engineering, Publications of the Mining and Metallurgical Divisions* was the title.

For some years after 1950 the Publications were temporarily suspended.

After the foundation of the Mechanical Engineering Faculty in Miskolc in 1949 and the movement of the Sopron Mining and Metallurgical Faculties to Miskolc, the Publications restarted with the general title *Publications of the Technical University of Heavy Industry* in 1955. Four new series - Series A (Mining), Series B (Metallurgy), Series C (Machinery) and Series D (Natural Sciences) - were founded in 1976. These came out both in foreign languages (English, German and Russian) and in Hungarian.

In 1990, right after the foundation of some new faculties, the university was renamed to University of Miskolc. At the same time the structure of the Publications was reorganized so that it could follow the faculty structure. Accordingly three new series were established: Series E (Legal Sciences), Series F (Economic Sciences) and Series G (Humanities and Social Sciences). The latest series, i.e., the series H (European Integration Studies) was founded in 2001. The eight series are formed by some periodicals and such publications which come out with various frequencies.

Papers on computational and applied mechanics were published in the

### **Publications of the University of Miskolc, Series D, Natural Sciences.**

This series was given the name Natural Sciences, Mathematics in 1995. The name change reflects the fact that most of the papers published in the journal are of mathematical nature though papers on mechanics also come out.

The series

### **Publications of the University of Miskolc, Series C, Fundamental Engineering Sciences**

founded in 1995 also published papers on mechanical issues. The present journal, which is published with the support of the Faculty of Mechanical Engineering and Informatics as a member of the Series C (Machinery), is the legal successor of the above journal.



## Contents

### Contributed Papers

- Olurotimi ADELEYE, Abdulahi ATITEBI and Ahmed YINUSA: Nonlinear vibrational and rotational analysis of microbeams in nanobiomaterials using Galerkin decomposition and differential transform methods 3–22
- István ECSEDI and Attila BAKSA: Deformation of a cantilever curved beam with variable cross section 23–36
- Lívia BODA, Istvan FARAGÓ and Tamás KALMÁR-NAGY: The average method is much better than average 37–56
- Ulrich GABBERT and Mathias WÜRKNER: Simulation of cellular structures with a coupled FEM-FCM approach based on CT data 57–70